Development and applications of microwave and optical atomic frequency standards

S. Bize

SORBONNE UNIVERSITÉ
CRÉATEURS DE FUTURS
DEPUIS 1257

DEVELOPMENT AND APPLICATIONS OF MICROWAVE AND OPTICAL ATOMIC FREQUENCY STANDARDS

HABILITATION À DIRIGER LES RECHERCHES

DISCIPLINE : PHYSIQUE

présentée le 25 juin 2018 par Sébastien BIZE

Composition du jury :

Pr.	Marie HOUSSIN	Rapporteur
Pr.	Gaetano MILETI	Rapporteur
Dr.	Pierre PILLET	Rapporteur
Dr.	Michel BRUNE	Examinateur
Pr.	Saïda GUELLATI-KHELIFA	Présidente du jury
Hon. Prof., Dr. rer. nat. habil.	Fritz RIEHLE	Examinateur

Travail de recherche effectué au

SYRTE (UMR 8630), Observatoire de Paris, Université PSL, CNRS,
Sorbonne Université, LNE

National Institute of Standards and Technology
NIST, Time and Frequency division, Boulder, CO, USA

Development and applications of microwave and optical atomic frequency standards

Sébastien BIZE

July 16, 2019

Contents

Chapter 1

Introduction

Researches presented here deal with the development and the use of atomic clocks with extreme stability and accuracy. This search for ever increased level of performance of atomic clock and more generally in atomic spectroscopy is motivated by the long-term vision that it has impact on science and society in the several different following ways:

- Search for extreme clock performance is advancing hand in hand with exploration in physics and better understanding of atomic systems. Increased clock performance reveals new phenomena and provides means to investigate them.

- Clocks with extreme level of performance are a tool of choice to test the structure of space-time and fundamental laws of nature. They provide experimental inputs to the quest for a unified theory of gravitation and quantum mechanics.

- Clocks with extreme level of performance are key to major applications with large impact in science and society, which are the realization of the base unit of time of the international systems of units (SI), timekeeping via the elaboration of the international atomic time (TAI) and the realization of master clock of global navigation satellite systems (GNSS).

- Search for extreme clock precision is a steady driver for innovation in multiple areas such as lasers, low noise electronics, ultra-stable oscillators. Also, it creates knowledge necessary to define tradeoff between performance and other requirements for applicability. This knowledge is often applicable not only to novel clocks but also extents to other classes of atom-based instruments.

– Increasing clock performance leads to new applications. For instance, clock comparisons with uncertainties of 10^{-18} foreseen with the new generation of optical clocks enable chronometric geodesy for Earth sciences, i.e. the use of clock as a new type of sensor for the measurement of Earth gravitational potential differences.

The work presented in this manuscript will give examples for several of these aspects. It mainly relates to the development of two experimental setups which are a dual atomic fountain clock, hereinafter called FO2, and a mercury optical lattice clocks, both developed at SYRTE. A third setup is a single mercury ion clock on which I worked during my postdoctoral stay in the team of J. Bergquist, in the ion trapping group, led by D. Wineland, at National Institute of Standards and Technology (NIST) in Boulder, CO (USA).

The manuscript is organized as follows:

Chapter 1 is the present *Introduction*.

Chapter 2 entitled *Clock physics* describes work undertaken to develop atomic frequency standards, to understand their physics and to improve their stability and uncertainty. Selected studies are related to two experiments : a dual Rb and Cs fountain and a Hg optical lattice clock.

Chapter 3 entitled *Ultra-stable oscillators* describes developments of ultra-stable oscillators which are key to the progress of atomic frequency standards while having their own interest. Three different topics are treated. First, the realization of ultra-stable microwave reference signals based on cryogenic sapphire oscillators and their applications. Then, the development of ultra-stable lasers. Finally and briefly, generation of ultra-low noise microwave signals using optical frequency combs.

Chapter 4 entitled *Metrology* deals with applications of atomic frequency standards in metrology, i.e. with the realization of frequency and time references, with comparisons between them and with the determination of reference values for atomic frequency ratios. One aspect of this work is to contribute some of the necessary steps toward a possible redefinition of the second of the international system of units based on optical transition(s).

Chapter 5 entitled *Fundamental tests* reports on several tests of fundamental physical laws making use of ultra-stable oscillators and atomic fre-

quency standards. These tests include tests of the stability of natural constants, tests of Lorentz invariance and search for dark matter.

Chapter 6 entitled *Conclusions and prospects* looks at possible continuations of the work reported in previous chapters. Prospect of developing novel application of atomic frequency standards to Earth's science, named chronometric geodesy, is mentioned.

Chapter 2

Clock physics

A key aspect in the development of atomic clocks with extreme performance lies in the understanding the physics of processes impacting the interrogation of the clock transition. The present chapter is devoted to studies of these aspects in the case of the dual Rb and Cs fountain FO2 and in a mercury lattice clock.

2.1 Atomic fountains

2.1.1 Principle of operation of atomic fountains

In this section, we provide a reminder of basic principles of operation of atomic fountains, which is necessary to understand the more advanced topics discussed later. Note that a description of atomic fountains and of the work done with them at SYRTE, written in French, can be found in [1].

A level diagram of Cs and Rb atoms and a schematic view of an atomic fountain is shown in Fig. 2.1. The clock transition is the M1 transition between the two hyperfine levels of the electronic ground states. The corresponding frequencies, indicated in Fig. 2.1, are 9.192631770 GHz and 6.834682610 GHz for Cs and Rb respectively. Atomic fountain clocks operate in a sequential manner. Atoms are first gathered in an optical molasses (2), made of set of 6 laser beams (1), with the proper geometry. The same laser beams are used to launch atoms upwards and to cool them, in the upward moving frame, to a temperature of ~ 1 μK. The subsequent steps of the clock sequence occur during the ballistic flight of the atomic sample in the ultra-high vacuum chamber. Atoms are selected in the $m_F = 0$ Zeeman sub-state of the lower hyperfine level, thanks to a combination of microwave interaction, applied in the state selection cavity (4) and a push laser beam

(5). Next, atoms interact with the interrogation microwave field, which is fed into the interrogation cavity (6). Interactions occur one time of the way up and a second time on the way down, forming the well-known Ramsey interrogation sequence. The separation in time between the up and down passages is typically ~ 0.6 s. When the interrogation field frequency matches the hyperfine frequency, atoms are promoted to the upper hyperfine level. On their way down, atoms cross the state selection and molasses region where all the fields (microwave and lasers) are off. They fall into the detection region (8) where the two hyperfine levels are detected independently by laser-induced fluorescence. From the number of atoms in the two hyperfine levels, one can estimate the transition probability, which in turn serves, during the clock operation, as a signal to lock the frequency of the interrogation field to the hyperfine transition. Typically, 10^6 atoms are detected. Stringent control of any field seen by the atoms in the interrogation region (7). This includes static electric and magnetic fields, microwave fields, light from lasers and thermal radiation. To this end, the interrogation region is surrounded by several layers of magnetic and thermal shields. The exact configuration of FO2 is described in [2][3]. Configurations of other fountains can be found, for instance, in [4][5][6][7][8][9][10][11][12].

2.1.2 Development of a dual Rb/Cs atomic fountain

One important aspect of the work reported here is development of the dual Rb/Cs fountain configuration of FO2. The use of ^{87}Rb in atomic fountains originates from the prediction [13] that the cold collision shift for ^{87}Rb would be more than one order of magnitude smaller than the large shift measured in ^{133}Cs [14][15]. The initial work focused on testing this prediction in a preliminary implementation of a ^{87}Rb fountain. After thorough investigations of atom number dependent shifts both at Yale University [16] and at SYRTE [17][18] confirming the minute cold collision shift in ^{87}Rb, the implementation of the dual fountain configuration was undertaken. Most likely, the minute cold collision shift was also one of the motivations for the United States Naval Observatory (USNO) to choose ^{87}Rb for their atomic fountain ensemble [19][20] aimed at improving the stability of the USNO Master Clock used for GPS.

On the left, Fig. 2.2 shows a schematic view of the FO2 dual fountain. On the right, it shows the pictures of the two key systems enabling the dual fountain configuration, i.e. the 11 dichroic collimators and the dual Ramsey cavity.

In the FO2 fountain, ^{87}Rb and ^{133}Cs atoms are gathered at the same location, in overlapped optical molasses, loaded from two 2D magneto-optic

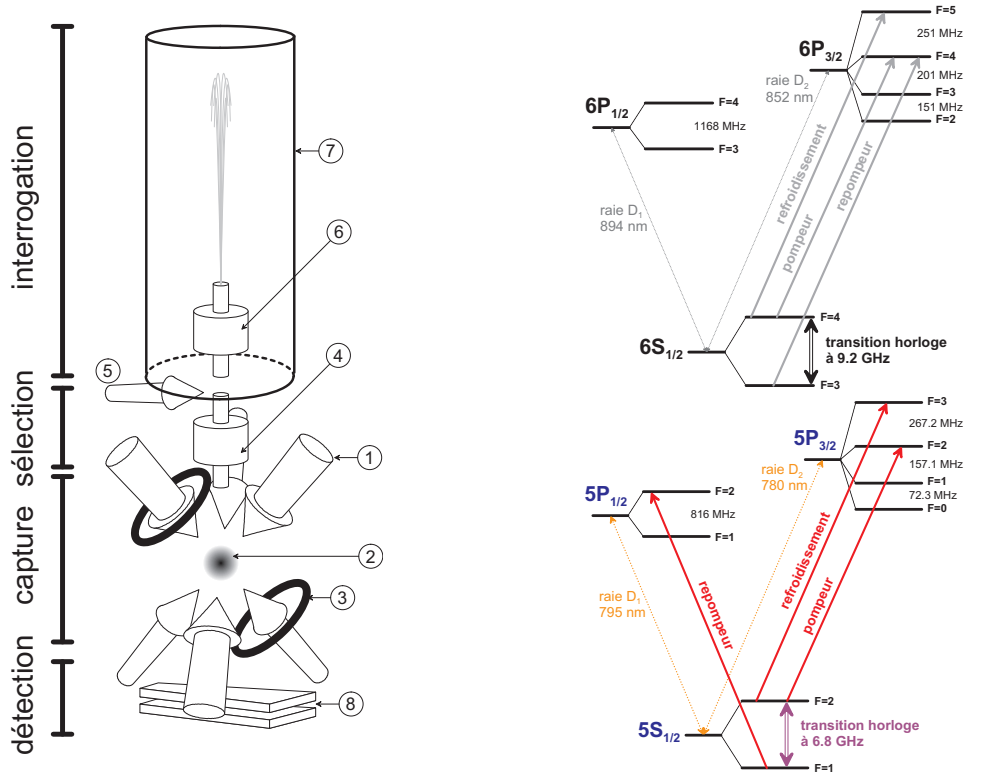

Figure 2.1: Level diagram of Cs and Rb atoms. Schematic view of an atomic fountain.

traps. This is made possible by dichroic collimators where the 780 nm and 852 nm laser lights, for ^{87}Rb and ^{133}Cs respectively, are brought by two polarizing optical fibers, superimposed with a dichroic beam splitter and collimated with an achromatic lens. These collimators have to match, for both wavelengths, stringent requirements needed for atomic fountains, i.e. alignment of laser beam axes with respect to a reference surface of the mechanical part to ~ 100 μrad, divergence of < 100 μrad and centering of the intensity profiles to 1 mm for a diameter of 26 mm. Designing, fabricating, tuning and characterizing these collimators turned out to be a demanding task which is described in [21].

Another feature of FO2 is the interrogation region shared by the two species. In order to keep the blackbody radiation shift under control, the temperature of the interrogation region must be homogenous to a high degree, typically to a few 10 mK. Consequently, the ^{87}Rb and ^{133}Cs Ramsey cavities cannot be independently tuned to their respectively atomic frequencies by their temperatures. Given this constraint, choice was made to make a single mechanical assembly comprising both cavities. The tuning of one cavity

Figure 2.2: Schematic view of the FO2 dual Rb/Cs fountain. Pictures of dichroic collimators and of Rb/Cs Ramsey cavity.

relative to the other, as required by the atomic frequencies is ensured by the precision to which mechanical parts are machined and assembled. In addition to this stringent dimensional requirement, the dual cavity has to match all other requirements for high accuracy, among which being completely non-magnetic, having no microwave leaks, having low and homogeneous wall resistive losses and having balanced coupling strengths for the 2 opposing microwave feeds. The implementation of the dual cavity assembly for FO2 was a challenging task which is described in [3] and [2].

Dichroic collimators and the dual Ramsey cavity enables truly simultaneous operation with ^{87}Rb and ^{133}Cs. To this end, fountain cycles of the ^{87}Rb and ^{133}Cs are made synchronous. ^{87}Rb and ^{133}Cs are first gathered simultaneously is the optical molasses. The 2 species are then launched with at slightly different times and with slightly different upwards velocities, such that the two atomic cloud move apart from each others during the ballistic flight, thereby avoiding interspecies interactions. Typically, parameters

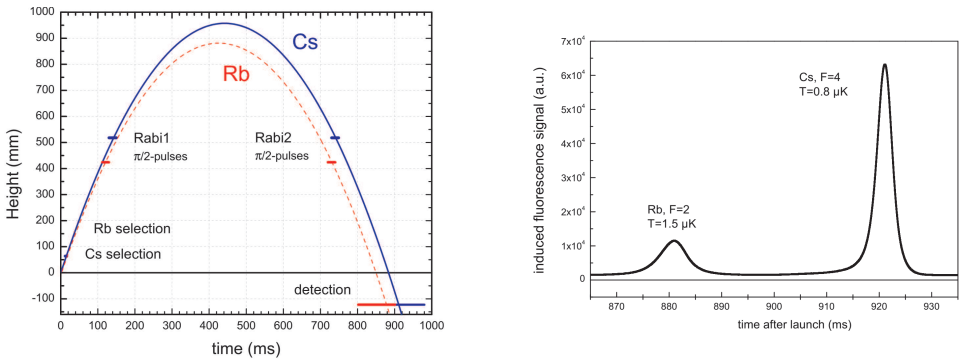

Figure 2.3: Left: trajectories of the ^{87}Rb and ^{133}Cs atomic clouds in FO2. Right: Experimental time of flight signals observed for simultaneous operation with the two species.

are chosen such that the ^{87}Rb and ^{133}Cs clouds cross their respective Ramsey cavity simultaneously, both on their way up and on their way down, as shown in Fig. 2.3. In such a typical configuration, the 2 clouds reach the detection region at different times, which provides the mean of detecting ^{87}Rb and ^{133}Cs separately with a fluorescence collection and photodiode system which does not distinguish 780 nm and 852 nm light. An example of time of flight signal is given in Fig. 2.3.

The first high-accuracy operation of FO2 in the dual Rb/Cs configuration is reported in [22]. The dual fountain configuration proved being a powerful setup for time and frequency metrology and its applications. Several examples are given in the present report. The FO2 dual fountain also offers several yet unexplored possibilities. For instance, the synchronization of the Rb and Cs part can be adjusted to overlap the two clouds during the interrogation in order to investigate Rb-Cs collisions. The dual configuration could also be used to extend the Lorentz local invariance tests performed with Cs [23].

2.1.3 Interrupted adiabatic passage to control atom number dependent frequency shifts

Frequency shift induced by cold collision are known to be large in ^{133}Cs since the early stages of atomic fountains [14][15]. One approach to mitigate this effect is to realize precise atomic density ratios which, in turn, enables precise extrapolation to zero atomic density of the clock frequency. This can be done using the state selection of the fountain cycle. Phases of state selection are shown in figure 2.4. Right after launch, all Zeeman sub-levels of the $F = 4$ hyperfine state are populated with approximatively equal populations. A

microwave excitation done in the state selection selectively drives the $|F = 4, m_F = 0\rangle \rightarrow |F = 3, m_F = 0\rangle$ transition. The selective excitation is enabled by a vertical magnetic field in the range of a few 100 nT to a few 10 μT, lifting the frequency degeneracy between all possible $F = 4 \rightarrow F = 3$ transitions. A laser beam, resonant with the $F = 4 \rightarrow F' = 5$, pushes away atoms remaining in the $F = 4$ level, leaving an almost pure $|F = 3, m_F = 0\rangle$ state for the interrogation.

The number of $|F = 3, m_F = 0\rangle$ can be varied by changing the characteristics of the microwave interaction. The most simple case is to drive a resonant Rabi oscillation. The duration and amplitude of the microwave pulse can be chosen to maximize the number of selected atoms, which corresponds to a Rabi flopping angle close to π for all atoms initially in $|F = 4, m_F = 0\rangle$. Instead, the amplitude can be lowered to induce a small Rabi flopping angle and select a smaller number of atoms. This simple method of varying the atom number does not produce precise atomic density ratio, because of the distribution of the microwave field inside the state selection cavity. Typically, the field amplitude can vary by 20% between the center and the edge of the region seen by the atoms. The spatial distribution of Rabi flopping angles and therefore of the transition probabilities vary when the atom number is changed. Consequently, atom density changes are not proportional to atom number changes, which prevents practical realization of accurate atom density ratios.

An alternative approach is to use adiabatic population transfer instead of Rabi flopping. To this end, the frequency detuning $\delta(t)$ and amplitude $\Omega_0(t)$ of the microwave field are modulated as shown in Fig. 2.4. In the Bloch vector picture, the effective magnetic field $\overrightarrow{\Omega}(t) = \delta(t)\overrightarrow{z} + \Omega_0(t)\overrightarrow{x}$ has the time evolution shown in Fig. 2.4. Within the adiabatic approximation, the Bloch vector representing the atomic state, which is initially aligned with $\overrightarrow{z}$, remains aligned with the effective magnetic field. As long as the adiabatic approximation is fulfilled for all atoms, one can see that the final transition probability is 1 after a complete adiabatic transfer. Similarly, when the adiabatic transfer is abruptly interrupted when the detuning is zero, the final transition probability is 1/2 independently of small changes of the field amplitude. In these two cases, the distribution of transition probability across the atomic cloud is precisely equal to 1 and 1/2, respectively. This can be used to realize two atomic samples for which both the atom number and the atomic density ratio are precisely equal to 1/2. Practically, this is done by interleaving measurements at full density and at half density, with typical durations of 50 to 100 fountain cycles for each of the two cases.

A first implementation of this scheme is reported in [24]. Ultimately, this

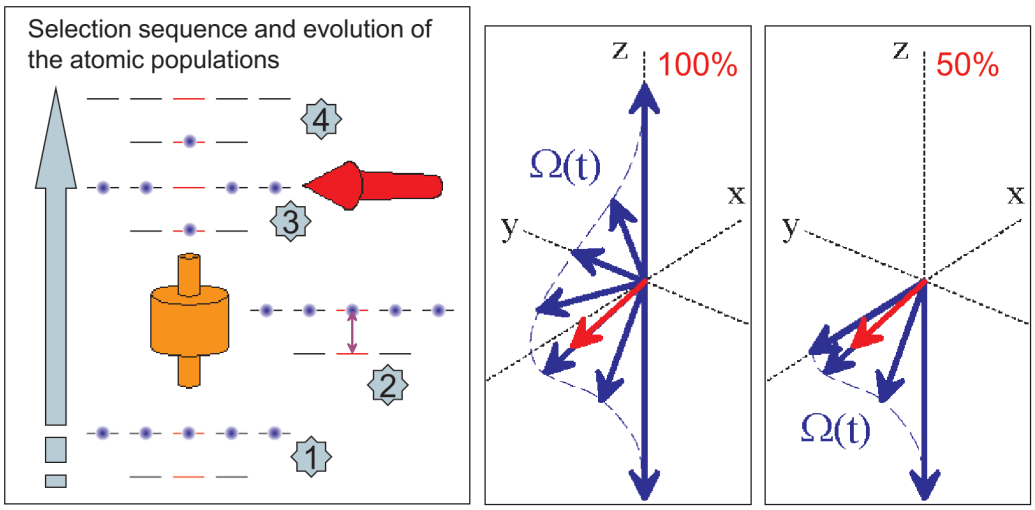

Figure 2.4: State selection in atomic fountains and interrupted adiabatic passage method.

method is limited by the degree to which the transfer remains adiabatic, given the number of constraints related to the fountain configuration. The available time for implementing the state selection is primarily limited to a few ms, due to the upward motion of the atomic cloud (at ~ 4 m.s^{-1}) and the size of the state selection cavity, taking into account that the interaction of the entire atomic cloud must be limited to central part of the state selection cavity where the amplitude is the highest and has less variations. Another limitation comes the neighboring transitions which must not be excited by the state selection interaction. Practically, for a proper implementation of the interrupted adiabatic passage method, an additional static vertical magnetic field of ~ 18 μT is pulsed to push the closest strongly coupled $|F = 4, m_F = \pm 1\rangle \rightarrow |F = 3, m_F = \pm 1\rangle$ transitions ± 126 kHz away from $|F = 4, m_F = 0\rangle \rightarrow |F = 3, m_F = 0\rangle$, and the marginally coupled $|F = 4, m_F = 0\rangle \rightarrow |F = 3, m_F = \pm 1\rangle$ transitions ± 63 kHz away. The strength of this magnetic field pulse is limited by the amount of perturbation that can be afforded inside the magnetic shields of the fountain. If too strong, this magnetic field pulse can perturb the control of the quantization axis after the state selection and cause permanent or transient perturbations inside the interrogation region, which is detrimental to the accuracy. The accurate implementation of the interrupted adiabatic passage also relies upon the degree to which the resonant condition is met when the interaction is switched off. Initially [24], a voltage controlled oscillator was used for the frequency sweep $\delta(t)$, the accuracy of which was

limiting the accuracy of the interrupted adiabatic passage to several 10^{-3}. Later, an arbitrary waveform generator was used. This enables adiabatic transfer accuracy of $< 10^{-4}$. At this level, the second order Zeeman shift from the biasing magnetic field must be taken into account to properly meet the resonant condition $\delta(t) = 0$ at interruption.

The realization of accurate density ratios is, in practice limited by the spurious residual atomic populations in the lower hyperfine states $|F = 3, m_F \neq 0\rangle$. These spurious populations come by two different channels. One channel is from atoms which are left in the $F = 3$ states after launch. In FO2-Cs, we found that the fraction of launched atoms in $F = 3$ states is about 10^{-4}, which gives a fraction of about 10^{-3} of the atomic sample after the state selection. A second channel is from atoms which are pumped from $F = 4$ to $F = 3$ by the push beam. The amount of such atoms increases when the push beam power is increased. It is therefore desirable to minimize the amount of push beam light yet preserving the effectiveness of the push beam. In FO2-Cs, we found that in optimal condition, atoms pumped by the push beam in $F = 3$ could represent a few 10^{-3} of the atomic sample after state selection. The presence of these spurious $|F = 3, m_F \neq 0\rangle$ atoms led us to study their effect in detail and to the observation of low ultra-low magnetic field Feshbach resonance related to these states (see 2.1.4).

Other approaches exist to control atom number dependent frequency shifts. Reference [25] proposes using a detuned state selection Rabi pulses at microwave amplitude which maximizes the transition probability. At zero detuning, this is identical to the usual π pulses which transfers all atoms from $|F = 4, m_F = 0\rangle$ to $|F = 3, m_F = 0\rangle$. For a detuned pulse, the transferred fraction is less than 1, providing the mean to vary the number of atoms in $|F = 3, m_F = 0\rangle$. Because the microwave amplitude is at an extremum, the transfer efficiency is highly homogeneous over the atomic sample, despite the spatial variation of the microwave field amplitude. Like the (interrupted-)adiabatic passage, this provides the mean to realize accurate atomic density ratios [25]. Since 2014, this method is used in FO2-Rb. It is also planned to use it in the cold atom space clock PHARAO. Another approach to mitigate the large collision shift of ^{133}Cs is described in [26][27]. The method is based on reducing the effective collision temperature to reach conditions where the contribution of the two clock states to the collision shift have opposing signs and similar values. In such conditions, the collision shift becomes smaller and it can further tuned to zero by adjusting the ratio of the two states using $< \pi/2$ Ramsey pulses. In practice, the effective collision temperature is reduced by reducing the initial atomic cloud size, using a tight magneto-optic trap.

2.1.4 Feshbach resonance at ultra-low magnetic fields in Cs

As explained in the above subsection, the presence of spurious atomic populations in $|F = 3, m_F \neq 0\rangle$ led us to study clock shifts due to these states. This work is reported in [28]. For the purpose of this study, an additional microwave field enables state selection of both usual clock level $|F = 3, m_F = 0\rangle$ and any chosen $|F = 3, m_F\rangle$. These two simultaneous excitations are done using adiabatic passage such that the space and velocity distributions of the two selected states are as similar as possible. Fig. 2.5 shows atomic populations after launch, the dual microwave excitation used for the state selection, atomic populations after state selection and the Ramsey interrogation, in the presence of $|F = 3, m_F\rangle$ population. To minimize the impact of uncertainties and fluctuations of the effective atomic density, a interleaved sequence of 3 configurations is used. The two first configurations correspond to the normal clock configurations with full and half densities of $|F = 3, m_F = 0\rangle$, the third configuration corresponds to the full density of both $|F = 3, m_F\rangle$ and the chosen $|F = 3, m_F\rangle$. As explained in [28], mean frequencies $\nu_0^{(1)}$, $\nu_0^{(1/2)}$ and $\nu_{0;m_f}^{(1)}$ and mean detected atom number N_0, $N_0/2$ and $N_0 + N_{m_f}$ in these three configurations can be used to compute the ratio:

$$R_{m_f;0}(B) = \frac{\nu_{0;m_f}^{(1)} - \nu_0^{(1)}}{(N_0 + N_{m_f}) - N_0} \times \frac{N_0 - N_0/2}{\nu_0^{(1)} - \nu_0^{(1/2)}}. \tag{2.1}$$

This quantity is independent of the detected atom numbers and is as close to intrinsic collisional properties as possible in our experiment. It represents, at a given magnetic field B, the ratio between clock shifts per effective density of the clock states and of $|F = 3, m_F\rangle$. $R_{m_f;0}(B)$ was measured for each of the $|F = 3, m_F \neq 0\rangle$ states and for magnetic fields ranging from 0 to 10 μT (100 mG). Here, we remind that the typical bias field in atomic fountains is < 200 nT. Over the explored range of magnetic field, we observe no change of the usual clock shift with B. Instead, as shown in Fig. 2.6, large variations of $R_{m_f;0}(B)$ are observed due to interactions of the additional $|F = 3, m_F\rangle$ with the clock states $|F = 3, m_F = 0\rangle$ and $|F = 4, m_F = 0\rangle$. These variations are due to molecular Feshbach resonances [29]. $R_{m_f;0}(B)$ span almost the entire range from -1 to $+1$ which means that the shift due to $|F = 3, m_F\rangle$ can be as large as the usual clock shift. In the experiment, this amounts to fractional shifts in the range $\pm 10^{-13}$ for effective densities of $\sim 2 \times 10^7$ cm^{-3} and detected atom numbers of $N_{m_f} \sim 2 \times 10^6$.

Experiment data of Fig. 2.6 exhibit narrow features, i.e. large change of the shift for changes of a few 100 nT only, and high signal-to-noise ratio,

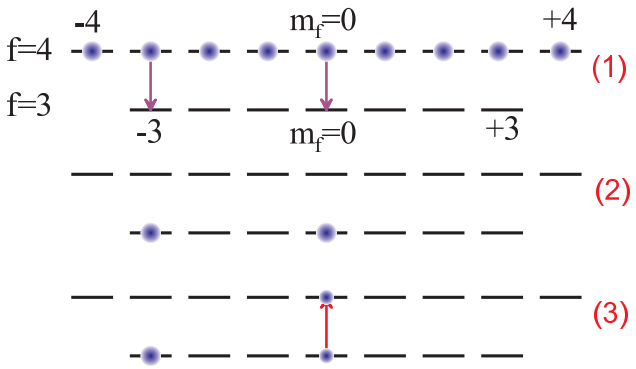

Figure 2.5: State selection for the measurement of the clock shift due to $|F = 3, m_F \neq 0\rangle$ states. (1) Populations after launch and transitions excite for the state selection. (2) Populations at the end of the state selection process, i.e. after a push laser beam removed $F = 4$ states. (3) Populations during the Ramsey interrogation.

which enables stringent comparisons with theory. One of goal is to explain the striking asymmetric shape of resonances. Another goal is to reproduce the resonant magnetic field values. To this end, a model of clock shift in the fountain configuration was developed. This model is based on a Monte-Carlo computation of the clock shift averaged over ballistic flight of the atomic cloud and the Ramsey interrogation, taking into account of space and velocity distributions and truncation of the atomic cloud by the microwave cavity. One output of this computation is to give the effective collision temperature, ~ 900 nK. The calculation computes in average shift from elementary pairwise collision shifts modelling a single Feshbach resonance. More details about this model can be found in [28]. This computation highlighted that, indeed, asymmetric line shapes are expected when the collision kinetic energy dominates over the strength of the coupling between the molecular bound state causing the resonance and the continuum states. Also, in the case of such asymmetric line shapes, the computation shows where to find the resonant field, namely at the extremum of the sharp feature. Fig. 2.7 shows results of this computation. The first graph shows shapes of the resonance for different coupling strengths. The second graph shows a fit of the model to the $m_F = 3$ resonance. A second part of the theoretical work is to predict positions of resonances from the molecular Hamiltonian. In a first attempt done at the time of the experiment (2003), theory predicted resonances at low magnetic field, in the vicinity of the experimental window $B = 0$ to $B = 10\ \mu T$. However, this theoretical prediction was far from agreement with experiment within the experimental resolution. Later (2012), knowl-

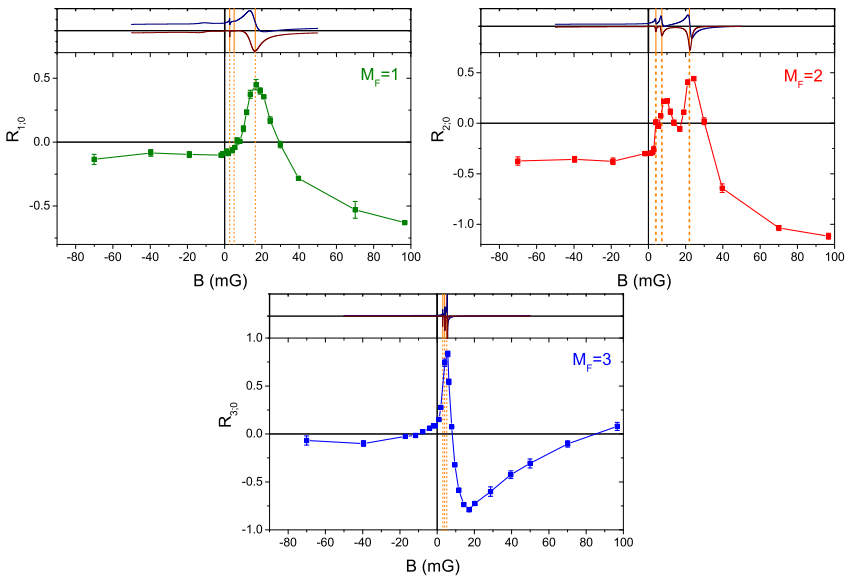

Figure 2.6: Measured collision frequency shift ratio $R_{m_f;0}(B)$, exhibiting Feshbach resonances at ultra-low magnetic for $m_F = 3$, $m_F = 2$ and $m_F = 1$. The effective temperature is 900 nK. Vertical lines show theoretical resonant field values (for a vanishing collision energy E).

edge of molecular properties and their modelling had made great progress. A new calculation was made showing excellent agreement with experiment. In Fig. 2.6, graphs on top of each experimental curves display the real and imaginary part of the scattering length from theory. Vertical bars show the position of resonances predicted by theory. A continuation of this work would be to combine the two approaches, i.e. use the theoretically calculated scattering lengths as function of the magnetic field in the Monte-Carlo computation of the fountain geometry. This would potentially enable more accurate determination of the resonant field.

For the uncertainty of collision shift in a Cs atomic fountains, measurements in Fig. 2.6 provides inputs to deal with shifts from spurious atoms left in $|F = 3, m_F \neq 0\rangle$ states after state selection. The two mechanisms leading to these spurious atomic populations were described in 2.1.3. Generally, they give a velocity distribution which differs from the velocity distribution of purposely selected atoms, whether in $|F = 3, m_F = 0\rangle$ (as for normal clock configuration) or in $|F = 3, m_F\rangle$ (as for the above experiment). In principle, this, together with the exact distribution of spurious atoms among the $|F = 3, m_F \neq 0\rangle$ states, should be taken into account to model the shift. In practice, the above measurements show that at the nominal magnetic field

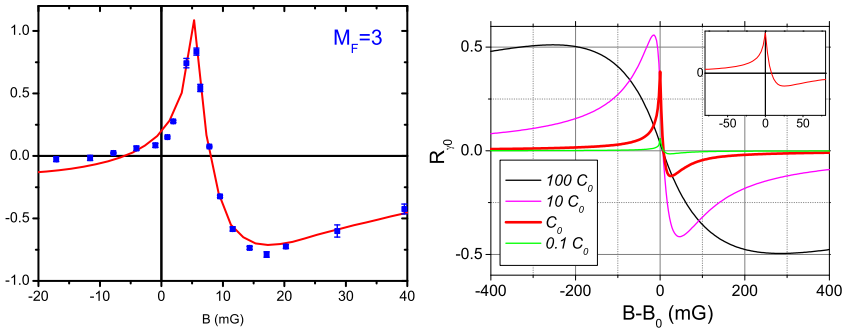

Figure 2.7: Model of collision shift around a Feshbach resonance in atomic fountains. The first graph shows a series of cases where the coupling strength between the resonant molecular state and the continuum C_0 is changed while all other parameters are the same. The second graph shows a fit of this model to the experimental $m_F = 3$ resonance.

(200 nT in FO2), the $R_{m_f;0}(B)$ collision shift ratio does not exceed 0.3 and has both positive and negative values depending on m_F. Also, $|F = 3, m_F \neq 0\rangle$ spurious populations are approximately equally distributed. With the above factors taken into account, the uncertainty due to collisions with spurious populations in $|F = 3, m_F\rangle$ states can be taken as the collision shift times the fraction of spurious atoms, which typically amount to 3×10^{-3}. This term typically amount to 10^{-16} in FO2-Cs.

In [30][31][32], these resonances and resonances connected to the $F = 4$ level are studied also in a fountain geometry. In this work, two clouds of $|F, m_F = 0\rangle$ and $|F, m_F \neq 0\rangle$ atoms are made to collide with each other. The scattered part of the wavefunction is isolated in the time of flight signal, which enable determining the phase difference between the scattered part and the unscattered part directly. Measuring the change of this phase difference versus magnetic field and collision velocity yields accurate determination of atomic scattering properties, independent of an accurate determination of atomic densities.

2.1.5 Distributed cavity phase shift

Atomic fountains are impacted by the first order Doppler effect. The scale of the fractional shift is v/c where v is the atomic velocity and c the speed of light. In atomic fountains, for a typical velocity of 3 m.s^{-1}, the scale of the fractional shift is extremely large: 10^{-8}. The shift is however largely suppressed by the reversal of the atomic trajectories due to gravity and by the high purity of the standing wave field in the interrogation microwave cavity. Despite the significant impact of this effect on the uncertainty budget of microwave clocks, there was for long a lack of precise quantitative comparisons between experiments and models of this effect. Below, we describe the work done to tackle this issue.

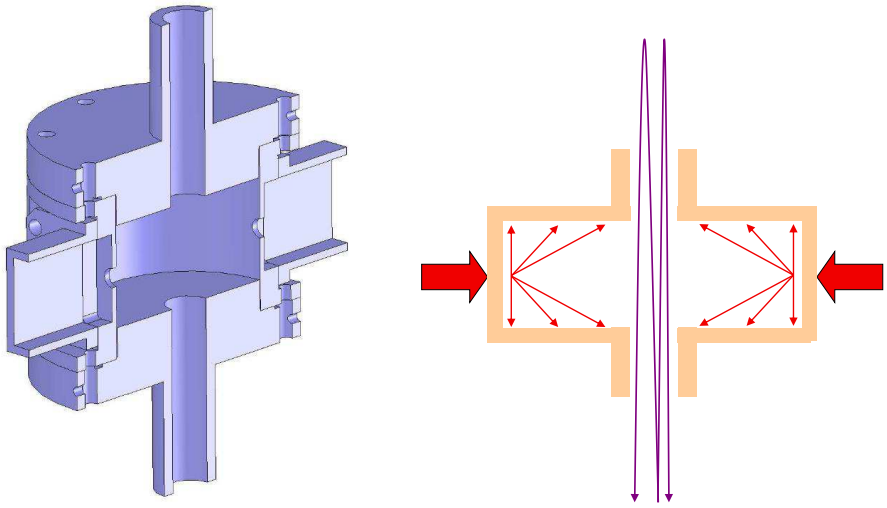

Figure 2.8: Schematic of the microwave cavity used in FO2-Cs atomic fountain.

Figure 2.8 a shows a schematic view of the interrogation cavity used in FO2-Cs. The cavity is designed and tuned to have its TE_{011} mode resonating at the Cs hyperfine frequency of 9.2 GHz. It is made of high purity oxygen-free high thermal conductivity copper. The microwave is fed by two irises located on the cavity midplane. The cavity is over coupled with a quality factor of $Q = 7000$. The unloaded quality factor, determined only by losses in copper walls of finite conductivity is $Q_0 \sim 27500$. As displayed on Fig. 2.8 b, power is fed into the cavity at the two feeds. This power is flowing towards the cavity walls where it is dissipated. This power flow corresponds to spatial variations of the phase of the microwave field, which therefore departs from a pure standing wave field. The phase distribution is unevenly sampled by the

atomic cloud, which leads to a residual first order Doppler shift, also called distributed cavity phase shift.

To highlight the significance of this shift and its dependence on many factors, Fig. 2.9 shows measurements of the fraction clock frequency difference between configurations where the cavity is fed from either of the two cavity feeds, as a function of the tilt of the fountain along cavity feeds and for several microwave amplitudes $\pi/2$, $3\pi/2$, $5\pi/2$, and $7\pi/2$. The dependence with tilt changes sign with the microwave amplitude and it almost reaches 5 parts in 10^{14}.

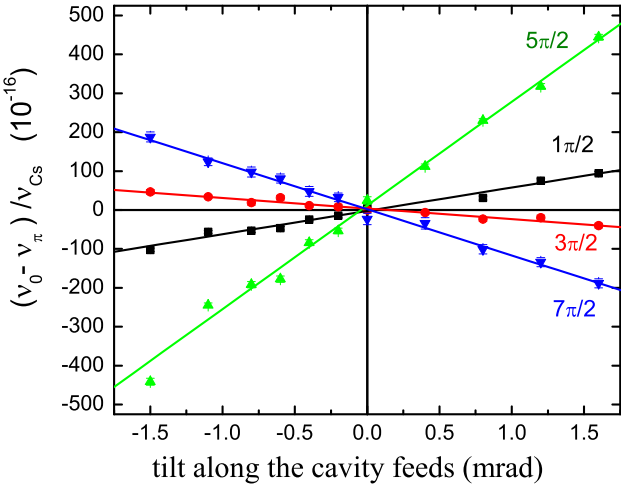

Figure 2.9: Distributed cavity phase shift for asymmetric feeds as a function of tilt along the cavity feeds.

After our first measurement of the tilt dependence [33], we engaged into a thorough investigation of the distributed cavity phase shift which eventually gave, with no free parameter, the first stringent test and quantitative confirmation of the key behavior of this shift. This work is described in [34]. Here, we highlight the main aspects and main conclusions.

Computing the phase distribution inside the cavity is a challenging task. Notably, the field has large variations over the scale of the skin near depth (0.7 μm) at the edge of the holes letting atoms through. This precludes 3D finite element calculations. Instead, with the azimuthal symmetry of the cavity, the difficult 3D problem can be decomposed into a series of 2D problems [35]. Furthermore, the atomic cloud interact with the cavity field only near its axis of symmetry, such that only the three lowest order terms of the azimuthal decomposition contribute significantly of the shift. In this approach, the magnetic field $\mathbf{H}(\mathbf{r})$ inside the cavity assumed to be tuned at

its resonance is written as follows.

$$\begin{aligned} \mathbf{H}(\mathbf{r}) &= \mathbf{H}_0(\mathbf{r}) + i\mathbf{g}(\mathbf{r}) \\ \mathbf{g}(\mathbf{r}) &= \sum_m \mathbf{g}_m(\rho, z)\cos(m\phi) \end{aligned} \tag{2.2}$$

$\mathbf{H}_0(\mathbf{r})$ is the unperturbed field, corresponding to perfectly conduction walls and no feed. $\mathbf{g}(\mathbf{r})$ is the perturbation of the field introduced by walls with finite conductivity and by feeds. For convenience, we may separate even and odd terms: $\mathbf{g}(\mathbf{r}) = \mathbf{g}_{\text{even}}(\mathbf{r}) + \mathbf{g}_{\text{odd}}(\mathbf{r})$. We have $\mathbf{g}_m(\rho, z) \propto \rho^m$. And because the atom trajectory are restricted to small values of ρ, $m = 0, 1\&2$ terms are enough to describe the distributed cavity shift in atomic fountain.

Another key aspect is the geometry of cloud expansion in the fountain. The initial atomic cloud space and velocity distribution are experimentally known with CCD camera to image to initial cloud and with the time of flight signals used to measure the transition probability. Additional information about the initial cloud center is also needed, which is also done with the camera looking upwards through the fountain and using neighbouring structures of the vacuum systems as references for the mechanical center of the fountain. Our investigation of the distributed cavity phase shift also highlighted the importance of the inhomogeneous spatial response of the detection. An atom falling off the center of the detection sees less detection light and emits its fluorescence light away from the optical axis of the light collection system leading to a smaller contribution to the signal than an atom at the center. This effect impacts the effective atomic distribution which interacts with interrogation cavity and finally, the distributed cavity phase shift. In order to quantify this effect, and more generally, to constrain the fountain geometry used to compute the distributed cavity phase shift, we measured the Rabi oscillation as a function of the microwave power injected into the cavity for three different cases [36]. The first case is the nominal Ramsey configuration (interaction on upwards and downwards passages), the second case is an interaction only on the way up (obtained by switching the microwave off during the downwards passage) and the third case is an interaction only on the way down. The result of this measurement is shown by data points in Fig. 2.10. On the same plot, lines show the result of model. The excellent agreement is achieved with only minor tuning of the initial cloud position and of the detection response curvature in one direction. All other inputs to the model are measured values. This Rabi oscillation test provides a independent constraint to the fountain geometry which is crucial to the validation of the distributed cavity phase shift model.

Measurements of clock frequency difference for the Ramsey cavity feed from either side, like these already shown in Fig 2.9, are directly related to

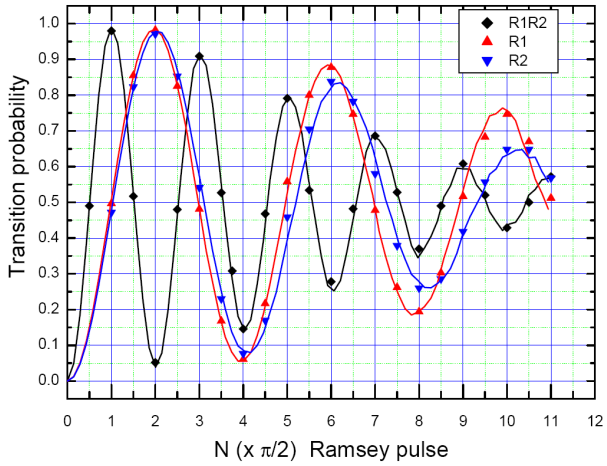

Figure 2.10: Rabi oscillation as a function of the microwave power injected into the cavity for three different cases. The first case is the nominal Ramsey configuration (R1R2, interaction on upwards and downwards passages), the second case is an interaction only on the way up (R1, obtained by switching the microwave off during the downwards passage) and the third case is an interaction only on on the way down (R2).

the odd part of the field perturbation $\mathbf{g}_{\text{odd}}(\mathbf{r})$ which, for its impact on the fountain can be reduced to the $m = 1$ term: $\mathbf{g}_1(\rho, z)$. Figure 2.11b shows the comparison between model and experiment for this term. Measurements are made at a tilt of 1.6 mrad for several microwave amplitudes of the field. The clock frequency shift is translated into a perturbation of the transition probability δP via the slope of the Ramsey fringe at the operation point, $dP/d\nu$ to give the plotted curve [34]. The magnitude of this odd term is inversely proportional to the loaded quality factor Q. With no free parameter, agreement in found between theory and model. Additional features of $\mathbf{g}_{\text{odd}}(\mathbf{r})$ were further tested, such as the dependence on the feed relative phase and on cavity detuning. Understanding $\mathbf{g}_{\text{odd}}(\mathbf{r})$ also led us to revisit and improved our feed balancing methods in order to optimize zeroing of odd terms for the nominal clock operation [34].

Effectively zeroing odd terms also opens the possibility to measure the much smaller effects of even terms. The result of this measurement is shown in Figure 2.11a. Here, the clock frequency is measured against other clock, for a null tilt and as a function of the microwave amplitude. Again, the perturbation of the transition probability δP is used on the plot. Measurements are compared to the model for the $m = 0$ term which is enough given the measurement uncertainties. This data set corresponds to a series of frequency

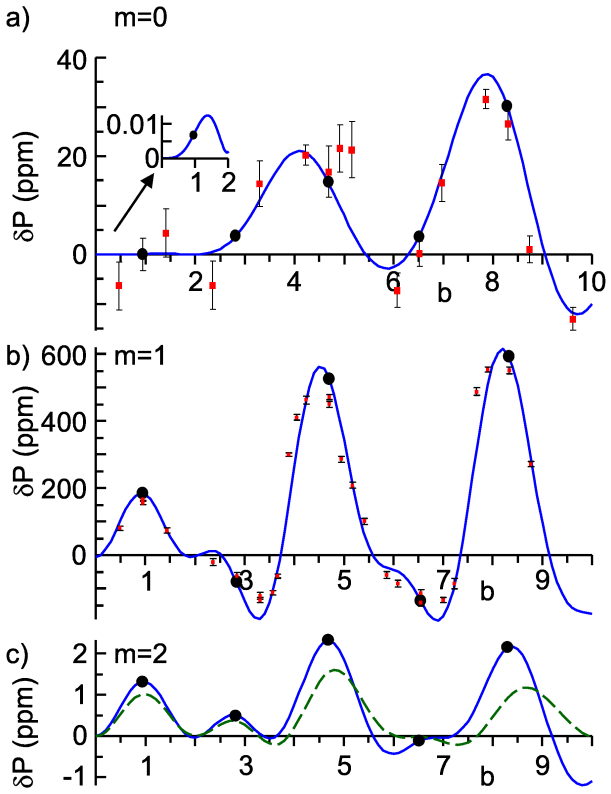

Figure 2.11: Distributed cavity phase shift $m = 0$, $m = 1$ and $m = 2$ terms. Comparison between model and experiments.

measurements with uncertainties a few 10^{-16} only, with configurations far from optimal clock parameters. All systematic shifts must be control at the best possible level. For instance, the collision shift needs to be measured and taken into account for each point, etc. Again, with no free parameter agreement is found between model and experiment. We note that in our cavity, the model predicts an extremely small $m = 0$ shift (4×10^{-19}) is the nominal clock condition.

Finally, while being unresolved in the $m = 0$ experiment, the $m = 2$ term still produces a shift that must be taken into account in accuracy budget of the most accurate clocks. The $m = 2$ term, computed based on our validated model, is shown in Fig. 2.11c. The estimated correction for this term is $(-7.5 \pm 5.5) \times 10^{-17}$. Physically, this term arises from the quadrupolar component of the phase distribution that is present in a two feed cavity. It gives a non vanishing shift when the fountain geometry also has a quadrupolar component that can be due, for instance, to an off-centered initial cloud

position or from quadrupolar inhomogeneity of the detection response.

Overall, for FO2-Cs, the correction and uncertainty for the distributed cavity phase shift is $(-0.9 \pm 0.9) \times 10^{-16}$. This study established a protocol for a complete evaluation of uncertainty for the distributed cavity phase shift [34], which was then applied to other fountains at SYRTE [37] and also in other institutes [38][39]. In addition to experimentally validating the approach and the model of [35][40] for the cavity phase distribution, this study contributed deeper understanding of the shift for designing better cavity geometries [40][41].

2.1.6 Improving stability

As we shall see in Chapter 4, accuracy of atomic fountains are in the low 10^{-16}. Studying systematic shifts at this level require the capability to measure with such resolution within a reasonable amount of time. 10^{-16} statistical uncertainty is typically reached within one day, and the full study of a particular systematic effect one to several months of actual measurement time. Consequently much effort was devoted to getting and maintaining the best possible short term stability. The short term fractional frequency instability of the fountain can be expressed as follows.

$$\sigma_y(\tau) = \frac{1}{\pi Q_{at}} \times \left(\frac{2\sigma^2_{\delta N_{det}}}{N^2_{det}} + \frac{1}{N_{det}} + \frac{1}{N_{det} n_{ph}} + \gamma^2_{det} + \gamma^2_{IO} \right)^{1/2} \times \sqrt{\frac{T_C}{\tau}} \quad (2.3)$$

Here, we have assumed that Ramsey fringes are perfectly contrasted, which is almost the case in atomic fountains, as can be seen in Fig. 2.10, where the transition probability at resonance is 0.985 for $\pi/2$ pulses. Q_{at} is the atomic quality factor, nominally $Q_{at} = 1.1 \times 10^{10}$ in FO2-Cs. T_C is the fountain cycle time. τ is the measurement time. N_{det} is the detected atom number. The first term represents the detection noise noise level expressed in terms of its equivalent cycle-to-cycle atom number fluctuation per channel $\sigma_{\delta N_{det}}$. In FO2-Cs, this noise is determined by the detection photodiode electronic noise and it amounts to ~ 450. The second term represents the atomic quantum projection noise. The third term represents the photon shot noise. It is negligible given a typical number of detected photons per atom $n_{ph} \sim 320$. The fourth term γ_{det} represents the transition probability measurement noise floor. The fifth and last term γ_{IO} corresponds to the limit introduced by the aliasing of the interrogation oscillator known as the Dick effect [42][43][44].

Initially, the stability of atomic fountain was limited by the interrogation oscillator noise γ_{IO} coming from quartz oscillators used at start of the microwave synthesis. It was then shown that the quantum projection noise

limit could be reached when using cryogenic sapphire oscillator [45], yielding stabilities of 4×10^{-14} at 1 s. Further work was then devoted to develop microwave synthesis schemes with lower γ_{IO} and to implement a fully operational ultra-low noise reference signal based on a continuously operated cryogenic oscillator. This work will be mentioned in Chapter 3. Figure 2.12 shows the best short term stability observed as the result of this work. Black points correspond to a detected atom number $N_{det} \simeq 5 \times 10^6$, for which the short term stability is 1.6×10^{-14} at 1 s. Red points correspond to a detected atom number divided by two. The ratio of stabilities at N_{det} and

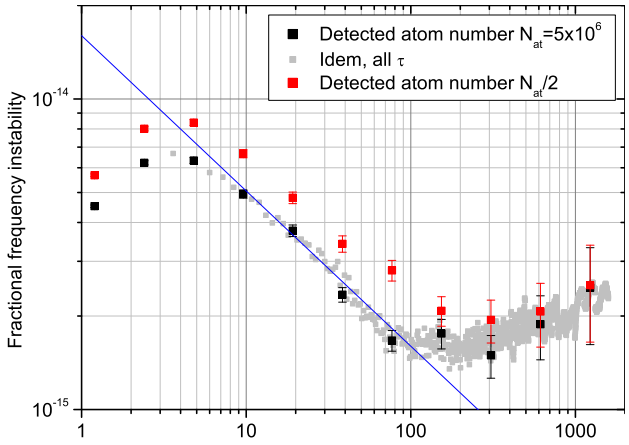

Figure 2.12: Short term stability obtained with FO2-Cs.

$N_{det}/2$ is close to $\sqrt{2}$, which indicates (once other factors are independently determined) that the main limitation is the quantum projection noise. One can further estimate the contribution of $\gamma_{det}^2 + \gamma_{IO}^2$. This term amounts to $\sim 9 \times 10^{-15}$ at 1 s, while the quantum projection noise alone corresponds to $\sim 1.3 \times 10^{-14}$ at 1 s for N_{det}. From the independent characterization of the latest microwave synthesizers [46], one can determine that γ_{IO} gives a limit in the low 10^{-15} at 1 s range. This leads to the conclusion that γ_{det} is significant at this level. It is therefore interesting to think about the possible phenomenon causing this limit. A contribution comes from the detection laser frequency and intensity noise. Because of a time delay of ~ 4 ms between the detection of the two hyperfine states, laser noises cause the two states to be detected with different and fluctuating efficiencies leading to an atom number independent floor in the measurement of transition probability. Estimation of this contribution is a few 10^{-15} at 1 s or less, too small to explain alone the observed limit [2]. A second contribution comes from what could be named atomic cross-talk, more precisely, fluctuations of atomic

cross-talk. In FO2-Cs, the $F = 4$ atomic state is detected in the upper detection beam. Atoms in this state are then pushed away. The $F = 3$ atomic state is detected in the lower detection beam. In practice, $F = 4$ atoms are not pushed perfectly and a small fraction, typically 10^{-2}, of them reach the lower detection. Fluctuations of this unpushed fraction give fluctuations of the transition probability which does not depend on N_{det}. Such fluctuations can be induced by fluctuations of the detection laser or fluctuations of the magnetic field affecting marginal trajectories of unpushed atoms. Fluctuations of a few percent of the fraction are enough to cause fluctuations of 10^{-4} of the measured transition probability, and a stability limit of $\sim 9 \times 10^{-15}$ at 1 s. A third contribution may come from spurious atoms which were depumped into $F = 3$ by the state selection push beam, as already mentioned in Sec. 2.1.3. Fluctuations of the depumped fraction can also give a limit to the stability which does not depend on N_{det}.

2.2 Mercury optical lattice clock

2.2.1 Motivations

Since 2000 and the demonstration of optical frequency combs [47][48], optical frequency metrology and optical clocks are developing at a high pace. In 2001, the idea of trapping atoms in a non-perturbing lattice dipole trap for making an optical clock [49, 50] initiated the development of optical lattice clocks, first with Sr [51] and Yb [52]. From the beginning, it was already known that the largest frequency shift in Sr and Yb lattice clocks is the blackbody radiation shift. The shift caused by the thermal electromagnetic background is $\sim -5.3 \times 10^{-15}$ in Sr and -2.4×10^{-15} in Yb at 300 K. Like Sr and Yb, Hg has an alkaline-earth-like electronic structure where the intercombination transition $^1S_0 - ^3P_0$ is well-suited for the optical lattice clock scheme. One interesting feature of Hg is its smaller blackbody radiation shift of -1.6×10^{-16} [53][54], about 30 times smaller than Sr and 15 less than Yb. The same ratios apply to the sensitivity to stray static electric field [55]. Hg has 7 isotopes, 2 fermionic and 5 bosonic. 6 of them have a natural abundance greater than 6%. Only the ^{196}Hg bosonic isotope has a small abundance of 0.15%. The ^{199}Hg fermionic isotope has a nuclear spin 1/2 for which the $^1S_0 - ^3P_0$ clock transition has no tensor light shift and therefore a simplified dependence to shifts induced by the lattice trap. Hg has a comparatively high vapor pressure at room temperature, which removes the need of using a high temperature oven and makes it possible to implement a 2 dimensional magneto-optical trap has high flux source of

precooled atoms. For applications to fundamental physics tests (see below Chap. 5), Hg has a fairly high sensitivity to a variation of the fine-structure constant α: $\delta\nu/\nu = 0.81 \times \delta\alpha/\alpha$ [56]. At the start of the experiment, Hg had never been laser-cooled. Its properties were therefore unexplored in the cold and ultra-cold regime.

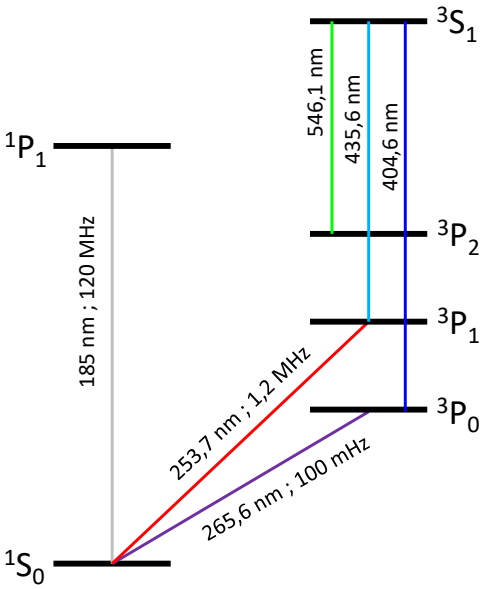

Figure 2.13: Low energy levels of Hg.

The main challenge of Hg lies in the need for deep UV laser sources. Figure 2.13 shows the lowest energy levels of Hg. The $^1S_0 - ^3P_0$ clock transition is at 265.6 nm. The transition used for laser cooling and detecting is the $^1S_0 - ^3P_1$ at 254 nm. The wavelength at which the dipole lattice trap does not shift the clock transition, the so-called magic wavelength, is at 362.6 nm. In the following, we describe the main steps taken toward the demonstration of a highly accurate optical lattice clock using Hg.

Note that a synthetic account of this work in French can be found in [57].

2.2.2 Laser-cooling of Hg

Figure 2.14 shows key elements of the ultrahigh vacuum chamber specifically developed for laser cooling of Hg. The vacuum chamber comprises a magneto-optic trap and a 2 dimensional magneto-optic trap, separated by a low conductance section. The magneto-optic trap side is pumped by a getter pump and an ion pump, down to a few 10^{-7} Pa. The 2 dimensional magneto-optic trap side is pumped by a second getter pump. Hg vapor source made

of 1 to 2 grams of Hg kept at -40^oC to -60^oC maintains a pressure of Hg of 10^{-5} to 10^{-4} Pa. Windows are made of UV grade fused silica with dielectric anti-reflection coatings for the 254 nm cooling light. They are glued to vacuum chamber parts made of titanium, whose one advantage is to have a low expansion coefficient, better suited than other materials to the expansion coefficient of fused silica. This configuration seems to be quite durable, especially with respect to exposure to Hg vapor. The same vacuum system has been in use for more than 10 years without showing sign of degradation. More details on the vacuum system can be found in [58].

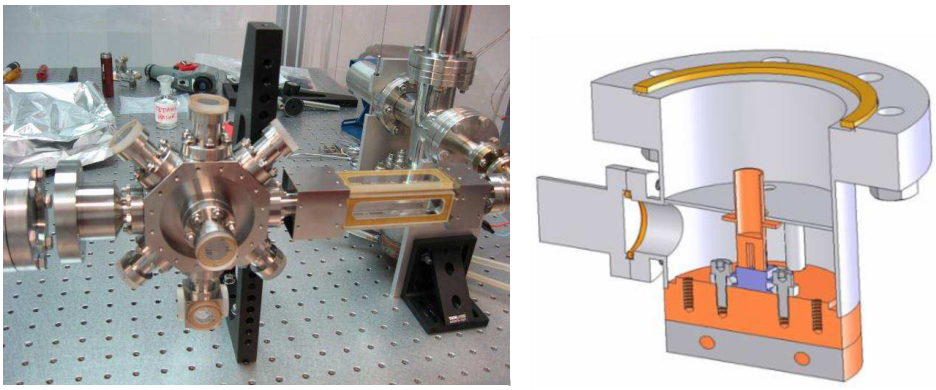

Figure 2.14: Ultrahigh vacuum chamber for the Hg optical lattice clock. On the left, a picture of the vacuum system at an early stage of assembly. One can see the magneto-optical trap area (octagonal shape) and the 2 dimensional magneto-optical trap (2D-MOT) area with rectangular shaped windows. On the right, a 3D schematic of the Hg source which is connected to the 2D-MOT, at the picture. 1 to 2 grams of Hg are held in a copper receptacle which cooled down to -40^oC to -60^oC with in-vacuum Peltier thermoelectric cooler.

Another key element for laser cooling of Hg is the laser source to address the $^1S_0 - ^3P_1$ transition at 254 nm. The natural linewidth of this transition is $\Gamma/2\pi = 1.2$ MHz and the saturation intensity 101 μW.mm^{-2}. The requirement for the source is to be continuous, single frequency, frequency stabilized and yet dynamically tunable, with a linewidth much lower than the natural linewidth of the transition and with a power of about 100 mW. A schematic of the source developed to meet these demanding requirements is shown in Fig. 2.15. The source is based on a 1015 nm thin disk laser whose output is frequency doubled two times by cavity enhanced second harmonic generation. A fraction of the 254 nm light is frequency shifted by two acousto-optic modulators and used to lock the thin disk laser frequency to the saturated

absorption spectrum of the ${}^1S_0 - {}^3P_1$ transition obtained in a room temperature, 1 mm thick Hg vapor cell. Measurements indicate that the linewidth at 254 nm of this laser is less than 100 kHz. Acousto-optic modulator AOM1 is used to dynamically change the main output detuning as required for the several phases of the atomic cloud manipulation and detection.

This 254 nm laser source enabled investigations and results reported below. Nevertheless, it was also the main limiting factor of the experiment because of its poor reliability. In the last few years, a new system was developed based on 1015 nm extended cavity diode laser, amplified using a Yb-doped fiber amplifier, and frequency doubled to the visible in a single-passed periodically-poled lithium niobate crystal. This approach reliably gives up to 2 W of optical power at the visible wavelength of 508 nm, removing the main impediment to the progress of Hg clock. More can be found about this laser source can be found in [59].

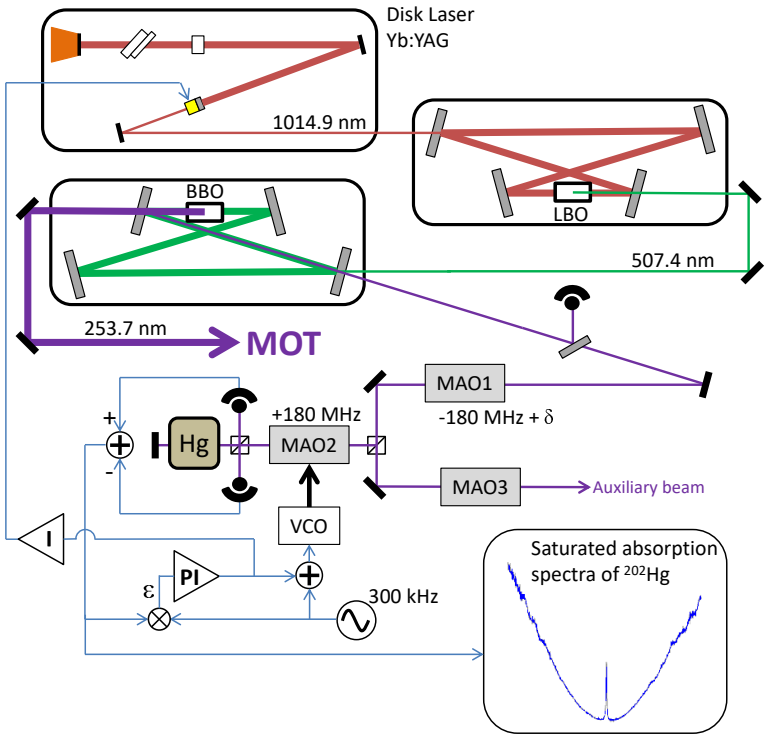

Figure 2.15: Overview of the laser source at 254 nm used to laser cool Hg atoms.

A third key element is the detection system. Hg atoms are detected using the fluorescence of the ${}^1S_0 - {}^3P_1$ transition at 254 nm. At this deep UV wavelength, it is still possible for have Si photodiodes with fairly high quantum

efficiency of 50% and electron multiplied, backside illuminate, thermoelectrically cooled CCD camera with quantum efficiency of 33%. Figure 2.16a is a schematic of the Hg detection system based on such camera. 10^6 atoms give about 1 nW of 254 nm light onto the CDD camera. Fluorescence light is detected along the same direction as one of the MOT beam and separated from it as shown in Fig. 2.16a. When operating the clock, the copropagating MOT beam is not used for detection in order to minimize stray light and optimize detection noise. Figure 2.16b shows a measurement of the atom number detection noise for optimized parameters: detection duration of 5 ms and a laser detuning of $-1 \times \Gamma$. The single shot detection noise is equivalent to ~ 40 atoms.

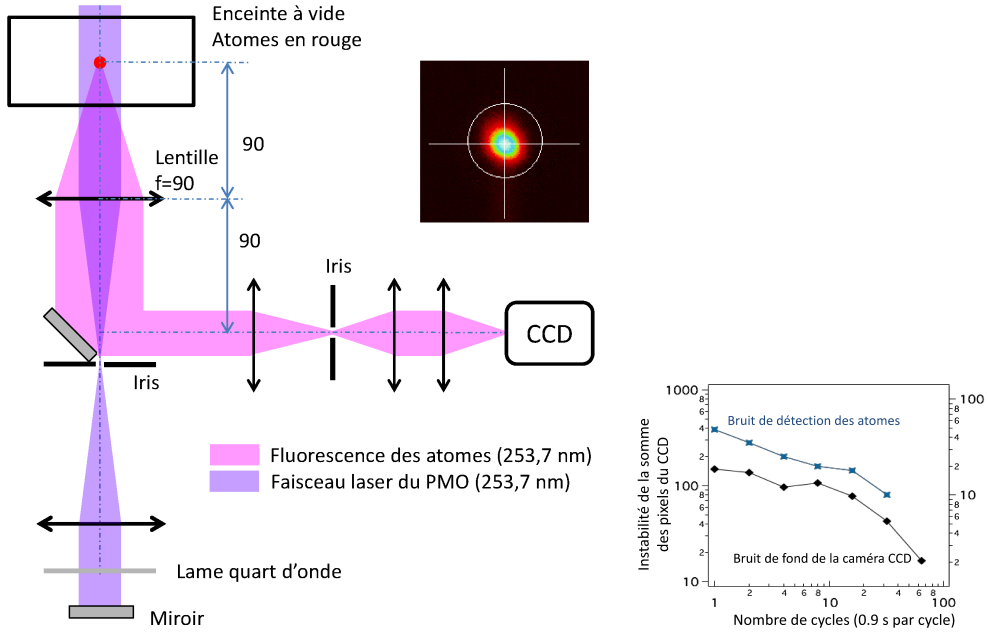

Figure 2.16: a) on the left: Detection of Hg atoms using a CCD camera. b) on the right: Measurement of the atom number detection noise.

With the above systems, we have observed, optimized and characterized magneto-optical trapping and laser cooling of Hg. Figure 2.17 shows on the left a magneto-optical trap loading curve for the ^{202}Hg isotope. On the right, in logarithmic scale, the graph shows the lifetime of the magneto-optical trap observed when turning off the 2D-MOT after reaching the MOT steady state. The lifetime curve is well described by a pure exponential decay whose time constant is identical to the loading curve time constant. These observations indicate that the MOT lifetime and atom number is mainly

limited by background gas collisions and by cold atom density effects. With low Hg pressure setting in the 2D-MOT, time constants as low as 2.5 s were observed, for a residual background pressure of about 3×10^{-7} Pa [60]. Number of atoms in the MOT was estimated in two different manners, one based on the fluorescence and one based on absorption of a probe beam. The two methods agreed to better than a factor of 2, which is reasonable for this type of measurements. Based on these measurements, up to 10^7 trapped atoms were observed for ^{202}Hg.

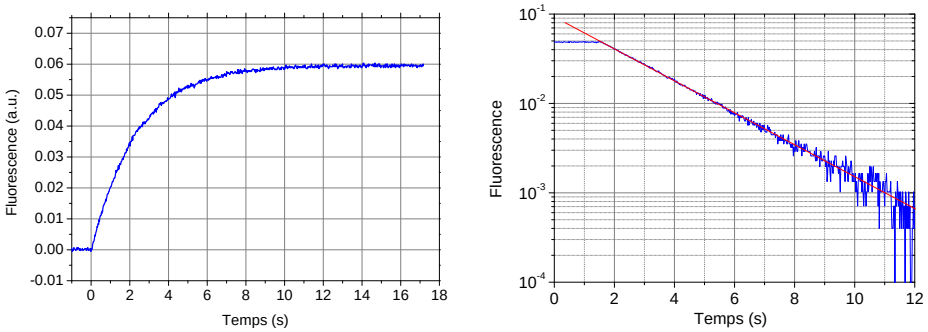

Figure 2.17: a) on the left: MOT loading curve. b) on the right: MOT deloading curve obtained when turning off the 2D-MOT after reaching the MOT steady state.

The temperature and size of Hg cloud release from the MOT were measured by analysing its ballistic expansion. With setup of Fig. 2.16, a series of image of the cloud are taken for several ballistic expansion duration after switching off the MOT. Images are analyzed to determine the initial size and the temperature. Figure 2.18 shows temperature as a function of the laser detuning for several isotopes. For ^{200}Hg and ^{202}Hg, measurements agree with the model based on the theory of Doppler cooling. For ^{199}Hg and ^{201}Hg, temperature much lower are observed which indicates that sub-Doppler cooling mechanisms are effective. These behaviors are expected. Bosonic isotopes ^{200}Hg and ^{202}Hg have no degeneracy in their $^1S_0$ ground state to leave room for sub-Doppler cooling. Fermionic isotopes ^{199}Hg and ^{201}Hg have spin 1/2 and 3/2 respectively in their ground state. The higher degeneracy in ^{201}Hg is expected to yield lower temperatures [61], as observed. The lowest observed temperature is ~ 30 μK. These values are confirmed by the Doppler width measured in the spectroscopy of the clock transition made on atom released from the MOT (see below and reference [62]).

We have measured atomic cloud sizes as low as 100 μm (root-mean-square of the distribution in one direction) and estimated densities up to $1.8 \times$

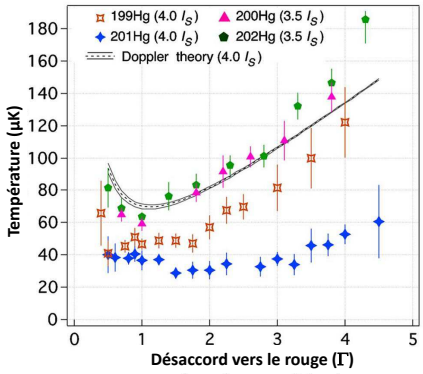

Figure 2.18: Temperature of the Hg atom cloud released for the MOT as a function of laser detuning and for 4 different isotopes.

10^8 mm^{-3}, a fairly high value, favorable for loading the optical lattice trap. This study of the Hg magneto-optical trap characteristics can be found in [63].

2.2.3 First laser spectroscopy of the Hg clock transition

At the start of this Hg optical lattice clock experiment, the frequency of the $^1S_0 - ^3P_0$ clock transition was known indirectly from the accurate wavelengths of spectral lines in Hg vapor lamps, with uncertainties of about 500 MHz, except for ^{198}Hg for which the uncertainty was 12 MHz [64][65][66][67][68]. An important step in the development of a Hg optical lattice clock was the first laser spectroscopy of the clock transition reducing these uncertainties by more than 4 orders of magnitude for the two fermionic isotopes ^{199}Hg and ^{201}Hg.

For this experiment, we used an ultra-stable interrogation laser source at 265.6 nm referenced to primary frequency standards which is described next in Chap. 3 and in [69][70]. This first laser spectroscopy of the clock transition was performed on cold atoms from the magneto-optical trap. During the initial search, the magneto-optical trap is left on continuously and reaches its stationary state. A vertical probe beam at 265.6 nm of a few milliwatts is sent through the trapped atomic cloud. When the probe beam hit the resonance with the clock transition, a fraction of $^1S_0$ atoms are excited into $^3P_0$ where they become insensitive to the magneto-optical trapping, start to accelerating under gravity, become detuned from the probe beam by the Doppler shift and finally fall out of the magneto-optical trap area. The steady state of the magneto-optical trap is modified by this additional loss

mechanism. In this way, spectroscopy of the clock transition is done by measuring the steady state magneto-optical trap fluorescence as a function of the probe laser frequency. Figure 2.19 shows one of the first spectra obtained with this method. At resonance, the effect on the magneto-optical trap is strong. Reduction of the steady state fluorescence by a factor of up to 10 were observed. In this measurement, the probe light is on concurrently

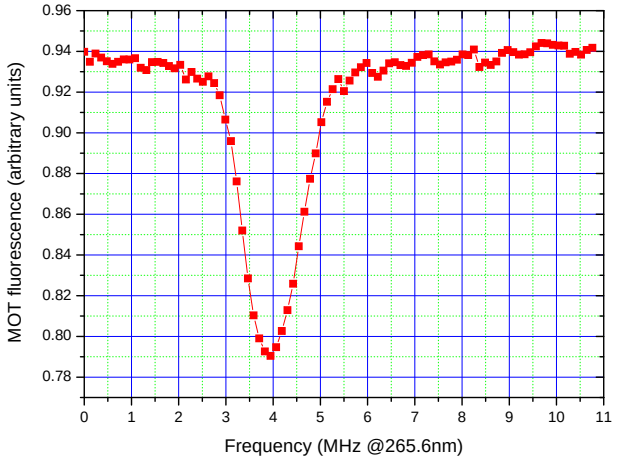

Figure 2.19: One of the first laser spectroscopy of the Hg ${}^1S_0 - {}^3P_0$ optical clock transition. The plot shows the steady state magneto-optical trap fluorescence as function of the probe laser detuning inducing additional losses.

with the 254 nm light for the magneto-optic trap. Spectroscopy is therefore impacted by the 254 nm light shift. In this experimental case, this light shift can be as high as ~ 1 MHz and it is inhomogeneous. It is one likely source of the broad linewidth and asymmetry in the spectrum of Fig. 2.19. For more accurate measurements, another sequence was used where the 254 nm light is periodically switched off when the probe is switched on and vice versa. Typically, the magneto-optic trap phase lasts for 50 ms and the probing phase for 5 ms. Under this cycle, which is faster that magneto-optical trap dynamics (see Fig. 2.17), the trap reaches its steady state equilibrium which again depends on losses induced by the probe. Also, to minimize Doppler shifts due to an initial velocity of atoms released from the magneto-optic trap and to their fall under gravity, a retro-reflected probe was used. As displayed in Fig. 2.20, spectroscopy made in this configuration shows Doppler-free recoil doublet [71]. The two components of the doublet are shifted by $\pm\nu_{\text{recoil}}$ with respect to the unperturbed frequency ν of the transition. The recoil frequency is $\nu_{\text{recoil}} = \nu \times (h\nu/2mc^2)$, where h is Planck's constant, c the speed of light and m the atomic mass. Here, $\nu_{\text{recoil}} = 14.2$ kHz. We verified that the

experiment was in agreement with this expectation. We also verified, when changing parameters of the sequence and in particular the probe time, that the doublet center was unchanged with respect to a stable frequency reference within ± 1 kHz. As shown in Fig. 2.20b, we observed that the width of the each peak has tendency to increase linearly with the probe duration τ, in a way which is well explained by the change of Doppler shift $\nu \times g\tau/c$ due to the free fall under gravity. For $\tau = 500$ μs, this Doppler induced chirp is 18 kHz. We quantified possible shifts due to the Zeeman effect and the probe light shift. As a result, of these experiments, we determined the absolute frequency of the $^1S_0 - ^3P_0$ clock transition for ^{199}Hg and ^{201}Hg with uncertainties of 5.6 kHz and 5.3 kHz, which corresponds to 5 parts in 10^{12}. More details can be found in [62].

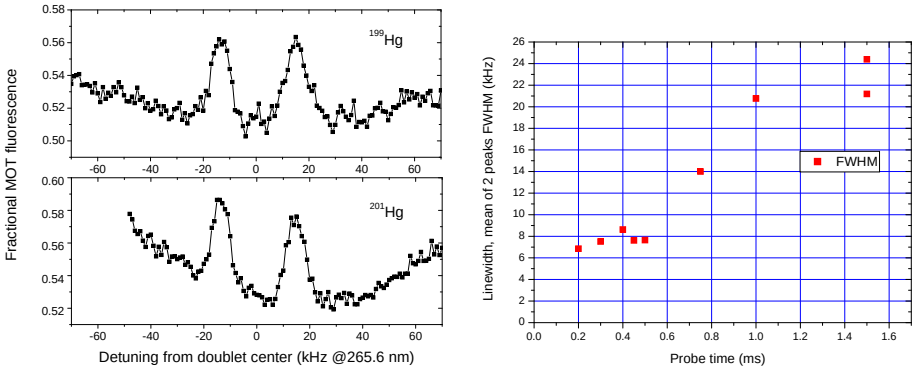

Figure 2.20: a) left: Recoil doublet observed in the spectroscopy of the clock transition made on atoms released from a magneto-optic trap. Measurements were taken for the two fermionic isotopes ^{199}Hg and ^{201}Hg. b) right: Variation of the width recoil doublet peaks as a function of the probe duration.

2.2.4 Lattice trapping and determination of the magic wavelength

At the start of this Hg optical lattice clock experiment, Hg had never been trapped in a dipole trap and theoretical estimations of the magic wavelength for the $^1S_0 - ^3P_0$ clock transition spread from 342 nm to 365 nm. Figure 2.21 shows the experimental setup developed for dipole lattice trapping of Hg and for measuring the magic wavelength. The laser source is based on a frequency doubled titanium:sapphire laser that provides tunability for the magic wavelength search and fairly high output power. The first series of experiment were made with 140 mW at 362 nm. A second notable feature

of the setup is an in-vacuum Fabry-Perot cavity at 362 nm for the dipole lattice trap. This configuration is required to make a deep enough lattice trap, given the wavelength, the available power and the comparatively small polarizability which is a counterpart to the small blackbody radiation shift. The relevant scale for the dipole lattice trap depth is the recoil energy, $E_R = \hbar^2 k^2_{\mathbf{lattice}}/2m$. $k_{\mathbf{lattice}}$ is the lattice light wave vector $k_{\mathbf{lattice}} = 2\pi/\lambda_{\mathbf{lattice}}$. For Hg, reaching a lattice trap depth of $100 \times E_R$ for trap waist of 100 μm requires a laser circulating power of 20 W at $\lambda_{\mathbf{lattice}} \sim 362$ nm. The in-vacuum Fabry-Perot cavity avoids vacuum windows placed inside the cavity and therefore permits high finesse and high build-up factor (see Fig. 2.21). In the first experiments, the lattice trap had a waist of 120 μm and a finesse of ~ 300. Degradation of the cavity optics at high power limited the trap depth to the modest value of $10 \times E_R$. Later, a new implementation was made with a waist of 69 μm and a finesse of 360. It gave access to trap depth higher than $100 \times E_R$.

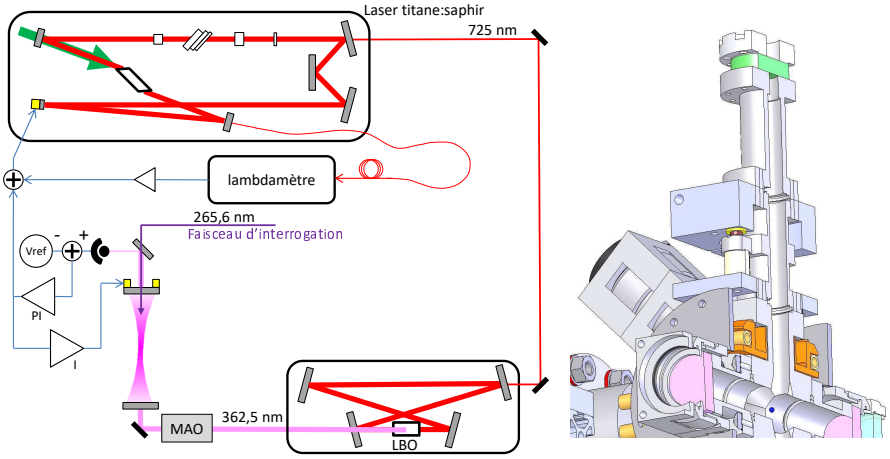

Figure 2.21: Left: Laser system used for lattice trapping of Hg. Right: Schematic view of the in-vacuum Fabry-Perot cavity of the lattice trap. In green, the top curved mirror of Fabry-Perot cavity is also the vacuum window. It is attached to a titanium part with a indium seal. The blue spot represents the cold atom cloud which is crossed by the fundamental mode of the Fabry-Perot.

The lattice cavity is aligned such that its waist coincides with the center of the magneto-optical trap. It is left on continuously and, with the depth achieved so far, it is as no significant effect on the magneto-optic trap. After gathering atoms, the laser detuning and the magnetic field gradient of the magnetic optical trap are changed to maximize density and minimize temperature. After this *compression* phase of 25 ms, the magneto-optic trap

laser beams after switched off. Atoms from the magneto-optic trap start to expand and fall, except for those whose initial position and velocity enable them to be confined in the dipole lattice trap. In early experiments, lattice trap depth was about $U_0 = 10 \times E_R$ which correspond to the temperature $U_0/k_\mathbf{B} = 3.7\ \mu$K. Efficiency of transfer from magneto-optic trap to lattice was limited to 10^{-3} and the number atoms in the lattice less than 2000. In more recent experiment, we have observed up to 10^4 lattice bound atoms. We have observed lattice lifetime up to 420 ms, mainly limited by background gas collisions at pressures of a few 10^{-7} Pa. Figure 2.22 shows an example of lattice lifetime measurement.

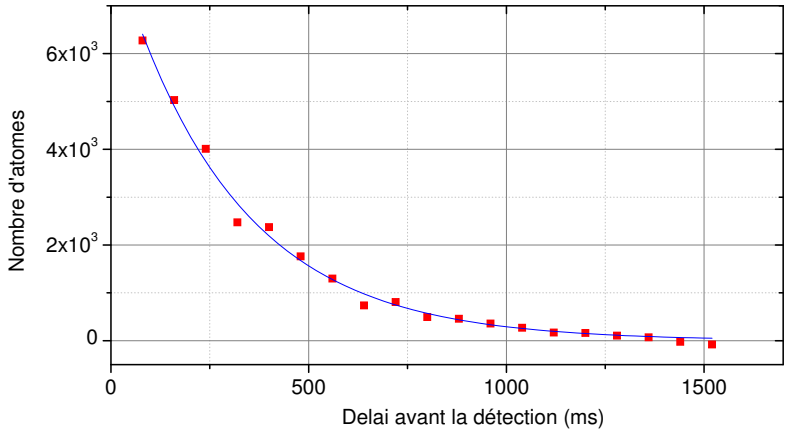

Figure 2.22: Measurement of the lifetime of Hg atoms trapped in a dipole lattice trap near the magic wavelength.

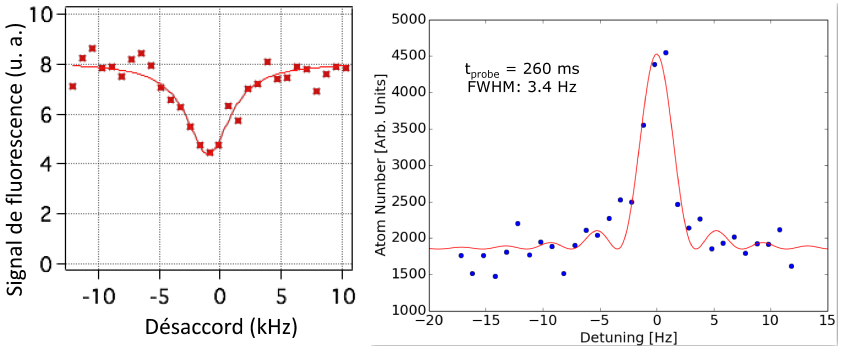

Figure 2.23: Spectroscopy of the ^{199}Hg optical clock transition on lattice bound atoms.

For lattice-bound spectroscopy, a downward-going laser beam at 265.6 nm

from the ultra-stable light source described next in Chap. 3 is overlapped with the lattice trap axis. In the initial phase, atoms were typically probed with a laser power of 200 μW and a probe pulse duration of 20 ms. When the frequency of this beam is resonant with $^1S_0 - ^3P_0$ clock transition, we detect the decrease of $^1S_0$ signal of the CCD camera (see Fig. 2.16). This setup enabled the first lattice-bound spectroscopy of the Hg optical clock transition. Figure 2.23 gives an example such spectrum. For determining the magic wavelength, we measured the center frequency of such spectra against a stable reference monitored by atomic fountains (see Chap. 3) for two trap depths of $10.1 \times E_R$ and $6.8 \times E_R$, and for a number of values of the lattice trap wavelength $\lambda_{\mathbf{lattice}}$. The result of these measurements is displayed in Fig. 2.24. These measurements give a determination of the magic wavelength for the $^1S_0 - ^3P_0$ clock transition in ^{199}Hg. A second determination was also made based on analyzing spectra asymmetrical broadening which appears when the lattice wavelength departs from the magic wavelength [51]. Altogether, this work gave the first experimental determination of the magic wavelength for the $^1S_0 - ^3P_0$ clock transition in ^{199}Hg: $\lambda_{\mathbf{magic}} = 362.53 \pm 0.21$ nm. It is reported in [72]. Subsequent work gave greatly improved magic wavelength determinations for Hg [73][74][59]. Best determination at SYRTE gives $\nu_{\mathbf{magic}} = 826\ 855\ 539 \pm 17$ MHz [59]. It is in agreement with the determination made at RIKEN: $\nu_{\mathbf{magic}} = 826\ 855\ 534 \pm 9$ MHz [74].

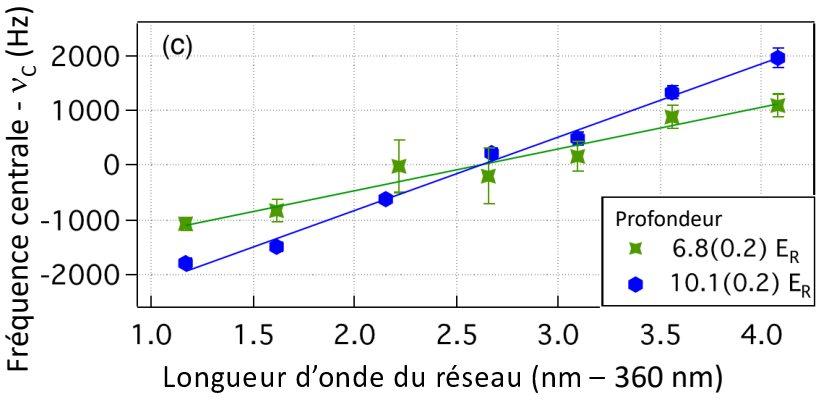

Figure 2.24: Measurements of the clock transition frequency for two trap depths as function of the lattice wavelength. These measurements yield the first experimental determination of the magic wavelength of Hg.

2.2.5 Lamb-Dicke spectroscopy and clock operation

Lattice-bound Lamb-Dicke spectroscopy was improved step by step, both in terms of linewidth and in terms of transition probability measurement noise. An example is given in Fig. 2.23b. Here, atoms were first state selected into one of the two Zeeman sublevels of $^3P_0$ in ^{199}Hg by means of a clock laser pulse on the $|^1S_0, m_F\rangle \longrightarrow |^3P_0, m_F\rangle$ in the presence of magnetic field of ~ 300 μT and of a cooling light pulse clearing $^1S_0$ atoms away. In this example, a 260 ms probe laser pulse is applied and atoms brought back into $^1S_0$ are detected. The spectrum of the clock transition has full width at half maximum of 3.4 Hz, which gives an atomic quality factor of 3.4×10^{14}.

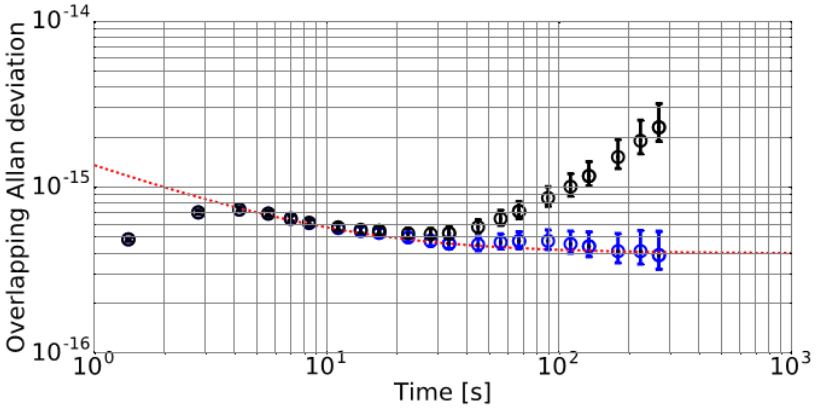

Figure 2.25: Fractional frequency instability of the Hg optical lattice clock.

Operation of the experiment as a clock by locking the probing laser to the atomic transition was achieved, and the frequency stability measured and gradually improved [75]. Figure 2.25 shows an example of such measurement. Conditions of this measurement are similar to the one described above for the narrow-line Lamb-Dicke spectroscopy, i.e. atoms are initially state selected in one of the $^3P_0$ sublevels. The probe time is 100 ms and the cycle time 700 ms. The stability is measured against the ultra-stable reference cavity of the clock laser (see Chap. 3). The stability quickly reaches the flicker frequency noise floor of the cavity of 4×10^{-16}. The ^{199}Hg optical clock short term stability is estimated to be $1.2 \times 10^{-15}\tau^{-1/2}$. The Dick effect from the aliasing of the probe laser high frequency noise is estimated to $4 \times 10^{-16}\tau^{-1/2}$. The additional noise which determines the stability has approximately equal contributions from the detection noise and from initial atom number fluctuations, the latter arising from the lack of normalized detection. The experiment still has much room for further improvement of the short term stability. One way for improvement is the implementation

of normalized detection combined with a further optimization of the CCD-image-based detection. A second one is the use of the 2D-MOT. As reported in Sec. 2.2.2, a 2D-MOT was already operated on the same setup, but weaknesses of the first generation 254 nm laser source did not allow routine use of this sub-system. The better laser source recently implemented on the experiment [59] shall finally make it possible to benefit from the 2D-MOT. With the 2D-MOT, the loading time should be greatly reduced and the clock duty cycle largely improved. Short term stabilities near 10^{-16} at 1 s shall be possible, with the existing ultra-stable laser. Even better stability will come from a new generation of ultra-stable lasers developed at SYRTE, combined with transfer of spectral purity via optical frequency combs [76].

2.2.6 Measurement of systematic shifts

Systematic shifts were measured at several stages of development of the Hg optical lattice clock [62][73][59]. So far, the overall fractional frequency uncertainty was improved down to 1.7×10^{-16}. Here, we will not give a full account this work, and rather discuss the prominent facts. One advantage of Hg is its low sensitivity to thermal radiation and to static electric fields. So far, the estimation of the blackbody radiation shift relied upon a theoretically determination of the differential Stark shift between the two clock levels [54], which gives a fractional shift of -1.60×10^{-16} at 300 K, with an estimated uncertainty of 10% of this value. The sensitivity to temperature of this shift is only -2.13×10^{-18} K^{-1} at 300 K. As a result, even a basic control of the thermal environment, the blackbody radiation shift was so far a small, non-limiting source of uncertainty of ~ 2 parts in 10^{17} [59]. Future work toward realizing the full potential of Hg will require experiments to better ascertain the differential Stark shift and the dynamical polarizability term and to better control the thermal environment.

At the start of the project, no prediction for the collision shift of the Hg lattice clock was available, but it was expected to be small and not limiting factor. At the same time, the case of the hyperfine transition in Cs (see Sec. 2.1.3 and 2.1.4) shows that peculiarly large shift do occur. Such accidentally large shift would depend on the specific isotope. Much attention was paid to measured the collision shift. Our recent measurement of this shift for the ^{199}Hg isotope gave collision shift of $(-6.5 \pm 7.8) \times 10^{-20}$ per atom, consistent with zero, and a corresponding fractional frequency correction of $(-5.2 \pm 6.4) \times 10^{-17}$ [59]. The measured collision shift refers to our experimental conditions: a one dimensional lattice trap with a depth of $\sim 50 \times E_R$ corresponding to ~ 18 μK, a waist of 69 μK and an atomic distribution resulting from loading from the 40 μK magneto-optic trap. In these conditions,

there are approximately 2.5 atoms per lattice site and the peak mean density is approximately 4×10^8 cm^{-3}. At the start of the interrogation, atoms are selected in a single $|^3P_0, m_F\rangle$ state. This measurement indicates that the collision shift shall not be an obstacle to uncertainties of 10^{-18} or less. Here, one should note that collisions in optical lattice clock have, in general, complex behaviors with respect to clock parameters [77][78][79], including non-linearity with respect to density or atom number.

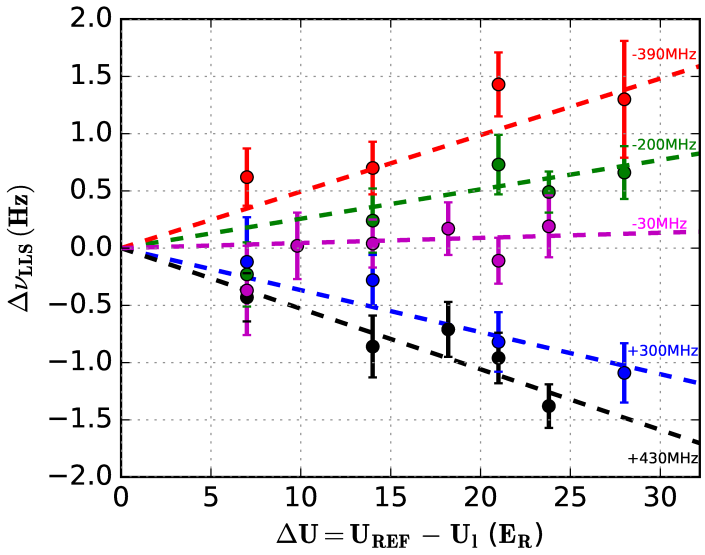

Figure 2.26: Measurement of the lattice light shift in a Hg optical lattice clock.

Another key systematic shift is the lattice light shift. Figure 2.26 shows a recent measurement of lattice light shift in Hg. The corresponding overall uncertainty related to this shift is 1.4×10^{-16} [59]. This uncertainty is mainly limited by the statistical uncertainty of measurements needed to ascertain the magic wavelength and by the uncertainty to which the lattice wavelength is controlled, here with a high-resolution wavemeter. On-going work will help overcoming these limits by improving the clock stability and by referencing the frequency of the lattice light to an optical frequency comb. Another source of uncertainty relates to non-linear light shifts. At the present level of uncertainty, measurements do not show non-linear dependencies, which is expected from theoretical estimations [80]. The non-linear light shift is currently estimated to be $(-6 \pm 3.6) \times 10^{-17}$. Observing and controlling these terms will be an important aspect of future work.

2.3 Personal publications relevant to chapter 2

[59] *Comparing a mercury optical lattice clock with microwave and optical frequency standards.*
R. Tyumenev, M. Favier, S. Bilicki, E. Bookjans, R. Le Targat, J. Lodewyck, D. Nicolodi, Y. Le Coq, M. Abgrall, J. Guéna, L. De Sarlo and S. Bize,
New J. Phys. **18**, 113002 (2016).

[81] *A mercury optical lattice clock at LNE-SYRTE.*
L. De Sarlo, M. Favier, R. Tyumenev and S. Bize,
Journal of Physics: Conference Series **723**, 012017 (2016), Proceedings of the 8th Symposium on Frequency Standards and Metrology.

[57] *Horloge à réseau optique à atomes de mercure.*
S. Bize, R. Chicireanu, S. Dawkins, L. De Sarlo, M. Favier, J. Guéna, Y. Lecoq, C. Mandache, D. Magalhães, J. Mcferran, S. Mejri, M. Petersen, R. Tyumenev and L. Yi
Revue Française de Métrologie **40**, 13 (2015).

[82] *Statistical uncertainty of* 2.5×10^{-16} *for the* ^{199}Hg $^1S_0 - ^3P_0$ *clock transition against a primary frequency standard.*
J. J. McFerran, L. Yi, S. Mejri, W. Zhang, S. Di Manno, M. Abgrall, J. Guéna, Y. Le Coq and S. Bize,
Phys. Rev. A **89**, 043432 (2014).

[28] *Feshbach Resonances in Cesium at Ultra-low Static Magnetic Fields.*
D. J. Papoular, S. Bize, A. Clairon, H. Marion, S. J. Kokkelmans and G.V. Shlyapnikov,
Phys. Rev. A **86**, 040701(R) (2012).

[75] *Laser locking to the* ^{199}Hg $^1S_0$–$^3P_0$ *clock transition with* $5.4 \times 10^{-15}\tau^{-1/2}$ *fractional frequency instability.*
J. J. McFerran, D. V. Magalhães, C. Mandache, J. Millo, W. Zhang, Y. Le Coq, G. Santarelli and S. Bize,
Opt. Lett. **37**, 3477 (2012).

[37] *Progress in atomic fountains at LNE-SYRTE.* Invited review article
J. Guéna, M. Abgrall, D. Rovera, P. Laurent, B. Chupin, M. Lours, G. Santarelli, P. Rosenbusch, M. E. Tobar, R. Li, K. Gibble, A. Clairon and S. Bize,
IEEE Trans. Ultr. Ferr. Freq. Contr. **59**, 391 (2012).

[73] *Neutral Atom Frequency Reference in the Deep Ultraviolet with Fractional Uncertainty* $= 5.7 \times 10^{-15}$.
J. J. McFerran, L. Yi, S. Mejri, S. Di Manno, W. Zhang, J. Guéna, Y. Le Coq and S. Bize,
Phys. Rev. Lett. **108**, 183004 (2012).

[60] *Ultraviolet laser spectroscopy of neutral mercury in a one-dimensional optical lattice.*
S. Mejri, J. J. McFerran, L. Yi and, Y. Le Coq and S. Bize,
Phys. Rev. A, **84**, 032507 (2011).

[34] *Evaluation of Doppler Shifts to Improve the Accuracy of Primary Atomic Fountain Clocks.*
J. Guéna, R. Li, K. Gibble, S. Bize and A. Clairon,
Phys. Rev. Lett. **106**, 130801 (2011).

[72] *Optical Lattice Trapping of* ^{199}Hg *and Determination of the Magic Wavelength for the Ultraviolet* $^1S_0 \leftrightarrow {}^3P_0$ *Clock Transition.*
L. Yi, S. Mejri, J. J. McFerran, Y. Le Coq and S. Bize,
Phys. Rev. Lett. **106**, 073005 (2011).

[63] *Sub-Doppler cooling of fermionic Hg isotopes in a magneto-optical trap.*
J. J. McFerran, L. Yi, S. Mejri and S. Bize,
Opt. Lett. **35**, 3078 (2010).

[22] *Demonstration of a Dual Alkali Rb/Cs Fountain Clock.*
J. Guéna, P. Rosenbusch, P. Laurent, M. Abgrall, D. Rovera, G. Santarelli, M. E. Tobar, S. Bize and A. Clairon,
IEEE Trans. Ultr. Ferr. Freq. Contr. **57**, 647 (2010).

[62] *Doppler-Free Spectroscopy of the 1S0-3P0 Optical Clock Transition in Laser-Cooled Fermionic Isotopes of Neutral Mercury.*
M. Petersen, R. Chicireanu, S. T. Dawkins, D. V. Magalhaes, C. Mandache, Y. Le Coq, A. Clairon and S. Bize,
Phys. Rev. Lett. **101**, 183004 (2008).

[83] *BNM-SYRTE Fountains: Recent Results.*
C. Vian, P. Rosenbusch, H. Marion, S. Bize, L. Cacciapuoti, S. Zhang, M. Abgrall, D. Chambon, I. Maksimovic, P. Laurent, G. Santarelli, A. Clairon, A. Luiten, M. Tobar, and C. Salomon,

IEEE Trans. Instrum. Meas. **54**, 833 (2005).

[84] *Cold atom clocks and applications.*
S. Bize, P. Laurent, M. Abgrall, H. Marion, I. Maksimovic, L. Cacciapuoti, J. Grünert, C. Vian, F. Pereira dos Santos, P. Rosenbusch, P. Lemonde, G. Santarelli, P. Wolf, A. Clairon, A. Luiten, M. Tobar and C. Salomon,
J. Phys. B: At. Mol. Opt. Phys. **38**, S449 (2005).

[85] *Advances in atomic fountains.*
S. Bize, P. Laurent, M. Abgrall, H. Marion, I. Maksimovic, L. Cacciapuoti, J. Grünert, C. Vian, F. Pereira dos Santos, P. Rosenbusch, P. Lemonde, G. Santarelli, P. Wolf, A. Clairon, A. Luiten, M. Tobar and C. Salomon,
C. R. Physique **5**, 829 (2004).

[24] *Controlling the Cold Collision Shift in High Precision Atomic Interferometry.*
F. Pereira Dos Santos, H. Marion, S. Bize, Y. Sortais, A. Clairon, and C. Salomon,
Phys. Rev. Lett. **89**, 233004 (2002).

[18] *Cavity Frequency Pulling in Cold Atom Fountains.*
S. Bize, Y. Sortais, C. Mandache, A. Clairon and C. Salomon,
IEEE Trans. on Instr. and Meas. **50**, 503 (2001).

[17] *Cold Collision Frequency Shifts in a ^{87}Rb Atomic Fountain.*
Y. Sortais, S. Bize, C. Nicolas, and A. Clairon, C. Salomon, C. Williams,
Phys. Rev. Lett. **85** (15), 3117 (2000).

Chapter 3

Ultra-stable oscillators

Ultra-stable oscillators are key to time and frequency metrology. There are essential to clocks and have a direct impact on their stability. There are also indispensable for timekeeping and for dissemination time and frequency references. They also have their own interest whether in fundamental science, like for instance in fundamental physics tests, or in applications, such as ultra-low noise microwave generation for radars. In this chapter, we describe work related to the development of several kinds of such ultra-stable oscillators both in the microwave domain and in the optical domain.

3.1 Ultra-stable references based on a cryogenic sapphire oscillator

Section 2.1.6 described how cryogenic sapphire oscillator gave the best stability ever reported for an atomic fountain. Given the tremendous benefits that come from such stability, a significant effort was devoted to obtaining the best from the cryogenic sapphire oscillator available at SYRTE and to making this performance benefit several experiments. Altogether, these developments yield an ultra-stable metrological reference, which has been in use for almost 2 decades. Next, we give an overview of the architecture that enabled this extended use. We also mention an experiment made in collaboration with the femto-st institute (UMR 6174) to test using a transportable, pulsed-tube based cryogenic oscillator with atomic fountains.

Figure 3.1 is a schematic showing the architecture of LNE-SYRTE ultra-stable metrological reference. This setup is designed to serve several purposes. A first one is to deliver to a variety of applications, a reference signal which has, as much as possible, the exquisitely low phase noise of the output of the cryogenic sapphire oscillator, combined with the mid- and long-term

stability of a hydrogen maser. A second purpose is to serve as a pivot for local high performance clock comparisons. A third one is to connect primary frequency standards (Cs fountains) and other highly accurate clocks (Rb fountain, Sr and Hg optical lattice clocks) to the local real-time physical representation of the coordinated universal time, the UTC(OP) timescale. A forth one is to connect, via UTC(OP), these same standards to remote time and frequency transfer systems which makes it possible for them to contribute to the elaboration of the international atomic time (TAI) and to be compared to similar standards developed in other institutes worldwide.

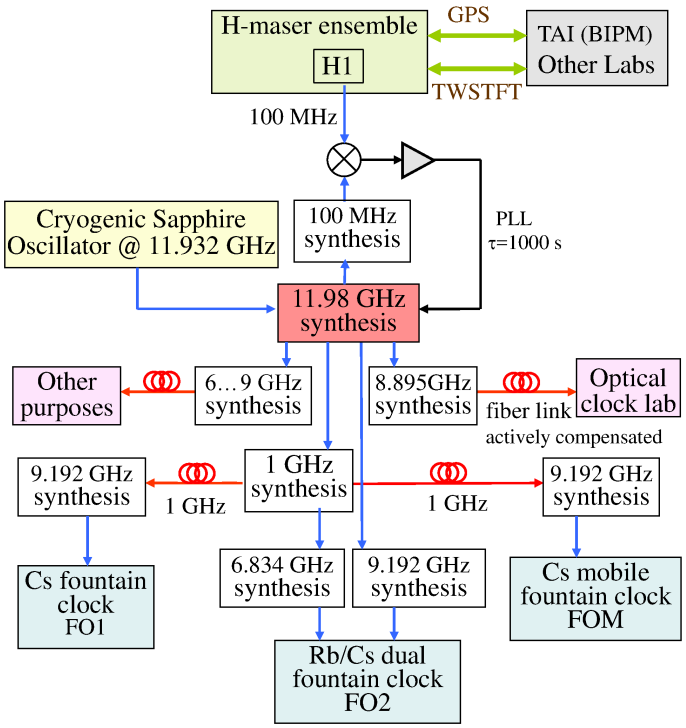

Figure 3.1: Architecture of LNE-SYRTE ultra-stable reference based on the cryogenic sapphire oscillator.

As shown in Fig. 3.1, the cryogenic sapphire oscillator itself is left free-running which avoids degradations of it characteristics that means of controlling it directly may introduce. Instead, an external 11.98 GHz signal, digitally-controlled finely-tunable (microhertz resolution corresponding to $\sim 10^{-16}$), is synthesized from the oscillator output. This 11.98 GHz signal is divided to generate a number of other signals, in particular at 1 GHz and 100 MHz. The 100 MHz signal is mixed to the 100 MHz from a hydrogen maser to provide a measurement of the phase difference between these

two signals. This phase difference is digitalized and used to implement a computer controlled digital phase locked loop which stabilized the phase of the 100 MHz derived from the cryogenic oscillator to the 100 MHz from the maser by tuning the frequency of the 11.98 GHz. This control system ensures long term coherence between the 11.98 GHz and all signals derived from it with the oscillation of the hydrogen maser. This, all reference signals, i.e. the 11.98 GHz and all signals derived from it, have the ultra-low phase noise and short term stability of the cryogenic sapphire oscillator (augmented with some synthesis noise) and the mid- and long-term frequency stability of the maser. Also, via the hydrogen maser, they are connected to the UTC(OP) timescale. The digital phase locked loop has a time constant of $\sim$ 1000 s, which corresponds to the time scale at which the cryogenic sapphire oscillator instability (predictable frequency drift removed) crosses the hydrogen maser instability. The 11.98 GHz has a fractional frequency instability below 2×10^{-15} between 1 s and 2000 s. Above 4000 s, it has the same stability as the maser, $< 10^{-15}$ at 10^4 s and $3 - 4 \times 10^{-16}$ at 1 d for high-performance active hydrogen masers use at SYRTE. Reference [86] gives further description and characterisation of this ultra-stable reference.

From LNE-SYRTE ultra-stable metrological reference, low noise interrogation microwave signals are synthesized for atomic fountains. Examples of such synthesis can be found in [46]. The phase noise power spectral density at 9.2 GHz is -97 dBrad^2.Hz^{-1} at a Fourier frequency of 1 Hz. This ultra-low phase noise signal enables quantum projection noise limited operation in atomic fountains, yielding record stability as shown in Fig 2.12. Operating LNE-SYRTE ultra-stable metrological reference for almost 2 decades also yield long term monitoring of the cryogenic oscillator against atomic references. It contributed characterizing long term behavior of sapphire resonator cryogenic oscillators, as reported in [87]. Applications to fundamental physics tests will be described in Chap. 5.

The femto-st institute (UMR 6174) developed a pulsed-tube based cryogenic oscillators including a transportable version [88][89][90]. One of these oscillators was moved to SYRTE for a few months, enabling the parallel operation of two ultra-stable references. These two references were compared directly, making possible to measured the phase modulation effect due to the pulse tube operation. They were also used to operated two fountains independently, which in turn were compared to each others, in order to specifically test using the transportable oscillator with atomic fountains [91], a configuration similar to the one used to test the flight model of the PHARAO cold atom space clock [92]. The latest implementation of this pulsed-tube based cryogenic oscillator is described in [93].

3.2 Ultra-stable lasers

Ultra-stable lasers are needed for optical clocks and have direct impact on their stability. Making ultra-stable lasers that enable quantum projection noise limited operation of optical lattice clocks was a challenge over the last 2 decades and it continues to be so. Together with the development of the Hg optical lattice clock described in Sec. 2.2, we developed a state-of-the-art ultra-stable laser at 1062.5 nm, which we describe next.

Shortly before this work was started, it was shown by the gravitational wave detector community that laser frequency stabilization to rigid Fabry-Perot cavities was limited by thermal brownian noise [94]. Thermal noise has three contributions from the spacer, mirror substrates and mirror coatings. It gives length fluctuations with a $1/f$ power spectral density, f being the Fourier frequency. It is related to dissipation of mechanical perturbations in materials. Noise in cavities made of broadly used ultra-low expansion glass is dominated by contribution from mirror substrates. With this in mind, we opted for a design based on fused silica mirror substrates. The much larger thermal expansion coefficient and sensitivity subsequent to this choice is mitigated with high level of active and passive protection against environment temperature variations. Note that another great mitigation approach is to use ultra-low expansion compensation rings [95]. We chose a 10 cm long cylindrical geometry, vertically mounted next to its mid-plane, a configuration which nominally gives a vanishing sensitivity to vibration. The exact shape was further optimized to take into account realistic support points and to null vibration induced mirror tilting, which keeps the sensitivity small even for an offset optical axis. Further description of the design can be found in [96]. This ultra-stable cavity design was the basis for a rigidly mounted transportable device developed with the space industry as a first step toward space qualified ultra-stable lasers [97]. It was followed by a second version described in [98].

In [70], the 1062.5 nm ultra-stable laser is described with some details and results of vibration sensitivity and temperature sensitivity measurements are given. Also, the effectiveness of passive shields is tested and shown to have a time constant of ~ 4 days providing reduced temperature fluctuations (< 10 nK) of for the cavity on timescale shorter than 1000 s. Figure 3.2 shows a schematic of the ultra-stable cavity and measurements of the 1062.5 nm ultra-stable laser against other ultra-stable references. The measurement of the frequency stability against another 1062.5 nm laser based on an horizontal cavity (see [96]) shows a flicker noise floor of 5.7×10^{-16} [75]. In this measurement, it is reasonable to assume that the two lasers contribute equally which places the flicker floor of a single laser near 4×10^{-16}, which is

consistent with what was observed later with the Hg clock (see Fig. 2.25 of Sec. 2.2). This is the state-of-the-art for a 10 cm long cavity and it matches estimations based on equations of reference [94]. The stability against LNE-SYRTE ultra-stable metrological reference is below 2 parts in 10^{15} up to 1000 s, once a linear drift of $\sim -6 \times 10^{-17}$ s^{-1} is removed. This verifies the effectiveness of thermal shields. Long term observation of the ultra-stable laser frequency indicates an isothermal creep of $\sim -6 \times 10^{-17}$ s^{-1} [75].

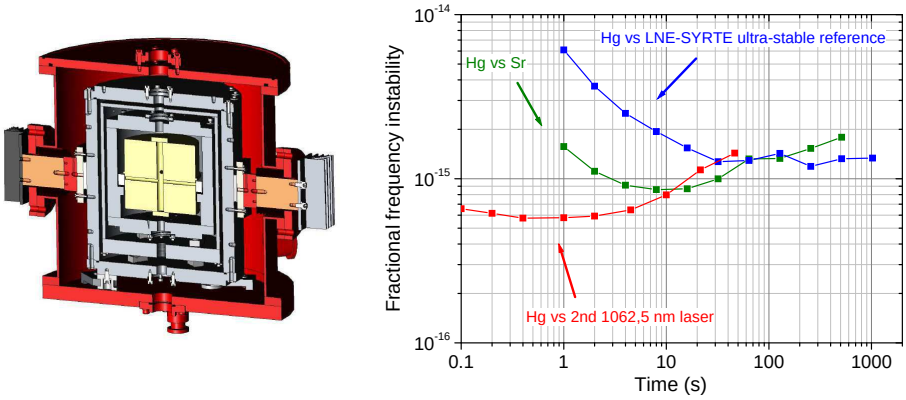

Figure 3.2: Left: Schematic of the 1062.5 nm ultra-stable cavity. Left: Comparison of the 1062.5 nm to other ultra-stable lasers. In the comparison with the LNE-SYRTE ultra-stable metrological reference based on a cryogenic oscillator and a hydrogen maser a linear drift of $\sim -6 \times 10^{-17}$ s^{-1} is removed.

For its use with the Hg optical clock, the 1062.5 nm ultra-stable laser is amplified and frequency doubled twice in resonant cavities to reach the frequency of the $^1S_0 - ^3P_0$ clock transition. This is described in [70]. The 1062.5 nm ultra-stable laser was also used for titanium:sapphire laser stabilization, for low noise microwave generation (see Sec. 3.3 below) and for transfer of spectral purity experiments [76].

3.3 Microwave generation

Microwave signals with ultra-low phase noise can be generated by detecting the repetition rate of an optical frequency comb locked to an ultra-stable laser. Even if the goal is the measurement of optical frequencies, locking frequency comb to an ultra-stable laser and using it as a frequency divider toward the microwave domain is beneficial. It makes the entire comb ultra-stable and thereby greatly extend its capability and readiness to measure

other optical frequencies with the same device. In [70], we describe the implementation of this approach to a titanium:sapphire comb. In this work, the carrier-envelop offset is classically detected with a $f - 2f$ interferometer. It is then electronically mixed out of each beatnote between the comb and lasers to be measured. Virtually, this give access to a comb free of the carrier-envelop offset, therefore with a single degree of freedom to control: the repetition rate. Closing a single stabilization phase-locked loop to the 1062.5 nm ultra-stable laser then makes this virtual carrier-envelop free comb ultra-stable and generates low noise microwave which is measured against LNE-SYRTE ultra-stable metrological reference. Microwave signals generated with this system was already had much better phase noise at 1 Hz than achievable with the best quartz oscillator based synthesis [70].

Fiber-based optical frequency combs at 1.5 μm offer a much higher reliability than titanium:sapphire based combs. They are therefore much better suited for a wide range of applications. With this in mind, SYRTE developed ultra-low noise microwave generation with fiber combs. In [99], we report such work where the above described method is again used to stabilize the comb. Microwave signal generated in this way is transmitted by an optical fiber link and compared to the LNE-SYRTE ultra-stable metrological reference. A fractional frequency instability of 3 parts in 10^{15} is observed at 1 s. The comb generated signal is then used to operation an atomic fountain is the quantum projection limited regime. SYRTE continued developing ultra-low noise microwave generation with fiber-based comb to the point of outclassing any other microwave source [100][101].

3.4 Personal publications relevant to chapter 3

[98] *Ultra-stable clock laser system development towards space applications.*
D. Swierad, S. Häfner, S. Vogt, B. Venon, D. Holleville, S. Bize, A. Kulosa, S. Bode, Y. Singh, K. Bongs, E. M. Rasel, J. Lodewyck, R. Le Targat, C. Lisdat and U. Sterr,
Scientific Reports **6**, 33973 (2016).

[91] *High-Stability Comparison of Atomic Fountains Using Two Different Cryogenic Oscillators.*
M. Abgrall, J. Guéna, M. Lours, G. Santarelli, M. Tobar, S. Bize, S. Grop, B. Dubois, G. C. Fluhr and V. Giordano,
IEEE Trans. Ultr. Ferr. Freq. Contr. **63**, 1198 (2016).

[97] *Prototype of an ultra-stable optical cavity for space applications.*

B. Argence, E. Prevost, T. Lévêque, R. Le Goff, S. Bize, P. Lemonde and G. Santarelli,
Optics Express **20**, 25409 (2012).

[75] *Laser locking to the* ^{199}Hg $^1S_0$–$^3P_0$ *clock transition with* $5.4 \times 10^{-15}\tau^{-1/2}$ *fractional frequency instability.*
J. J. McFerran, D. V. Magalhães, C. Mandache, J. Millo, W. Zhang, Y. Le Coq, G. Santarelli and S. Bize,
Opt. Lett. **37**, 3477 (2012).

[70] *An ultra-stable referenced interrogation system in the deep ultraviolet for a mercury optical lattice clock.*
Dawkins, S., Chicireanu, R., Petersen, M., Millo, J., Magalhães, D., Mandache, C., Le Coq, Y. and S. Bize,
Appl. Phys. B **99**, 41 (2010).

[96] *Ultra-stable lasers based on vibration insensitive cavities.*
J. Millo, D. V. Magalhaes, C. Mandache, Y. Le Coq, E. M. L. English, P. G. Westergaard, J. Lodewyck, S. Bize, P. Lemonde, and G. Santarelli,
Phys. Rev. A **79**, 053829, (2009).

[99] *Ultralow noise microwave generation with fiber-based comb and application to atomic fountain clock.*
J. Millo, M. Abgrall, M. Lours, E. M. L. English, H. Jiang, J. Guéna, A. Clairon, S. Bize, Y. Le Coq, G. Santarelli, and M. E. Tobar,
Appl. Phys. Lett. **94**, 141105, (2009).

[46] *Design and metrological features of microwave synthesizers for atomic fountain frequency standard.*
D. Chambon, M. Lours, F. Chapelet, S. Bize, M.E. Tobar, A. Clairon and G. Santarelli,
IEEE Trans. Ultr. Ferr. Freq. Contr. **54**, 729 (2007).

[87] *Long Term Operation and Performance of Cryogenic Sapphire Oscillators.*
M.E. Tobar, E.N. Ivanov, C.R. Locke, P.L. Stanwix, J.G. Hartnett, A.N. Luiten, R.B. Warrington, P.T.H. Fisk, M.A. Lawn, M.J. Wouters, S. Bize, G. Santarelli, P. Wolf, A. Clairon, P. Guillemot,
IEEE Trans. Ultrason. Ferroelect. Freq. Contr., **53**, 2386 (2006).

[86] *Design and realization of a flywheel oscillator for advanced time and fre-*

quency metrology.
D. Chambon, S. Bize, M. Lours, F. Narbonneau, H. Marion, A. Clairon, and G. Santarelli A. Luiten and M. Tobar,
Rev. Sci. Instrum. **76**, 094704 (2005).

Chapter 4

Metrology

Atomic frequency standards and ultra-stable oscillators like the ones described in Chap. 2 and 3 find one of their main applications in the field of pure time and frequency metrology. In this chapter, we describe the work done in this direction.

4.1 Comparison of primary frequency standards

In Chap. 2, we reported studies of systematic shifts in microwave and optical frequency standards. A comprehensive study of systematic shifts in a given device establishes an uncertainty budget for this particular standard. Comparisons between highly accurate frequency standards provides the mean of challenging and validating uncertainty budgets. They check that actual realization of frequency reference is done with all systematic shifts under control over a planed period of use. They are key to the credibility and the advancement of the field.

	FO1	FO2-Cs	FOM	FO2-Rb
Quadratic Zeeman shift	-1274.5 ± 0.4	-1915.9 ± 0.3	-305.6 ± 1.2	-3465.5 ± 0.7
Blackbody radiation	172.6 ± 0.6	168.0 ± 0.6	165.6 ± 0.6	122.8 ± 1.3
Collisions and cavity pulling	70.5 ± 1.4	112.0 ± 1.2	28.6 ± 5.0	2.0 ± 2.5
Distributed cavity phase shift	-1.0 ± 2.7	-0.9 ± 0.9	-0.7 ± 1.6	0.4 ± 1.0
Spectral purity and leakage	<1.0	<0.5	<4.0	<0.5
Ramsey and Rabi pulling	<1.0	<0.1	<0.1	<0.1
Microwave lensing	-0.7 ± 0.7	-0.7 ± 0.7	-0.9 ± 0.9	-0.7 ± 0.7
Second-order Doppler shift	<0.1	<0.1	<0.1	<0.1
Background collisions	<0.3	<1.0	<1.0	<1.0
Total	-1033.1 ± 3.5	-1637.5 ± 2.1	-113.0 ± 6.9	-3341.0 ± 3.3

Figure 4.1: Uncertainty budget of LNE-SYRTE atomic fountain frequency standards as of 2012, reproduced from [37].

Figure 4.1 shows uncertainty budget of FO2-Cs and other LNE-SYRTE atomic fountains. Over the course of the development of these frequency standards, many comparisons where made with improving uncertainties. In doing so, availability of the cryogenic sapphire oscillator and of the LNE-SYRTE ultra-stable metrological reference described in Sec. 3.1 was a great advantage. It enabled high stability operation of atomic fountains and yielded stringent comparisons in a comparatively short time [83][37]. Typically, in such comparisons, cumulated measurement time yield statistical uncertainty $\sim 10^{-16}$ such that the overall uncertainty is fully dominated by systematic uncertainties. In general, over almost two decades of developments, the results of such comparisons showed agreement and supported uncertainty budget established for atomic fountains. In some case, comparison showed statistically resolved non vanishing difference between two fountains (difference of 5.7×10^{-16} for an overall uncertainty of 6.0×10^{-16}) [37].

Atomic fountain frequency standards are used to calibrate and steer TAI (see next). In turn, the process by which the BIPM realizes TAI provides the mean of comparing fountains worldwide. References [102][103][104][105] report on such comparisons. Here also, statistically significant differences are found in some cases but these differences are well consistent with stated accuracies of standards. In these comparisons, instability of satellite time transfer methods used for linking atomic fountains to TAI is dominant at short time. However, cumulated effective comparison time (hundreds of days) is sufficient to average down this noise contribution to the point where systematic uncertainties of standards dominate the overall uncertainty (see, for instance, [106]).

In 2004, a dedicated and coordinated remote comparison campaign was organised between PTB, NIST, NPL, INRIM and LNE-SYRTE using satellite methods TWSTFT, GPS TAI P3 and GPS CP. About 20 days of fountain comparisons could be cumulated between NPL-CsF1, INRIM-CsF1 and LNE-SYRTE-FO2-Cs leading to a link uncertainty of less than 10^{-15}. FO2-Cs and NPL-CsF1 were found in agreement with an overall uncertainty of 1.7×10^{-15}. INRIM-CsF1 was found to differ for the two others by two standard deviations [107].

Recently, coherent optical fiber link [108] between SYRTE and PTB (Physikalisch-Technische Bundesanstalt, Germany) enabled remote fountain comparisons. In this experiment, the link instability has negligible contribution and fountains are compared remotely just as well as if they were next of one another. This gave stringent comparisons between 4 primary frequency standards. The largest difference is 2.7×10^{-16} with an overall uncertainty of 5.0×10^{-16}. Other differences are closer to zero and the lowest overall uncertainty is 4.2×10^{-16} [109].

4.2 Absolute frequency measurements, optical frequency ratios and reference values

Highly accurate absolute frequency measurements of microwave and optical atomic frequencies provide reference values for atomic transitions which can then be used in applications. A typical example are optical transitions used for practical realization of the meter. Another example is the Rb hyperfine transition which is widely used in commercial frequency standards and in other type of atomic sensors. Since 2001, anticipating the development of optical frequency standards outclassing microwave standards, the CIPM defined secondary representations of the seconds (SRS) as atomic transitions that are measured with uncertainties close the accuracy of the primary frequency standards. The CIPM, via the CCTF and the BIPM, maintains a list of recommended values for such SRS [110], as a preparation for possible redefinition of the second. Highly accurate absolute frequency measurements contribute building this list and linking the optical and the microwave domains at the best possible level. It is also a mean of checking consistency of independent measurements and of consolidating progress of the field.

With atomic fountains and optical lattice clocks at SYRTE, we perform some of the most accurate absolute frequency measurements to date. Using FO2-Rb and Cs fountains, we performed a series of highly accurate absolute frequency measurements of the ^{87}Rb hyperfine frequency. Based on the earliest of these measurements (with uncertainty 1.2×10^{-15} for the best one) [111][112][85][84], this transition became the first secondary representation of the second recognized by the CIPM. Later on, we performed many more measurements while uncertainties of both FO2-Rb and Cs fountains was improved [22][37], bringing the uncertainty on ^{87}Rb hyperfine frequency down to 4.4×10^{-16} [113]. The already mentioned optical fiber link comparison provided the opportunity to further improve to 3.1×10^{-16} [109].

We performed absolute frequency measurements of the ^{88}Sr [114] and ^{87}Sr optical lattice clocks [115][116][117]. For the latter, we made some of the most accurate measurements with uncertainties down to 2.8 parts in 10^{16}. These measurements, together with measurements made at PTB [**?**](and a few other institutes but with significantly worse uncertainties), provide the most stringent link to date between optical and microwave domains.

We performed absolute frequency measurements of the ^{201}Hg and ^{199}Hg $^1S_0 - ^3P_0$ optical clock transitions observed on free-falling laser-cooled atoms released from a magneto-optical trap (see Sec. 2.2.3) [62]. Later on, we made measured the ^{199}Hg transition in the optical lattice clock configuration [73][59] to an uncertainty of 3.8×10^{-16}, which led this transition to

enter the CIPM list of recommended values and to later become a secondary representation of the second.

We performed $^{87}Sr/^{87}Rb$ [117] and $^{199}Hg/^{87}Rb$ [59] optical-to-microwave frequency ratio measurements. Finally, we performed an optical-to-optical frequency measurement (for the first time at SYRTE) of $^{199}Hg/^{87}Sr$, with an uncertainty of 1.8×10^{-16} limited by Hg [59]. The measurement is in agreement with another measurement of the same quantity (uncertainty 8.4×10^{-17}) made at RIKEN (Japan) [74]. This ratio is one of the few optical frequency ratios measured independently at two different institutes and with uncertainties beyond the realization of the SI second.

Altogether, with the above measurements, SYRTE had a large contribution to the CIPM list of recommended values, to linking the optical and the microwave domain and to advancing toward a possible redefinition of the SI second.

4.3 Contribution to timekeeping

International Atomic Time (TAI) and Coordinated Universal Time (UTC) are global resources of high importance for science and society. Approximately 400 commercial clocks from many institutes worldwide are used by the BIPM, together with satellite time transfer data, to construct the free atomic timescale (EAL). EAL alone has high stability and reliability but poor accuracy. The frequency of EAL is steered based on calibrations of its scale interval by primary frequency standards so as to realize TAI with a scale interval nominally coinciding with the SI second (see for instance [118]). 16 primary frequency standards, among which 14 Cs atomic fountains, contributed in recent years, from 10 institutes. The vast majority of primary calibrations comes from 3 or 4 institutes only. LNE-SYRTE fountain ensemble was developed taking into account demanding requirements for providing TAI calibrations. This includes capability of stand-alone operation for long period of time, at least 5 days but more typically months, while maintaining and ascertaining the nominal accuracy, via real-time measurements of frequency shifts (collisions) and of key parameters. This includes also capability to deliver finalized measurements of month long data taking within a few days, according to the TAI calibration reporting scheme. This also includes devoting extended periods of time to this applications and not only to investigating a specific frequency shift or performing other experiments. Over the last 15 years, LNE-SYRTE fountains provided more than 200 TAI calibrations, which represents more than 40% of all calibrations worldwide. Calibrations reports and their use in TAI are publicly available on the BIPM

website, in particular in *Circular T* [119].

After the ^{87}Rb hyperfine transition was adopted by the CIPM as a secondary representation of the second (see above), we supplied TAI calibrations made with FO2-Rb. For the first time, TAI started being calibrated and steered using a SRS [113]. Given the limited number of standards actually and effectively contributing to the elaboration of TAI, this additional possibility was significant and FO2-Rb provided many calibrations. Also this enabled setting up rules and processes for standards based on SRS to contribute to TAI. Figure 4.2 shows data from *Circular T* and highlights calibrations from LNE-SYRTE fountain ensemble.

The increase of TAI calibrations by atomic fountains from less than 1 per month to 4-5 per months over the last 15 years yield significant improvement of TAI and UTC long term stability and accuracy [105][118]. Via the elaboration of TAI, the long term stability and accuracy of atomic fountains are made accessible to users and applications. For instance, it enables highly accurate SI-traceable frequency measurements without a local primary frequency [120].

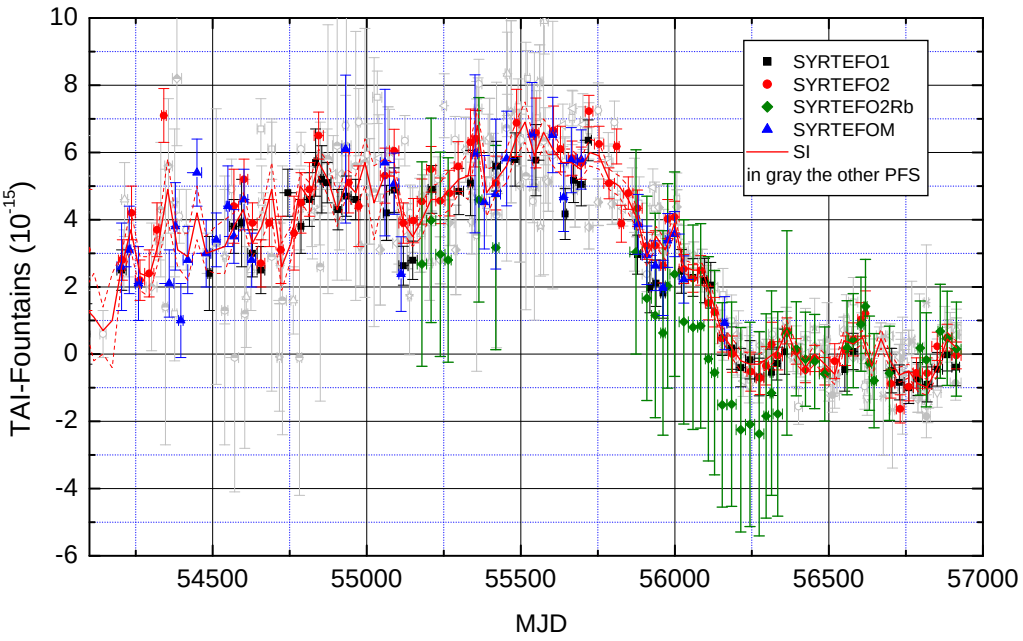

Figure 4.2: Calibration of TAI with primary and secondary frequency standards.

Another important aspect of timekeeping is the realization of real-time physical representations of UTC. At Observatoire de Paris, LNE-SYRTE is

realizing such a timescale called UTC(OP). Since October 2012, UTC(OP) is making use of frequency measurements from atomic fountains. Specifically, one or several fountains are used to measure the frequency of a hydrogen maser whose output is used a generate UTC(OP). Fountain data are collected and processed automatically to determine mean frequency of the hydrogen maser over a day. The algorithm then use these data point to determine, on a daily basis, frequency offsets to be applied to the compensate for frequency fluctuations of the hydrogen maser and for steering the frequency and phase of UTC(OP) to UTC, based UTC(OP)-UTC time differences published in *Circular T* on a monthly basis. The process is made robust against gaps in fountain data and enables, when necessary, switching to another fountain. This new realization of UTC(OP) using atomic fountain frequency standards is described in [121]. It improved the stability of UTC(OP) which became one of the best realization of UTC, together with a few other institutes using fountains to generate their timescales [122][20]. The time difference |UTC(OP)-UTC| remains well below 10 ns and has a rms values of less than 3 ns. UTC(OP) is the legal timescale for France [123] and it is the basis for many applications and services, such dissemination via the French atomic time network (TA(F)) to demanding users, contributions to the development of the european GNSS GALILEO and to EGNOS (European Geostationary Navigation Overlay Service), etc. Many of these services are grouped under the Action Nationale d'Observation CNRS/INSU-Astronomie-Astrophysique-Horloges and under the time and frequency activities of the Réseau National de la Métrologie Française coordinated by LNE (Laboratorie National de Métrologie et d'Essais). High performance realizations of UTC are also a resource of assessing and pushing limits of remote time transfer methods [107][124][125].

UTC(OP) and together with continuously operated highly accurate atomic fountains will be a key parts of the ground segment of the ACES space mission [92][126][127].

4.4 Personal publications relevant to chapter 4

[109] *First international comparison of fountain primary frequency standards via a long distance optical fiber link.*
J. Guéna et al.,
Metrologia **54**, 348 (2017).

[59] *Comparing a mercury optical lattice clock with microwave and optical frequency standards.*

R. Tyumenev, M. Favier, S. Bilicki, E. Bookjans, R. Le Targat, J. Lodewyck, D. Nicolodi, Y. Le Coq, M. Abgrall, J. Guéna, L. De Sarlo and S. Bize,
New J. Phys. **18**, 113002 (2016).

[121] *UTC(OP) based on LNE-SYRTE atomic fountain primary frequency standards.*
G. D. Rovera, S. Bize, B. Chupin, J. Guéna, Ph. Laurent, P. Rosenbusch, P. Uhrich and M. Abgrall,
Metrologia **53**, S81 (2016).

[117] *Optical to microwave clock frequency ratios with a nearly continuous strontium optical lattice clock.*
J. Lodewyck, S. Bilicki, E. Bookjans, J.-L. Robyr, C. Shi, G. Vallet, R. Le Targat, D. Nicolodi, Y. Le Coq, J. Guéna, M. Abgrall, P. Rosenbusch and S. Bize,
Metrologia **53**, 1123 (2016).

[128] *Atomic fountains and optical clocks at SYRTE: Status and perspectives.*
M. Abgrall, B. Chupin, L. De Sarlo, J. Guéna, P. Laurent, Y. Le Coq, R. Le Targat, J. Lodewyck, M. Lours, P. Rosenbusch, G. D. Rovera and S. Bize,
C. R. Physique **16**, 461 (2015).

[113] *Contributing to TAI with a Secondary Representation of the SI Second.*
J. Guéna, M. Abgrall, A. Clairon and S. Bize,
Metrologia **51**, 108 (2014).

[116] *Experimenting an optical second with strontium lattice clocks.*
R. Le Targat, L. Lorini, Y. Le Coq, M. Zawada, J. Guéna, M. Abgrall, M. Gurov, P. Rosenbusch, D. G. Rovera, B. Nagórny, R. Gartman, P. G. Westergaard, M. E. Tobar, M. Lours, G. Santarelli, A. Clairon, S. Bize, P. Laurent, P. Lemonde and J. Lodewyck,
Nature Comm. **4**, 2109 (2013).

[129] *Optical Lattice Clocks as Candidates for a Possible Redefinition of the SI Second.*
M. Gurov, J. J. McFerran, B. Nagorny, R. Tyumenev, Z. Xu, Y. Le Coq, R. Le Targat, P. Lemonde, J. Lodewyck, and S. Bize,
IEEE Trans. Instrum. Meas. **62**, 1568 (2013).

[73] *Neutral Atom Frequency Reference in the Deep Ultraviolet with Fractional Uncertainty* $= 5.7 \times 10^{-15}$.

J. J. McFerran, L. Yi, S. Mejri, S. Di Manno, W. Zhang, J. Guéna, Y. Le Coq and S. Bize,
Phys. Rev. Lett. **108**, 183004 (2012).

[1] *Réalisation et diffusion de la seconde au LNE-SYRTE fondées sur l'utilisation d'horloges en fontaine atomique.*
S. Bize et al.,
Revue Française de Métrologie **18**, 13 (2009).

[130] *An optical lattice clock with spin-polarized ^{87}Sr atoms.*
X. Baillard, M. Fouché, R. Le Targat, P.G. Westergaard, A. Lecallier, F. Chapelet, M. Abgrall, G.D. Rovera, P. Laurent, P. Rosenbusch, S. Bize et al.,
Eur. Phys. J. D **48**, 11 (2008).

[114] *Accuracy evaluation of an optical lattice clock with bosonic atoms.*
X. Baillard, M. Fouché, R. Le Targat, P.G. Westergaard, A. Lecallier, Y. Le Coq, G.D. Rovera S. Bize and P. Lemonde,
Opt. Lett. **32**, 1812 (2007).

[107] *Comparison between frequency standards in Europe and the USA at the 10^{-15} uncertainty level .*
A. Bauch, J. Achkar, S. Bize, D. Calonico, R. Dach, R. Hlavac, L. Lorini, T. Parker, G. Petit, D. Piester, K. Szymaniec, P. Uhrich,
Metrologia **43**, 109 (2006).

Chapter 5

Fundamental tests

As mentioned in the Introduction, accurate atomic frequency standards find applications in testing fundamental physical laws. Physics is based on two fundamental theories : general relativity and the standard model of particle physics. These two theories are extremely successful in describing a huge number of observations. Nonetheless, these two theories do have some difficulties. One is to require the introduction of dark energy and cold dark matter, representing 95% of the energy and mass in the Universe, to match the observed accelerating expansion and rotation curves of galaxies, in the so-called ΛCDM cosmological model of the Universe. A second difficulty is that the standard model is a quantum field theory whereas general relativity is not, giving an heterogeneous picture of the 3 fundamental interactions.

In this context, accurate atomic frequency standards provide laboratory tests, complementary to geophysical and astronomical observations, to investigate the pending question in modern physics of elaborating a unified theory of gravitation, electroweak and strong interactions. They could be one way to reveal physics beyond general relativity and the standard model. One of the interest of these tests is that their interpretation is independent of any particular cosmological model and that they provide information at the present epoch. In this chapter, we report on some fundamental tests done with atomic frequency standards. These experiments provide tests of Einstein's equivalent principle which one of the founding principle of general relativity. More specially, they test local position invariance and local lorentz invariance. The third component of Einstein's equivalence principle, the universality of free fall is not directly tested by clock experiments.

Overview of tests of fundamental laws, including tests not based on clocks, tests on geological an cosmological timescale, etc. can be found in [131][132]. A more complete view on testing general relativity with clocks can be found in [133].

5.1 Local position invariance: stability of natural constants

The frequency of atomic transitions A can, in principle, be expressed as a function of fundamental constants of the standard model, in the following generic manner :

$$\nu_A = R_\infty c \times f_A(\alpha, \Lambda_{\rm QCD}, m_e, m_u, m_d, ...) \tag{5.1}$$

where the dimension is given by the Rydberg constant expressed in frequency units $R_\infty c$ and where f_A is a dimensionless function of parameters of fundamental interactions and of elementary particles. α is the fine structure constant, $\Lambda_{\rm QCD}$ the mass scale of quantum chromodynamics, m_e the electron mass, m_u the up quark mass, etc. Atomic frequency ratios are experimentally accessible quantities which depends on fundamental constants as :

$$\nu_B/\nu_A = f_B(\alpha, \Lambda_{\rm QCD}, m_e, m_u, m_d, ...)/f_A(\alpha, \Lambda_{\rm QCD}, m_e, m_u, m_d, ...). \tag{5.2}$$

Function f_A is, by far, not know as accurately as atomic transition can be realized and compared in highly accurate clock. But, derivatives of f_A with respect to parameters can be computed with small enough uncertainties for the purpose of tests discussed here (see e.g. [134][135][136][137]). Also, for these tests, one can restrict the analysis to 3 leading parameters : α, $m_e/\Lambda_{\rm QCD}$ and $m_q/\Lambda_{\rm QCD}$. Alternatively, one can choose α, $\mu = m_e/m_p$, $m_q/\Lambda_{\rm QCD}$. Despite the fact that m_p is not an elementary, this choice is convenient because μ naturally appears as a scale factor when expressing atomic frequencies. In this framework, a given atomic transition A is characterized by its sensitivities k_A^α, k_A^μ and k_A^q, such that :

$$\frac{d\nu_A}{\nu_A} = k_A^\alpha \times \frac{d\alpha}{\alpha} + k_A^\mu \times \frac{d\mu}{\mu} + k_A^q \times \frac{d(m_q/\Lambda_{\rm QCD})}{(m_q/\Lambda_{\rm QCD})}. \tag{5.3}$$

A given frequency ratio is characterized by the corresponding sensitivity differences. Three well-chosen atomic frequency comparisons can test a putative change of the 3 parameters k_A^α, k_A^μ and k_A^q, which tests both the strong and the electroweak interactions. More than three comparisons provide redundant and predictive tests in case of a non zero observation. Given the dramatic implications of such finding, this possibility and the possibility to redo the experiments are distinct advantages of this type of laboratory tests.

For the purpose of these tests, electronic transitions are sensitive to α only, hyperfine transitions are sensitive of the 3 parameters, with sensitivity $k_{\rm hfs}^\mu = 1$ to μ (since $\nu_{\rm hfs} \sim g \times \mu \times \alpha^2 F(\alpha)$ with g the nuclear g-factor), molecular vibrational and rotational transitions are sensitive to μ with sensitivity

1/2 and 1 respectively, etc. Sensitivities are estimated from theory. k_A^α coefficients are determined from quantum electrodynamics (QED) calculations in atoms with uncertainties of 1% to 10%. k_A^μ are typically known to much better than 1%. k_A^q coefficients depend on quantum chromodynamics and on proton and nuclei structure calculations. They are the less well known, with uncertainties of 10% to 100%.

One can search for two main types of variations, slow drift with time and variations correlated with the Earth motion. In the most basic interpretation of such variations, drift with time at present epoch is associated with evolution of the Universe at cosmological timescale. Variations correlated with time can be related to the variation of Sun gravitational potential at the clocks due the elliptic Earth orbit (the amplitude of this annual sinusoidal modulation of the potential is 1.65×10^{-10}). They can be described as a null gravitational redshift test between clocks in the gravitational potential of the Earth. They can also be described as a test for variation of fundamental constants with gravity. These variations can also be considered as variations (gradients) of fundamental constants in space, explored by the motion of the Earth around the Sun and of the Sun in the galaxy, with respect of a preferred frame, like the frame of the cosmic microwave background.

Going one step further, such experiments can be analyzed to test alternative theories developed with the aim to tackle difficulties of the framework defined by general relativity and the standard models. There are many different categories of such alternative theories, which can lead to different picture or explanation for variation of constants. The result of experiments stated in terms of variations or bound to variations of k_A^α, k_A^μ and k_A^q provides unambiguous information to constrain a given theory or class of theories. Here, we will briefly mention one type of theories, where it is assumed that an addition field φ adds to the metric tensor $g_{\mu\nu}$ of general relativity as a mediator for long range interactions between masses, and that some of parameters of the standard model ($\alpha, \Lambda_{\rm QCD}, m_e, m_u, m_d, ...$) becomes effective constants weakly depending on φ. Within such framework, the interpretation of slow drift can be that the expectation value of φ at the clock is changing in relation, for instance, the cosmological evolution, itself consistently modelled within the alternative framework. Within such comprehensive theory, present epoch variations can be related to variations at cosmological timescale tested by astronomical observations (see e.g. [138][139][140][141][142]) and, overall, test the proposed theory. The whole approach becomes even more relevant when including several other observation also constraining the value of constants over geological or cosmological timescale (see the review [131]). Within the same framework, variations correlated with the Earth motion can be described due to the modulation of φ at the clock position with respect to the

source of φ: the Sun, the galaxy. In some case, φ and the overall alternative theory can be itself an effective manifestation in the 4-dimensional space-time of a more fundamental overlaying theory (see e.g. [143][144]), etc.

Over the years, we applied high accuracy atomic frequency standard comparisons to testing the stability of natural constants. In [112], we pioneered using laser-cooled atomic fountains of ^{87}Rb and ^{133}Cs. The Rb/Cs ratio is sensitive to the combination of constant $g_{\rm Rb}/g_{\rm Cs}\alpha^{-0.49}$ where $g_{\rm Rb}$ and $g_{\rm Cs}$ are the nuclear g-factors [134]. When further adding inputs from nuclear structure models, one can finally relate this atomic hyperfine frequency ratio to $\alpha^{-0.49}(m_q/\Lambda_{\rm QCD})^{-0.021}$ [135]. In [145][128], we presented an updated version of this test where both time variation and coupling to gravity are considered. Variations of the Rb/Cs frequency ratio are constrained at the level of $d\ln(\nu_{\rm Rb}/\nu_{\rm Cs})/dt = (-11.6 \pm 6.1) \times 10^{-17}{\rm yr}^{-1}$ and $c^2 d\ln(\nu_{\rm Rb}/\nu_{\rm Cs})/dU = (7.4 \pm 6.5) \times 10^{-7}$, which are some of the tightest constrains to date for any frequency ratio, if not the tightest. This tested is supported by a large data set spanning more than 15 years and cumulating more than 1000 days of measurements. The same constraints apply to $\alpha^{-0.49}(m_q/\Lambda_{\rm QCD})^{-0.021}$.

As described previously in Sec. 3.1 and Sec. 4.3, one or several hydrogen masers are permanently used as part of the LNE-SYRTE ultra-stable reference and of UTC(OP) timescale generation. Hydrogen masers are based on the hyperfine transition in hydrogen at 1.4 GHz. In [146], we exploit the Cs/H and Rb/H frequency ratio measurements over 8 yr and 5 yr respectively to perform two other null redshift tests : $|c^2 d\ln(\nu_{\rm Cs}/\nu_{\rm H})/dU| < 4.8 \times 10^{-6}$ and $|c^2 d\ln(\nu_{\rm Rb}/\nu_{\rm H})/dU| < 10^{-5}$. Cs/H and Rb/H frequency ratios are sensitive to $\alpha^{0.83}(m_q/\Lambda_{\rm QCD})^{0.102}$ and $\alpha^{0.34}(m_q/\Lambda_{\rm QCD})^{0.081}$ respectively. Here, the lack of accuracy and long term stability of hydrogen masers prevent using these comparisons for searching for time variations of natural constants. Instead, redshift tests rely upon searching for periodic modulation at specific frequencies (annual and sidereal) such that other part of the spectrum (e.g. diurnal period) can be used bound the influence of systematic biases and instabilities in masers.

In [147], we reported a series of absolute frequency measurements of the $^{199}{\rm Hg}^+$ single ion optical clock against a Cs fountain, an experiment done at NIST (Boulder, USA). At the time, this experiment gave the most accurate absolute frequency for an optical transition, with an uncertainty of 1 part in 10^{14} almost entirely limited by the $^{199}{\rm Hg}^+$ clock. Measurements were used to test the stability of constants. We found $|d\ln(\nu_{\rm Cs}/\nu_{\rm Hg^+})/dt| < 7 \times 10^{-15}{\rm yr}^{-1}$, which constrains $\alpha^{5.77}\mu(m_q/\Lambda_{\rm QCD})^{0.002}$ to the same level. Here, we see the quite high sensitivity of this comparison to a putative variation of α. Heavy atoms and ions with tend to have high relativistic corrections, yielding

high sensitivity to α. The $5d^{10}6s\ ^2S_{1/2} - 5d^9 6s^2\ ^2D_{5/2}$ electric quadrupole transition in $^{199}Hg^+$ also has a negative sensitivity to α, which is rather unusual. The large negative sensitivity of Hg^+ $k^{\alpha}_{Hg^+} = -2.94$ combines with a high positive sensitivity of hyperfine transition (α^2 and relativistic correction factor) $k^{\alpha}_{Cs} = +2.83$ to give a tight constraint on putative α variation.

Absolute frequency measurements of the ^{87}Sr like the one described in Sec. 4.2 can be used in a similar manner [148]. In [116][128], we report constraints using both latest high accurate measurements made at SYRTE and measurements made by other institutes. In this case, given the many institutes running Sr optical lattice clock experiments, it is beneficial and relevant to combine from all places. We had $d\ln(\nu_{Cs}/\nu_{Sr})/dt = (2.3 \pm 1.8) \times 10^{-16}\mathrm{yr}^{-1}$ and $c^2 d\ln(\nu_{Cs}/\nu_{Sr})/dU = (1.3 \pm 1.5) \times 10^{-6}$. The same constraints apply to $\alpha^{2.77}\mu(m_q/\Lambda_{QCD})^{0.002}$. These results will for sure improve significantly in a near future, given the continuing efforts of many institutes to develop highly accurate Sr optical lattice clocks and to link them to primary frequency references [149][117][120].

The work done with LNE-SYRTE fountain ensemble included comparing with the transportable fountain FOM with FO2 and participating to improving FOM. The transportable was moved several times to Max-Planck-Institute for Quantum Optics (Garching, Germany) to measure the frequency of the 1S-2S transition in hydrogen [150], which yielded yet another of test based on the Cs/H(1S-2S) ratio [151]. In 2004, the constraint was at the level of $(3.2 \pm 6.3) \times 10^{-15}\mathrm{yr}^{-1}$. New realizations of this measurement and of the subsequent test can be found in [152][153]. Incidentally, it worth noting here that highly accurate absolute frequency measurements of the 1S-2S transition in hydrogen are key to determining the Rydberg constant R_∞ and the proton charge radius r_p [154], which gives another important input of highly accurate atomic frequency measurements to physics. The inputs are not only for establishing reference values of key natural constants. They are also for deeper understanding atomic and nuclear properties, here for unveiling and investigating the proton size puzzle [155][156][157].

All the above tests becomes more robust when combined together. In [145], we gave such analysis an concluded that putative fractional variations of α, μ and m_q/Λ_{QCD} are constrained at the level of $(-2.5 \pm 2.6) \times 10^{-17}\mathrm{yr}^{-1}$, $(1.5 \pm 3.0) \times 10^{-16}\mathrm{yr}^{-1}$ and $(7.1 \pm 4.4) \times 10^{-15}\mathrm{yr}^{-1}$ respectively for time variations, and at the level of $(0.5 \pm 2.7) \times 10^{-6}$, $(-0.4 \pm 1.5) \times 10^{-5}$ and $(-0.5 \pm 2.8) \times 10^{-5}$ for variations with the gravitational potential. Progress of clocks in the last few years and progress to come will significantly improved upon these values and increase the diversity and redundancy of experiments. Also, it should be noted here that even if most tests of the type discussed here

are using clocks with the highest accuracy, it is also possible to use atomic transitions selected not for their potential for high accuracy but for their extreme sensitivity. Competitive tests using Dysprosium are using this approach [158], i.e. RF transitions used in Dy make very poor atomic frequency standards and the sensitivity is orders of magnitudes higher $|k^{\alpha}_{\mathrm{Dy}}| \sim 10^6 - 10^7$. Largely enhanced sensitivity can appear for transitions between accidentally quasi-degenerate states of different configuration compositions. In Dy, these are two electronic levels of different parities. Proposals ave been made to exploit coincidences between hyperfine and rotational energies in diatomic molecules [159]. The isomeric nuclear transition in ^{229}Th [160] is another example where accidental quasi-degeneracy yields magnified sensitivity [134]. Highly charged ions can also support transitions with enhanced sensitivities by this mechanism and other factors [161]. All these promising alternative approaches are yet to be brought into reality.

5.2 Search for dark matter

Highly accurate atomic frequency ratio measurements can also be used to search for dark matter [162][163][164][165]. Here, we will focus on the case of massive scalar field as a model of dark matter. In the previous section 5.1, we mentioned alternative theories where an additional scalar field φ is introduced. Such field, if massive, can be a candidate for dark matter which exhibits oscillatory behaviour at frequency $m_{\varphi}c^2/h$, where m_{φ} is the mass characterizing the field. Under the further assumption that φ has a non-zero coupling to standard model fields, oscillatory behaviour of α, Λ_{QCD}, m_e, m_u, m_d,... will be induced (see [165][166] and references therein). And in turn, an oscillation of atomic transition frequency ratios will emerge, whose amplitude relates to the k^{α}_A, k^{μ}_A and k^{q}_A of transitions, to the couplings parameters between φ and the standard model and to the local density of dark matter ρ_{DM} (≈ 0.4 GeV.cm^{-3}), which is given by galaxy rotation curves and mass models here specifically applied to the Milky Way [167].

Owing to their high filling factor over the last 6 years, measurements of the Rb/Cs frequency ratio made with FO2 support the determination of the power spectral density of fluctuations of this ratio. Within the above described framework, a bound to couplings between dark matter and standard model fields can be deduced, as a function of the scalar field mass. The result of this analysis is displayed in Fig. 5.1. Couplings constants between light scalar dark matter are tests for $10^{-24}\mathrm{eV} < m_{\varphi} < 10^{-17}\mathrm{eV}$, a range of mass determined by the range of frequencies reached by the measurements, itself determined by corresponding to the durations (bin time and overall dura-

tion). The Rb/Cs tests both the coupling with the electroweak interaction via the fine-structure constant $\alpha(\varphi)$ and the couling with the strong interaction via $m_q(\varphi)/\Lambda_{\mathrm{QCD}}(\varphi)$. The level of the constraint goes from 10^{-8} to 10^{-4} depending on the mass [166]. This test provides is both complementary and competitive with the previous similar test using RF spectroscopy of Dy isotopes [168].

In [169], the same experiments are analyzed in a modified theoretical framework where couplings of light scalar dark matter with Higgs boson, with photon and with light quark are considered and tested.

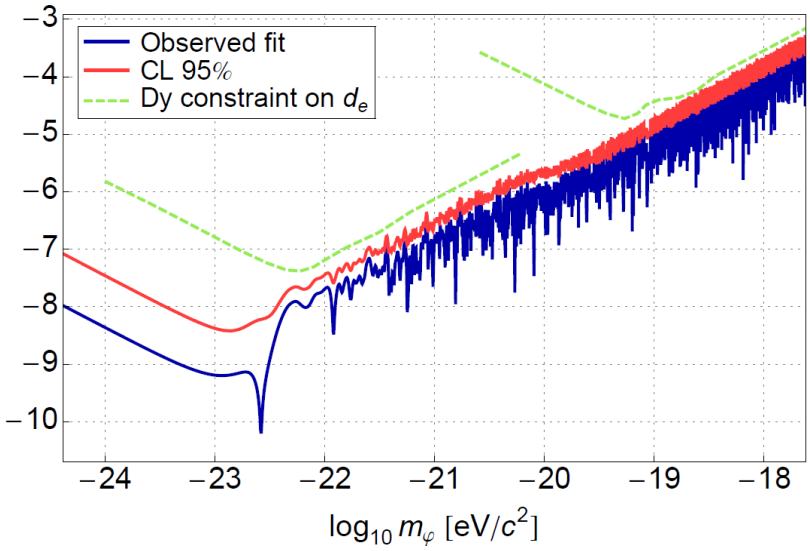

Figure 5.1: Search for dark matter using the Rb/Cs ratio measured with atomic fountain frequency standards: Constraint on coupling constants between a massive scalar field and the standard model as a function of the scalar field mass.

5.3 Local Lorentz invariance in the photon sector

Accurate atomic frequency standards and ultra-stable oscillators also find applications in testing local Lorentz invariance. These tests are modern versions of Michelson-Morley [170], Kennedy-Thorndike [171] and Ives-Stilwell [172] experiments. Here, we used the LNE-SYRTE ultra-stable reference (see Sec. 3.1) to compare the frequency of the ultra-stable cryogenic oscillator and

the frequency of hydrogen masers. As already seen, the frequency of the hydrogen maser is connected to the 1.4 GHz hyperfine transition is atomic hydrogen. The frequency of the cryogenic oscillator instead is the frequency of a particular mode of the electromagnetic field inside a sapphire resonator kept at cryogenic temperature. The frequency of this mode (~ 11.932 GHz) is defined by the dimensions of this macroscopic object. The comparison between the two frequencies is therefore a ratio between an atomic frequency and the frequency defined by the propagation of the electromagnetic field within boundary conditions defined by a macroscopic object. To test local Lorentz invariance, one look for change of this frequency ratio correlated with changes of velocity and orientation of the experiment with respect to the supposedly preferred frame, a natural candidate being the frame of the cosmic microwave background [173]. In our experiment, we rely on the Earth motion to induce changes in velocity and orientation. Putative violations of local Lorentz invariance induce sinusoidal modulations of the ratio, with specific phases, at specific frequency related to the sidereal angular frequency $\omega_\oplus$ and the angular frequency of the Earth orbital motion $\Omega_\oplus$.

In [174][175][176][177], we analyse up to 6 years of quasi-continuous comparison. We assessed and bound perturbations (e.g. due to magnetic field, temperature, atmospheric pressure, tilt, gravity) of the cryogenic oscillator and of hydrogen masers that could mimic the above signatures. A simple alternative framework for analyzing the experiment is the Robertson, Mansouri and Sexl framework [178][179][180][181], where modifications of Lorentz transformation laws are introduced and mathematically described by 3 parameters $\alpha_{\rm rms}, \beta_{\rm rms}, \delta_{\rm rms}$. In special relativity, $\alpha_{\rm rms} = -1/2, \beta_{\rm rms} = 1/2, \delta_{\rm rms} = 0$. Also, in this framework, Michelson-Morley experiments test $P_{\rm MM} = 1/2 - \beta_{\rm rms} + \delta_{\rm rms}$, Kennedy-Thorndike experiments test $P_{\rm KT} = \beta_{\rm rms} - \alpha_{\rm rms} - 1$ and Ives-Stilwell experiments test $P_{\rm IS} = \alpha_{\rm rms} + 1/2$. $P_{\rm MM}$, $P_{\rm KT}$ and $P_{\rm IS}$ are equal to zero in special relativity. Analyzed in this framework, our experiment tests both $P_{\rm MM}$ and $P_{\rm KT}$. In the first analysis [174], it matched the best previous Michelson-Morley experiment [182] and improved the best previous Kennedy-Thorndike experiment [183] by a factor of 30. Analyzing longer data set [177] improved the Kennedy-Thorndike test by another factor of 8, giving $P_{\rm KT} = (-4.8 \pm 3.7) \times 10^{-8}$. To date, this experiment remains the most constraining Kennedy-Thorndike test by more than 2 orders of magnitude. Therefore, it plays an important role in establishing the validity of special relativity. Our Michelson-Morley test was supersede by experiments using rotating pairs of cryogenic resonators allowing for faster averaging of the noise and better assessment of systematic biases [184][185] and then by rotating pairs of optical resonators [186].

Another framework for analyzing this test is the Standard Model Ex-

tension framework [187][188][189]. One of the aim of this framework is to include all possible Lorentz violating terms for all standard model fields. A benefit of this approach is to place many different experiments in single comprehensive framework. In this way, different tests can be compared if they address the same sector. Also, untested sectors are better identified which can motivate new experiments to fill the gaps. As counterpart, the standard model extension has a very large number of parameters and does not give insight on the nature of the possible fundamental overlaying theories. In [175][176], our experiment is analyzed in the standard model extension framework and compared to an experiment based on rotating pairs of optical resonators [190]. Our experiment is sensitive to 7 parameters out of 19 of the photon sector. A summary of Lorentz violation tests in the standard model extension framework is given in [191][192].

5.4 Local Lorentz invariance in the matter sector

Highly accurate atomic spectroscopy can test isotropy of space and mass in modern versions of Hugues-Drever experiments [193][194][195]. FO2-Cs atomic fountain was used to design and implement such a test. The experiment relies on measuring the frequency ν_{+3} and ν_{-3} of the $|F = 3, m_F = +3\rangle \leftrightarrow |F = 4, m_F = +3\rangle$ and $|F = 3, m_F = -3\rangle \leftrightarrow |F = 4, m_F = -3\rangle$ transitions and to search for variations of these frequencies correlated with changes of orientation of the quantization axis (defined by the vertical magnetic field applied in the fountain) with respect to a supposedly preferred reference frame. As for previously described tests, changes of orientation are provided by the motion of the Earth . ν_{+3} and ν_{-3} have a first order Zeeman shift and therefore are sensitive to magnetic field fluctuations. To limit their impact on the test, FO2-Cs was set to run 3 interleaved configurations measuring ν_{+3}, ν_{-3} and ν_0, the frequency of the usual clock transition $|F = 3, m_F = 0\rangle \leftrightarrow |F = 4, m_F = 0\rangle$. The quantity $\nu_c = \nu_{+3} + \nu_{-3} - 2\nu_0$ can then be extracted and correlated with the orientation of the quantization axis. This quantity is immune to the first order Zeeman shift and to frequency fluctuations of the reference hydrogen maser. It largely minimises two of the main sources of noise and biases in the test. We ran two sessions of measurements of 21 and 14 days respectively. We analyzed and bounded potential biases in the test, in particular, biases that could come from unperfect cancellation of the first order Zeeman effect, due to non-identical space and velocity distributions of $m_F = +3$ and $m_F = -3$ atoms and to magnetic field

gradients. As a result, sidereal and semi-sidereal modulations of ν_c could be bound at the level of 60 μHz (which is equivalent to the fT level in terms of magnetic field and to the 10^{-28} GeV range in terms of energy).

The test was analyzed within the already mentioned standard model extension framework. Here, the matter sector is addressed. The complete interpretation of the test requires to determine its sensitivity to parameters pf standard model extension describing violations for different elementary particles. In [196], such sensitivities are calculated. The quantity of interest in this test $\nu_{+3} + \nu_{-3} - 2\nu_0$ connects to Lorentz violating terms via the momentum quadrupole moment of the nucleons in the ^{133}Cs nucleus. With the Schmidt model of the nucleus, only the valence shell proton contributes and our test constrains standard model extension parameters of the proton solely [23]. Recently, this analysis was revisited based on state-of-the-art nuclear structure models (Self-Consistent Relativistic Mean Field, see [197] and references therein), which gave a more accurate value for the sensitivity to proton parameters and showed that the experiment has a non zero sensitivity to neutron parameters. Sensitivity coefficients are $\gamma^p = 8.32 \times 10^{-4}$ and $\gamma^n = 1.76 \times 10^{-5}$. Within a factor close to 1, these dimensionless coefficients relate modulations of ν_c express in energy, i.e. $h\nu_c$, to standard model extension parameters also expressed in energy. As a result, our experiment provided constraints on 9 Lorentz violating parameters, at levels as low as 10^{-24} GeV for the proton and 10^{-22} GeV for the neutrons [197]. For several parameters, this experiment provides the most stringent constraint by many (up to 13) orders of magnitudes [23][197]. See the summary of Lorentz violation tests in the standard model extension framework is given in [191][192].

5.5 Personal publications relevant to chapter 5

[197] *Lorentz-symmetry test at Planck-scale suppression with nucleons in a spin-polarized* ^{133}Cs *cold atom clock.*
H. Pihan-Le Bars, C. Guerlin, R.-D. Lasseri, J.-P. Ebran, Q. G. Bailey, S. Bize, E. Khan and P. Wolf,
Phys. Rev. D **95**, 075026 (2017).

[166] *Searching for an Oscillating Massive Scalar Field as a Dark Matter Candidate Using Atomic Hyperfine Frequency Comparisons.*
A. Hees, J. Guéna, M. Abgrall, S. Bize, and P. Wolf,
Phys. Rev. Lett. **117**, 061301 (2016).

[146] *Testing local position and fundamental constant invariance due to peri-*

odic gravitational and boost using long-term comparison of the SYRTE atomic fountains and H-masers.
M. E. Tobar, P. L. Stanwix, J. J. McFerran, J. Guéna, M. Abgrall, S. Bize, A. Clairon, Ph. Laurent, P. Rosenbusch, D. Rovera and G. Santarelli,

Phys. Rev. D **87**, 122004 (2013).

[145] *Improved tests of Local Position Invariance using* ^{87}Rb *and* ^{133}Cs *fountains.*
J. Guéna, M. Abgrall, D. Rovera, P. Rosenbusch, M. E. Tobar, Ph. Laurent, A. Clairon and S. Bize,
Phys. Rev. Lett. **109**, 080801 (2012).

[177] *Testing local Lorentz and position invariance and variation of fundamental constants by searching the derivative of the comparison frequency between a cryogenic sapphire oscillator and hydrogen maser.*
M. E. Tobar, P. Wolf, S. Bize, G. Santarelli, and V. Flambaum,
Phys. Rev. D **81**, 022003 (2010).

[23] *Cold Atom Clock Test of Lorentz Invariance in the Matter Sector.*
P. Wolf, F. Chapelet, S. Bize, and A. Clairon,
Phys. Rev. Lett. **96**, 060801 (2006).

[175] *Improved test of Lorentz invariance in electrodynamics.*
P. Wolf, S. Bize, A. Clairon, G. Santarelli, M.E. Tobar and A.N. Luiten,
Phys. Rev. D **70**, 051902(R) (2004).

[151] *New Limits to the Drift of Fundamental Constants from Laboratory Measurements.*
M. Fischer, N. Kolachevsky, M. Zimmermann, R. Holzwarth, Th. Udem, T.W. Haensch, M. Abgrall, J. Gruenert, I. Maksimovic, S. Bize, H. Marion, F. Pereira Dos Santos, P. Lemonde, G. Santarelli, P. Laurent, A. Clairon, C. Salomon, M. Haas, U.D. Jentschura and C.H. Keitel,
Phys. Rev. Lett. **92**, 230802 (2004).

[176] *Whispering Gallery Resonators and Tests of Lorentz Invariance.*
P. Wolf, M.E. Tobar, S. Bize, A. Clairon, A.N. Luiten and G. Santarelli,
Gen. Rel. Grav. **36**, 2352 (2004).

[147] *Testing the Stability of Fundamental Constants with the* $^{199}Hg^{+}$ *Single-Ion Optical Clock.*

S. Bize, S.A. Diddams, U. Tanaka, C.E. Tanner, W.H. Oskay, R.E. Drullinger, T.E. Parker, T.P. Heavner, S.R. Jefferts, L. Hollberg, W.M. Itano, and J.C. Bergquist,
Phys. Rev. Lett. **90**, 150802 (2003).

[174] *Tests of Lorentz Invariance using a Microwave Resonator.* P. Wolf, S. Bize, A. Clairon, A.N. Luiten, G. Santarelli and M.E. Tobar,
Phys. Rev. Lett. **90**, 060402 (2003).

[112] *Search for Variations of Fundamental Constants using Atomic Fountain Clocks.*
H. Marion, F. Pereira Dos Santos, M. Abgrall, S. Zhang, Y. Sortais, S. Bize, I. Maksimovic, D. Calonico, J. Grünert, C. Mandache, P. Lemonde, G. Santarelli, Ph. Laurent, A. Clairon and C. Salomon,
Phys. Rev. Lett. **90**, 150801 (2003).

Chapter 6

Conclusions and prospects

6.1 Conclusions and prospects

We will now discuss possible continuations of the above described researches.

In the coming years, the ACES space mission is scheduled to fly between the second half of 2018 and the end 2021. During this period of time, having the best possible realization the Cs hyperfine transition on ground is key, in particular, for the gravitational redshift test. To this end, LNE-SYRTE fountain ensemble will be run continuously at its best level of performance. Before that, additional systematic shifts studies shall be considered, if time allows. These are relevant both for fountain standards but also specifically for the PHARAO cold Cs atomic clock onboard ACES. For instance, experiments on microwave lensing and background gas collision shifts would have high value to build confidence and possibly reduce stated uncertainties [198]. Elaboration of the UTC(OP) experiments and connecting it to the ACES ground terminal will be just as important for all objectives of the mission. Of course, these tasks are compatible with most other applications of fountain standards, which will continue during the ACES mission.

The Hg experiment offers many possibilities. Developing the setup as a highly accurate optical frequency standard will remain one of the main directions. Realizing the full potential of this atom is far from being done. One of key enabling step, yet to be accomplished, will be to make the 2 dimensional magneto-optical trap (2D-MOT) a permanent resource for experiments. The 2D-MOT shall give many advantages and possibilities. All other things being equal, it shall increase the loading rate of atom into the magneto-optic trap by a factor of at least 10. The most straightforward exploitation would be to largely reduce the cycle time and simultaneously improve the duty cycle of the clock sequence. Short term stability in the low 10^{-16} at 1 s shall

follow, with the same interrogation laser. With lasers under development at SYRTE, which are expected to match or surpass current state of the art [199][200][201][202], Hg lattice clock equipped with a 2D-MOT shall give stability $< 10^{-16}$ at 1 s needed for investigating individual shifts at the $< 10^{-18}$ level. The 2D-MOT will also allow increased atom number for collision studies. It will yield reduced the background of hot Hg atoms, which is turn will increase the lifetime of atoms in the lattice and lower the background gas shift. Currently, the blackbody radiation sensitivity of Hg comes from theory [54]. To bring the uncertainty down to 10^{-18}, it is necessary to address this effect experimentally. One approach would be to do precise Stark shift determination and possibly additional measurements as in [203][204][205]. Another approach would be to set up cryogenic environment. The blackbody radiation shift of Hg is less than 10^{-18} at liquid nitrogen temperature (77 K). Measurements at cryogenic temperature and room temperature could be use to determine the room temperature shift. The sensitivity of blackbody shift of Hg at room temperature is only $2.3 \times 10^{-18}\mathrm{K}^{-1}$. A moderately demanding control of the environment would then enable high reproducibility and accuracy. One key aspect to study will be lattice induced light shifts. On the positive side, the ^{199}Hg isotope has a spin 1/2 and therefore no tensor light shift sensitivity. On the down side, theory points toward comparatively higher non-linear light shifts in Hg [80][206]. Measuring these effects will help confirming theoretical predictions (which differ significantly between [80] and [206]). They might define the ultimate accuracy achievable with Hg. We can expect that this limit will be in the low 10^{-18} or less.

Many other possible studies could be done the Hg experiment. One could investigate methods to further cool and manipulate atoms in the lattice trap, for instance, using side-band cooling with the optical clock transition. One could measure lifetime of atomic levels and contribute narrowing down atomic structure calculations. These studies would likely benefit the lattice clock. Collisions and photo-associative collisions with the many isotopes of Hg in the laser-cooled regime are little explored. Studying is relevant for the lattice clock and would help defining the best route toward quantum degenerate gases of Hg and cold molecules. Investigating potential specific interest of other isotopes than ^{199}Hg for the clock could be done as well, and yield highly accurate isotope shifts. In turn, advancing knowledge in atomic properties of laser cooled Hg will allow better defining whether and how to undertake other research, for instance to detect the nuclear anapole moment of Hg via light shift measurements [207].

One major prospect in the field of optical frequency metrology is to further develop and exploit optical fiber links [108]. One benefit will be to enlarge the number and diversity of atomic frequency ratio that can be mea-

sured accurately and used for fundamental physics tests. In this respect, Hg is particularly attractive because it is at the same a candidate of extreme accuracy, a frequency standard with high sensitivity of α variations and an atomic species not used elsewhere in Europe for frequency standards. European optical fiber links will give access to several yet unmeasured optical frequency ratios involving Hg, like for instance Hg/Yb^+(E3), Hg/Yb^+(E2), Hg/$^{88}Sr^+$. Adding this new ratios will enhance fundamental physics tests by making them more stringent and more robust.

Atomic frequency standards emerged as a tool to search for dark matter. Tests like the one reported in Section 5.2 will continue and improve as a result of developments considered previously. They will enrich as a result of progress in accuracy and operability made by optical frequency standards and optical fiber links. With theorists, new investigations will be considered to exploit all possibilities offered by the clock ensemble at SYRTE, by its optical fiber link connections and by the original configuration of the dual Rb and Cs fountain. One could see how different types of hypothetical dark matter could be tested or constrained.

Optical frequency standards surpass atomic fountain primary frequency standards by up to 2 orders of magnitude in terms of stability and uncertainty. A redefinition of the second of the international system of units based on optical transition(s) is therefore logical and desirable. For such a redefinition to be agreed upon and implemented, criteria others than the pure best performance achieved by a particular standard must be accounted for. Continuity between the current and the new definition must be guaranteed. Equivalence of realizations based on the new definition must be checked and means to check on regular basis must be durable. Capability to continue realizing TAI at the same level or better must be proven. Sufficiently wide dissemination of realizations based on the new definition shall be effective, possibly through measurements beforehand of optical frequency ratios. Dedicated efforts will be made with the SYRTE clock ensemble to contribute fulfilling these requirements and to prepare for after the redefinition. Of course, only the sum of coordinated efforts of a wide community will bring readiness for redefinition. In its strategy document, the consultative committee for time and frequency (CCTF) of the international committee for weights and measures (CIPM) anticipates that redefinition could be possible at the 2026 general conference on weights and measures (CGPM) at the earliest.

Accuracy of atomic frequency standards and of means of comparing them remotely is such that effects of Earth's gravity on space-time must be taken into account in most applications. The first and foremost effect is Einstein's gravitational redshift [208]: two identical frequency standards located in dif-

ferent gravitational potentials appear to have different frequencies when compared remotely [209]. This effect can be understood as coming from the fact that proper time at the two frequency standard locations is modified depending on the local value of the gravitational potential. The effect comes from the structure of space-time modified by massive object. It does not depend on the nature of the two identical frequency standards: $\nu_2/\nu_1 = [1-(U_2-U_1)/c^2]$ where U_1 and U_2 refer to the gravitational potential at the two frequency standard positions. Near the Earth's surface the gravitational redshift amount to $\sim 10^{-16}\mathrm{m}^{-1}$. One readily sees that realization of global timescale such as TAI in the vicinity of the Earth is only possible in the framework of general relativity with the gravitational redshift precisely taken into account. Similarly so for global navigation satellite systems and for any comparison of frequency standards. This is one of the main goals of the ACES mission to measure the gravitational redshift with increased precision [92][126][127].

Conversely, remote comparisons of frequency standards near the Earth's surface can be viewed as a way to gain knowledge on the gravitational potential. This leads to the idea of chronometric geodesy [210] and of using frequency standards as sensors for Earth sciences. The advent of optical frequency metrology at the 10^{-18} level means the possibility to reach 1 cm resolution in height. One interesting prospect of the field is therefore to assess the potential of this novel approach and to further develop it into a method of observation for geodesy and Earth sciences. With these ideas in mind, SYRTE initiated a collaboration with Laboratoire de recherche en géodésie (LAREG) de l'Institut national de l'information géographique et forèstière (IGN). Joint work led to one of the first quantitative study of how chronometric geodesy can improve high spatial resolution gravity field models [211]. More studies of this type will help defining cases of highest interest for pilot future experiments. On the experimental and instrumental side, several group worldwide started developing transportable optical frequency standards [212][213]. Coherent optical fiber links provide means to compare optical frequency standards to better than 10^{-18} up to continental scales. They recently enabled proof-of-principle experiments [108][214]. Fiber links will be crucial to further advance chronometric geodesy. They nevertheless will always remain restricted in their geographic coverage. It would therefore be of high interest to develop means of comparing to 10^{-18} everywhere. Free space ground-air-ground optical links [215][216] bridging distances of a few 100 km and extending the capability of fiber links would be a way forward.

6.2 Personal publications relevant to chapter 6

[211] *Determination of a high spatial resolution geopotential model using atomic clock comparisons.*
G. lion, I. Panet, P. Wolf, C. Guerlin, S. Bize and P. Delva,
Journal of Geodesy **91**, 597 (2017).

Appendix A

Bibliography

[1] S. Bize and et al., "Réalisation et diffusion de la seconde au lne-syrte fondées sur l'utilisation d'horloges en fontaine atomique," *Revue Française de Métrologie*, vol. 18, p. 13, 2009.

[2] S. Bize, "Tests fondamentaux à l'aide d'horloges à atomes froids de rubidium et de cesium," Ph.D. dissertation, Université de Paris VI, 2001.

[3] Y. Sortais, "Construction d'une fontaine double à atomes froids de ^{87}Rb et de ^{133}Cs, étude des effets dépendant du nombre d'atomes dans une fontaine." Ph.D. dissertation, Université de Paris VI, 2001.

[4] S. Weyers, U. Hübner, R. Schröder, C. Tamm, and A. Bauch, "Uncertainty evaluation of the atomic caesium fountain CSF1 of the PTB," *Metrologia*, vol. 38, p. 343, 2001.

[5] V. Gerginov, N. Nemitz, S. Weyers, R. Schroder, D. Griebsch, and R. Wynands, "Uncertainty evaluation of the caesium fountain clock ptb-csf2," *Metrologia*, vol. 47, no. 1, pp. 65–79, 2010. [Online]. Available: http://stacks.iop.org/0026-1394/47/65

[6] K. Szymaniec, W. Chalupczak, P. B. Whibberley, S. N. Lea, and D. Henderson, "Evaluation of the primary frequency standard npl-csf1," *Metrologia*, vol. 42, no. 1, p. 49, 2005. [Online]. Available: http://stacks.iop.org/0026-1394/42/i=1/a=007

[7] K. Szymaniec, S. E. Park, G. Marra, and W. ChaÅĆupczak, "First accuracy evaluation of the npl-csf2 primary frequency standard," *Metrologia*, vol. 47, no. 4, p. 363, 2010. [Online]. Available: http://stacks.iop.org/0026-1394/47/i=4/a=003

[8] S. Jefferts, J. Shirley, T. Parker, T. Heavner, D. Meekhof, C. Nelson, F. Levi, G. Costanzo, A. DeMarchi, R. Drullinger, L. Hollberg, W. Lee, and F. Walls, "Accuracy evaluation of NIST-F1," *Metrologia*, vol. 39, p. 321, 2002.

[9] T. P. Heavner, E. A. Donley, F. Levi, G. Costanzo, T. E. Parker, J. H. Shirley, N. Ashby, S. Barlow, and S. R. Jefferts, "First accuracy evaluation of NIST-F2," *Metrologia*, vol. 51, no. 3, p. 174, 2014. [Online]. Available: http://stacks.iop.org/0026-1394/51/i=3/a=174

[10] F. Levi, D. Calonico, C. E. Calosso, A. Godone, S. Micalizio, and G. A. Costanzo, "Accuracy evaluation of ITCsF2: a nitrogen cooled caesium fountain," *Metrologia*, vol. 51, no. 3, p. 270, 2014. [Online]. Available: http://stacks.iop.org/0026-1394/51/i=3/a=270

[11] F. Levi, D. Calonico, L. Lorini, and A. Godone, "Ien-csf1 primary frequency standard at inrim: accuracy evaluation and tai calibrations," *Metrologia*, vol. 43, no. 6, p. 545, 2006. [Online]. Available: http://stacks.iop.org/0026-1394/43/i=6/a=010

[12] Y. Ovchinnikov and G. Marra, "Accurate rubidium atomic fountain frequency standard," *Metrologia*, vol. 48, no. 3, p. 87, 2011. [Online]. Available: http://stacks.iop.org/0026-1394/48/i=3/a=003

[13] B. Kokkelmans, B. Verhaar, K. Gibble, and D. Heinzen, "Predictions for laser cooled Rb clocks," *Phys. Rev. A.*, vol. 56, p. R4389, 1997.

[14] K. Gibble and S. Chu, "A laser cooled Cs frequency standard and a measurement of the frequency shift due to ultra-cold collisions," *Phys. Rev. Lett.*, vol. 70, p. 1771, 1993.

[15] A. Clairon, P. Laurent, G. Santarelli, S. Ghezali, S. Lea, and M. Bahoura, "A cesium fountain frequency standard: recent results," *IEEE Trans. on Inst. and Meas.*, vol. 44, no. 2, p. 128, 1995.

[16] C. Fertig and K. Gibble, "Measurement and cancellation of the cold collision frequency shift in an ^{87}Rb fountain clock," *Phys. Rev. Lett.*, vol. 85, p. 1622, 2000.

[17] Y. Sortais, S. Bize, C. Nicolas, A. Clairon, C. Salomon, and C. Williams, "Cold collision frequency shifts in a ^{87}Rb fountain," *Phys. Rev. Lett.*, vol. 85, p. 3117, 2000.

[18] S. Bize, Y. Sortais, C. Mandache, A. Clairon, and C. Salomon, "Cavity frequency pulling in cold atom fountains," *IEEE Trans. on Instr. and Meas.*, vol. 50, p. 503, 2001.

[19] S. Peil, S. Crane, J. Hanssen, T. Swanson, and C. Ekstrom, "An ensemble of atomic fountains," in *Frequency Control Symposium (FCS), 2012 IEEE International*, may 2012, pp. 1–4.

[20] S. Peil, J. L. Hanssen, T. B. Swanson, J. Taylor, and C. R. Ekstrom, "Evaluation of long term performance of continuously running atomic fountains," *Metrologia*, vol. 51, no. 3, p. 263, 2014. [Online]. Available: http://stacks.iop.org/0026-1394/51/i=3/a=263

[21] F. Chapelet, "Fontaine atomique double de Césium et de Rubidium avec une exactitude de quelques 10^{-16} et applications," Ph.D. dissertation, Université de Paris XI, 2008.

[22] J. Guéna, P. Rosenbusch, P. Laurent, M. Abgrall, D. Rovera, G. Santarelli, M. Tobar, S. Bize, and A. Clairon, "Demonstration of a dual alkali Rb/Cs fountain clock," *Ultrasonics, Ferroelectrics and Frequency Control, IEEE Transactions on*, vol. 57, no. 3, p. 647, 2010. [Online]. Available: https://doi.org/10.1109/TUFFC.2010.1461

[23] P. Wolf, F. Chapelet, S. Bize, and A. Clairon, "Cold atom clock test of Lorentz Invariance in the matter sector," *Phys. Rev. Lett.*, vol. 96, no. 6, p. 060801, 2006. [Online]. Available: http://link.aps.org/abstract/PRL/v96/e060801

[24] F. Pereira Dos Santos, H. Marion, S. Bize, Y. Sortais, A. Clairon, and C. Salomon, "Controlling the cold collision shift in high precision atomic interferometry," *Phys. Rev. Lett.*, vol. 89, p. 233004, 2002.

[25] K. Gibble, "Fountain clock accuracy," in *Proceedings of the 2012 European Frequency and Time Forum*, 2012, pp. 16–18.

[26] K. Szymaniec, W. Chałupczak, E. Tiesinga, C. J. Williams, S. Weyers, and R. Wynands, "Cancellation of the collisional frequency shift in caesium fountain clocks," *Phys. Rev. Lett.*, vol. 98, no. 15, p. 153002, 2007.

[27] K. Szymaniec and S. E. Park, "Primary frequency standard NPL-CsF2: Optimized operation near the collisional shift cancellation point," *Instrumentation and Measurement, IEEE Transactions on*, vol. 60, no. 7, pp. 2475 –2481, 2011.

[28] D. J. Papoular, S. Bize, A. Clairon, H. Marion, S. J. J. M. F. Kokkelmans, and G. V. Shlyapnikov, "Feshbach resonances in cesium at ultralow static magnetic fields," *Phys. Rev. A*, vol. 86, p. 040701, Oct 2012. [Online]. Available: http://link.aps.org/doi/10.1103/PhysRevA.86.040701

[29] C. Chin, R. Grimm, P. Julienne, and E. Tiesinga, "Feshbach resonances in ultracold gases," *Rev. Mod. Phys.*, vol. 82, no. 2, pp. 1225–1286, Apr 2010.

[30] R. A. Hart, X. Xu, R. Legere, and K. Gibble, "A quantum scattering interferometer," *Nature*, vol. 446, no. 7138, pp. 892–895, Apr. 2007. [Online]. Available: http://dx.doi.org/10.1038/nature05680

[31] S. D. Gensemer, R. B. Martin-Wells, A. W. Bennett, and K. Gibble, "Direct observation of resonant scattering phase shifts and their energy dependence," *Phys. Rev. Lett.*, vol. 109, p. 263201, Dec 2012. [Online]. Available: http://link.aps.org/doi/10.1103/PhysRevLett.109.263201

[32] A. Bennett, K. Gibble, S. Kokkelmans, and J. M. Hutson, "Atomic clock measurements of quantum scattering phase shifts spanning feshbach resonances at ultralow fields," *Phys. Rev. Lett.*, vol. 119, p. 113401, Sep 2017. [Online]. Available: https://link.aps.org/doi/10.1103/PhysRevLett.119.113401

[33] F. Chapelet, S. Bize, P. Wolf, G. Santarelli, P. Rosenbusch, M. Tobar, P. Laurent, C. Salomon, and A. Clairon, "Investigation of the distributed cavity phase shift in an atomic fountain," in *Proceedings of the 2006 EFTF, Braunschweig, Germany*, 2006.

[34] J. Guéna, R. Li, K. Gibble, S. Bize, and A. Clairon, "Evaluation of Doppler shifts to improve the accuracy of primary atomic fountain clocks," *Phys. Rev. Lett.*, vol. 106, no. 13, p. 130801, Apr 2011. [Online]. Available: https://doi.org/10.1103/PhysRevLett.106.130801

[35] R. Li and K. Gibble, "Phase variations in microwave cavities for atomic clocks," *Metrologia*, vol. 41, no. 6, pp. 376–386, 2004. [Online]. Available: http://stacks.iop.org/0026-1394/41/376

[36] J. Guéna, S. Bize, A. Clairon, R. Li, and K. Gibble, "Quantitative evaluation of distributed cavity phase shifts to improve the accuracy of SYRTE FO2," in *Frequency Control and the European Frequency and Time Forum (FCS), 2011 Joint Conference of the IEEE International*, may 2011, p. 61.

[37] J. Guéna, M. Abgrall, D. Rovera, P. Laurent, B. Chupin, M. Lours, G. Santarelli, P. Rosenbusch, M. Tobar, R. Li, K. Gibble, A. Clairon, and S. Bize, "Progress in atomic fountains at LNE-SYRTE," *Ultrasonics, Ferroelectrics and Frequency Control, IEEE Transactions on*, vol. 59, no. 3, pp. 391–410, march 2012. [Online]. Available: https://doi.org/10.1109/TUFFC.2012.2208

[38] R. Li, K. Gibble, and K. Szymaniec, "Improved accuracy of the NPL-CsF2 primary frequency standard: evaluation of distributed cavity phase and microwave lensing frequency shifts," *Metrologia*, vol. 48, no. 5, p. 283, 2011. [Online]. Available: http://stacks.iop.org/0026-1394/48/i=5/a=007

[39] S. Weyers, V. Gerginov, N. Nemitz, R. Li, and K. Gibble, "Distributed cavity phase frequency shifts of the caesium fountain ptb-csf2," *Metrologia*, vol. 49, no. 1, p. 82, 2012. [Online]. Available: http://stacks.iop.org/0026-1394/49/i=1/a=012

[40] R. Li and K. Gibble, "Evaluating and minimizing distributed cavity phase errors in atomic clocks," *Metrologia*, vol. 47, no. 5, p. 534, 2010. [Online]. Available: http://stacks.iop.org/0026-1394/47/i=5/a=004

[41] K. Gibble, S. Lea, and K. Szymaniec, "A microwave cavity designed to minimize distributed cavity phase errors in a primary cesium frequency standard," in *Precision Electromagnetic Measurements (CPEM), 2012 Conference on*, 2012, pp. 700–701.

[42] G. Dick, "Local oscillator induced instabilities in trapped ion frequency standards," in *Proc. of Precise Time and Time Interval*, Redendo Beach, 1987, pp. 133–147.

[43] G. J. Dick, J. D. Prestage, C. A. Greenhall, and L. Maleki, "Local oscillator induced degradation of medium-term stability in passive atomic frequency standards," *Proc. of te 22nd PTTI*, 1990.

[44] G. Santarelli, C. Audoin, A. Makdissi, P. Laurent, G. J. Dick, and A. Clairon, "Frequency stability degradation of an oscillator slaved to a periodically interrogated atomic resonator," *IEEE Trans. on Ultr., Ferr. and Freq. Contr.*, vol. 45, p. 887, 1998.

[45] G. Santarelli, P. Laurent, P. Lemonde, A. Clairon, A. G. Mann, S. Chang, A. N. Luiten, and C. Salomon, "Quantum projection noise in an atomic fountain: A high stability cesium frequency standard," *Phys. Rev. Lett.*, vol. 82, no. 23, p. 4619, 1999.

[46] D. Chambon, M. Lours, F. Chapelet, S. Bize, M. E. Tobar, A. Clairon, and G. Santarelli, "Design and metrological features of microwave synthesizers for atomic fountain frequency standard," *IEEE Trans. Ultr. Ferr. Freq. Contr.*, vol. 54, p. 729, 2007.

[47] J. L. Hall, "Nobel lecture: Defining and measuring optical frequencies," *Reviews of Modern Physics*, vol. 78, no. 4, p. 1279, 2006. [Online]. Available: http://link.aps.org/abstract/RMP/v78/p1279

[48] T. W. Hansch, "Nobel lecture: Passion for precision," *Reviews of Modern Physics*, vol. 78, no. 4, p. 1297, 2006. [Online]. Available: http://link.aps.org/abstract/RMP/v78/p1297

[49] H. Katori, "Spectroscopy of strontium atoms in the Lamb-Dicke confinement," in *Proc. of the 6th Symposium on Frequency Standards and Metrology*. World scientific, Singapore, 2001, p. 323.

[50] H. Katori, M. Takamoto, V. G. Pal'chikov, and V. D. Ovsiannikov, "Ultrastable optical clock with neutral atoms in an engineered light shift trap," *Phys. Rev. Lett.*, vol. 91, no. 17, p. 173005, Oct 2003.

[51] M. Takamoto and H. Katori, "Spectroscopy of the $s1 - p3$ clock transition of $sr87$ in an optical lattice," *Phys. Rev. Lett.*, vol. 91, no. 22, p. 223001, Nov 2003.

[52] Z. W. Barber, C. W. Hoyt, C. W. Oates, L. Hollberg, A. V. Taichenachev, and V. I. Yudin, "Direct excitation of the forbidden clock transition in neutral ^{174}Yb atoms confined to an optical lattice," *Phys. Rev. Lett.*, vol. 96, p. 083002, Mar 2006. [Online]. Available: http://link.aps.org/doi/10.1103/PhysRevLett.96.083002

[53] 2004, V.G. Pal'chikov, private communication (2004) and H. Katori et al., in proc. of the XIX International Conference on Atomic Physics (2004).

[54] H. Hachisu, K. Miyagishi, S. G. Porsev, A. Derevianko, V. D. Ovsiannikov, V. G. Pal'chikov, M. Takamoto, and H. Katori, "Trapping of neutral mercury atoms and prospects for optical lattice clocks," *Phys. Rev. Lett.*, vol. 100, p. 053001, 2008.

[55] J. Lodewyck, M. Zawada, L. Lorini, M. Gurov, and P. Lemonde, "Observation and cancellation of a perturbing dc stark shift in strontium optical lattice clocks," *Ultrasonics, Ferroelectrics and Frequency Control, IEEE Transactions on*, vol. 59, no. 3, pp. 411 –415, march 2012.

[56] E. J. Angstmann, V. A. Dzuba, and V. V. Flambaum, "Relativistic effects in two valence-electron atoms and ions and the search for variation of the fine-structure constant," *Phys. Rev. A*, vol. 70, p. 014102, 2004.

[57] S. Bize and et al., "Horloge à réseau optique à atomes de mercure," *Revue française de métrologie*, vol. 40, p. 13, 2015.

[58] M. M. Petersen, "Laser-cooling of neutral mercury and laser-spectroscopy of the 1s0-3p0 optical clock transition," Ph.D. dissertation, Université de Paris VI, 2009.

[59] R. Tyumenev, M. Favier, S. Bilicki, E. Bookjans, R. L. Targat, J. Lodewyck, D. Nicolodi, Y. L. Coq, M. Abgrall, J. Guéna, L. D. Sarlo, and S. Bize, "Comparing a mercury optical lattice clock with microwave and optical frequency standards," *New Journal of Physics*, vol. 18, no. 11, p. 113002, 2016. [Online]. Available: http://stacks.iop.org/1367-2630/18/i=11/a=113002

[60] S. Mejri, J. J. McFerran, L. Yi, Y. Le Coq, and S. Bize, "Ultraviolet laser spectroscopy of neutral mercury in a one-dimensional optical lattice," *Phys. Rev. A*, vol. 84, p. 032507, Sep 2011. [Online]. Available: http://link.aps.org/doi/10.1103/PhysRevA.84.032507

[61] Y. Castin and K. Mølmer, "Monte carlo wave-function analysis of 3d optical molasses," *Phys. Rev. Lett.*, vol. 74, no. 19, pp. 3772–3775, May 1995.

[62] M. Petersen, R. Chicireanu, S. T. Dawkins, D. V. Magalhaes, C. Mandache, Y. L. Coq, A. Clairon, and S. Bize, "Doppler-free spectroscopy of the $^1S_0$-$^3P_0$ optical clock transition in laser-cooled fermionic isotopes of neutral mercury," *Phys. Rev. Lett.*, vol. 101, no. 18, p. 183004, 2008. [Online]. Available: http://link.aps.org/abstract/PRL/v101/e183004

[63] J. J. McFerran, L. Yi, S. Mejri, and S. Bize, "Sub-doppler cooling of fermionic hg isotopes in a magneto-optical trap," *Opt. Lett.*, vol. 35, no. 18, pp. 3078–3080, 2010. [Online]. Available: http://ol.osa.org/abstract.cfm?URI=ol-35-18-3078

[64] K. Burns, K. B. Adams, and J. Longwell, "Interference measurements in the spectra of neon and natural mercury," *J. Opt. Soc. Am.*, vol. 40, no. 6, pp. 339–344, 1950. [Online]. Available: http://www.opticsinfobase.org/abstract.cfm?URI=josa-40-6-339

[65] K. Burns and K. B. Adams, "Energy levels and wavelengths of the isotopes of mercury -199 and -200," *J. Opt. Soc. Am.*, vol. 42, p. 716, 1952.

[66] ——, "Energy levels and wavelengths of the isotopes of mercury -198 and -202," *J. Opt. Soc. Am.*, vol. 42, p. 56, 1952.

[67] C. J. Sansonetti, M. L. Salit, and J. Reader, "Wavelengths of spectral lines in mercury pencil lamps," *Appl. Opt.*, vol. 35, no. 1, pp. 74–77, Jan 1996. [Online]. Available: http://ao.osa.org/abstract.cfm?URI=ao-35-1-74

[68] E. B. Saloman, "Wavelengths, energy level classifications, and energy levels for the spectrum of neutral mercury," *Journal of Physical and Chemical Reference Data*, vol. 35, pp. 1519–1548, 2006.

[69] J. Millo, S. Dawkins, R. Chicireanu, D. Magalhaes, C. Mandache, D. Holleville, M. Lours, S. Bize, P. Lemonde, and G. Santarelli, "Ultra-stable optical cavities: Design and experiments at lne-syrte," in *Frequency Control Symposium, 2008 IEEE International*, may 2008, pp. 110 –114.

[70] S. Dawkins, R. Chicireanu, M. Petersen, J. Millo, D. Magalhães, C. Mandache, Y. Le Coq, and S. Bize, "An ultra-stable referenced interrogation system in the deep ultraviolet for a mercury optical lattice clock," *Appl. Phys. B: Lasers and Optics*, vol. 99, p. 41, 2010. [Online]. Available: http://dx.doi.org/10.1007/s00340-009-3830-3

[71] J. L. Hall, C. J. Bordé, and K. Uehara, "Direct optical resolution of the recoil effect using saturated absorption spectroscopy," *Phys. Rev. Lett.*, vol. 37, pp. 1339–1342, 1976.

[72] L. Yi, S. Mejri, J. J. McFerran, Y. Le Coq, and S. Bize, "Optical lattice trapping of ^{199}Hg and determination of the magic wavelength for the ultraviolet $^1S_0 \leftrightarrow {}^3P_0$ clock transition," *Phys. Rev. Lett.*, vol. 106, no. 7, p. 073005, 2011.

[73] J. J. McFerran, L. Yi, S. Mejri, S. Di Manno, W. Zhang, J. Guéna, Y. Le Coq, and S. Bize, "Neutral atom frequency reference in the deep ultraviolet with a fractional uncertainty $= 5.7 \times 10^{-15}$," *Phys. Rev. Lett.*, vol. 108, p. 183004, May 2012. [Online]. Available: http://link.aps.org/doi/10.1103/PhysRevLett.108.183004

[74] K. Yamanaka, N. Ohmae, I. Ushijima, M. Takamoto, and H. Katori, "Frequency ratio of ^{199}Hg and ^{87}Sr optical lattice clocks beyond the SI limit," *Phys. Rev. Lett.*, vol. 114, p. 230801, Jun 2015. [Online]. Available: http://link.aps.org/doi/10.1103/PhysRevLett.114.230801

[75] J. J. McFerran, D. V. M. aes, C. Mandache, J. Millo, W. Zhang, Y. L. Coq, G. Santarelli, and S. Bize, "Laser locking to the hg199s01−p03 clock transition with 5.4×10−15/τ fractional frequency instability," *Opt. Lett.*, vol. 37, no. 17, pp. 3477–3479, Sep 2012. [Online]. Available: http://ol.osa.org/abstract.cfm?URI=ol-37-17-3477

[76] D. Nicolodi, B. Argence, W. Zhang, R. Le Targat, G. Santarelli, and Y. Le Coq, "Spectral purity transfer between optical wavelengths at the 10^{-18} level," *Nat Photon*, vol. 8, p. 219, Jan. 2014. [Online]. Available: http://dx.doi.org/10.1038/nphoton.2013.361

[77] K. Gibble, "Decoherence and collisional frequency shifts of trapped bosons and fermions," *Physical Review Letters*, vol. 103, no. 11, p. 113202, 2009. [Online]. Available: http://link.aps.org/abstract/PRL/v103/e113202

[78] M. Bishof, Y. Lin, M. D. Swallows, A. V. Gorshkov, J. Ye, and A. M. Rey, "Resolved atomic interaction sidebands in an optical clock transition," *Phys. Rev. Lett.*, vol. 106, p. 250801, Jun 2011. [Online]. Available: http://link.aps.org/doi/10.1103/PhysRevLett.106.250801

[79] M. J. Martin, M. Bishof, M. D. Swallows, X. Zhang, C. Benko, J. von Stecher, A. V. Gorshkov, A. M. Rey, and J. Ye, "A quantum many-body spin system in an optical lattice clock," *Science*, vol. 341, no. 6146, pp. 632–636, 2013. [Online]. Available: http://www.sciencemag.org/content/341/6146/632.abstract

[80] H. Katori, V. D. Ovsiannikov, S. I. Marmo, and V. G. Palchikov, "Strategies for reducing the light shift in atomic clocks," *Phys. Rev. A*, vol. 91, p. 052503, May 2015. [Online]. Available: http://link.aps.org/doi/10.1103/PhysRevA.91.052503

[81] L. D. Sarlo, M. Favier, R. Tyumenev, and S. Bize, "A mercury optical lattice clock at lne-syrte," *Journal of Physics: Conference Series*, vol. 723, no. 1, p. 012017, 2016. [Online]. Available: http://stacks.iop.org/1742-6596/723/i=1/a=012017

[82] J. J. McFerran, L. Yi, S. Mejri, W. Zhang, S. Di Manno, M. Abgrall, J. Guéna, Y. Le Coq, and S. Bize, "Statistical uncertainty of 2.5×10^{-16} for the $^{199}hg\ ^{1}s_0 - ^{3}p_0$ clock transition against a primary frequency standard," *Phys. Rev. A*, vol. 89, p. 043432, Apr 2014. [Online]. Available: http://link.aps.org/doi/10.1103/PhysRevA.89.043432

[83] C. Vian, P. Rosenbusch, H. Marion, S. Bize, L. Cacciapuoti, S. Zhang, M. Abgrall, D. Chambon, I. Maksimovic, P. Laurent, G. Santarelli, A. Clairon, A. Luiten, M. Tobar, and C. Salomon, "BNM-SYRTE Fountains: Recent Results," *IEEE Trans. Instrum. Meas.*, vol. 54, p. 833, 2005. [Online]. Available: https://doi.org/10.1109/TIM.2005.843573

[84] S. Bize, P. Laurent, M. Abgrall, H. Marion, I. Maksimovic, L. Cacciapuoti, J. Grünert, C. Vian, F. Pereira dos Santos, P. Rosenbusch, P. Lemonde, G. Santarelli, P. Wolf, A. Clairon, A. Luiten, M. Tobar, and C. Salomon, "Cold atom clocks and applications," *J. Phys. B: Atomic, Molecular and Optical Physics*, vol. 38, no. 9, pp. S449–S468, 2005. [Online]. Available: http://stacks.iop.org/0953-4075/38/S449

[85] ——, "Advances in ^{133}Cs fountains," *C. R. Physique*, vol. 5, p. 829, 2004.

[86] D. Chambon, S. Bize, M. Lours, F. Narbonneau, H. Marion, A. Clairon, G. Santarelli, A. Luiten, and M. Tobar, "Design and realization of a flywheel oscillator for advanced time and frequency metrology," *Rev. Sci. Instrum.*, vol. 76, p. 094704, 2005.

[87] M. Tobar, E. Ivanov, C. Locke, P. Stanwix, J. Hartnett, A. Luiten, R. Warrington, P. Fisk, M. Lawn, M. Wouters, S. Bize, G. Santarelli, P. Wolf, A. Clairon, and P. Guillemot, "Long-term operation and performance of cryogenic sapphire oscillators," *Ultrasonics, Ferroelectrics and Frequency Control, IEEE Transactions on*, vol. 53, no. 12, pp. 2386 –2393, december 2006.

[88] S. Grop, P. Y. Bourgeois, N. Bazin, Y. Kersalé, E. Rubiola, C. Langham, M. Oxborrow, D. Clapton, S. Walker, J. D. Vicente, and V. Giordano, "ELISA: A cryocooled 10 GHz oscillator with 10^{-15} frequency stability," *Rev. Sci. Instrum.*, vol. 81, no. 2, p. 025102, 2010. [Online]. Available: http://link.aip.org/link/?RSI/81/025102/1

[89] S. Grop, W. Schafer, P. Bourgeois, Y. Kersale, M. Oxborrow, E. Rubiola, and V. Giordano, "Unprecedented long-term frequency stability with a microwave resonator oscillator," *Ultrasonics, Ferroelectrics and Frequency Control, IEEE Transactions on*, vol. 58, no. 8, pp. 1694–1697, 2011.

[90] S. Grop, B. Dubois, P. Y. Bourgeois, Y. Kersalé, E. Rubiola, G. Haye, and V. Giordano, "Uliss: A mobile cryogenic ultra-stable oscillator," in *2011 Joint Conference of the IEEE International Frequency Control and the European Frequency and Time Forum (FCS) Proceedings*, May 2011, pp. 1–4.

[91] M. Abgrall, J. Guéna, M. Lours, G. Santarelli, M. E. Tobar, S. Bize, S. Grop, B. Dubois, C. Fluhr, and V. Giordano, "High-stability comparison of atomic fountains using two different cryogenic oscillators," *IEEE Transactions on Ultrasonics, Ferroelectrics, and Frequency Control*, vol. 63, no. 8, pp. 1198–1203, Aug 2016. [Online]. Available: https://doi.org/10.1109/TUFFC.2016.2570898

[92] P. Laurent, D. Massonnet, L. Cacciapuoti, and C. Salomon, "The ACES/PHARAO space mission," *Comptes Rendus Physique*, vol. 16, no. 5, pp. 540 – 552, 2015, the measurement of time / La mesure du temps. [Online]. Available: http://www.sciencedirect.com/science/article/pii/S1631070515000808

[93] C. Fluhr, B. Dubois, S. Grop, J. Paris, G. L. Tetû, and V. Giordano, "A low power cryocooled autonomous ultra-stable oscillator," *Cryogenics*, vol. 80, pp. 164 – 173, 2016. [Online]. Available: http://www.sciencedirect.com/science/article/pii/S0011227516302363

[94] K. Numata, A. Kemery, and J. Camp, "Thermal-noise limit in the frequency stabilization of lasers with rigid cavities," *Phys. Rev. Lett.*, vol. 93, no. 25, p. 250602, 2004. [Online]. Available: http://link.aps.org/abstract/PRL/v93/e250602

[95] T. Legero, T. Kessler, and U. Sterr, "Tuning the thermal expansion properties of optical reference cavities with fused silica mirrors," *J. Opt. Soc. Am. B*, vol. 27, no. 5, pp. 914–919, May 2010. [Online]. Available: http://josab.osa.org/abstract.cfm?URI=josab-27-5-914

[96] J. Millo, D. V. Magalhaes, C. Mandache, Y. L. Coq, E. M. L. English, P. G. Westergaard, J. Lodewyck, S. Bize, P. Lemonde, and G. Santarelli, "Ultrastable lasers based on vibration insensitive

cavities," *Phys. Rev. A*, vol. 79, no. 5, p. 053829, 2009. [Online]. Available: http://link.aps.org/abstract/PRA/v79/e053829

[97] B. Argence, E. Prevost, T. Lévèque, R. L. Goff, S. Bize, P. Lemonde, and G. Santarelli, "Prototype of an ultra-stable optical cavity for space applications," *Opt. Express*, vol. 20, no. 23, pp. 25 409–25 420, Nov 2012. [Online]. Available: http://www.opticsexpress.org/abstract.cfm?URI=oe-20-23-25409

[98] D. Swierad, S. Häfner, S. Vogt, B. Venon, D. Holleville, S. Bize, A. Kulosa, S. Bode, Y. Singh, K. Bongs, E. M. Rasel, J. Lodewyck, R. Le Targat, C. Lisdat, and U. Sterr, "Ultra-stable clock laser system development towards space applications," *Scientific Reports*, vol. 6, p. 33973, Sep. 2016. [Online]. Available: http://dx.doi.org/10.1038/srep33973

[99] J. Millo, M. Abgrall, M. Lours, E. M. L. English, H. Jiang, J. Guéna, A. Clairon, M. E. Tobar, S. Bize, Y. L. Coq, and G. Santarelli, "Ultralow noise microwave generation with fiber-based optical frequency comb and application to atomic fountain clock," *Applied Physics Letters*, vol. 94, no. 14, p. 141105, 2009. [Online]. Available: http://link.aip.org/link/?APL/94/141105/1

[100] W. Zhang, Z. Xu, M. Lours, R. Boudot, Y. Kersalé, G. Santarelli, and Y. L. Coq, "Sub-100 attoseconds stability optics-to-microwave synchronization," *Appl. Phys. Lett.*, vol. 96, no. 21, p. 211105, 2010. [Online]. Available: http://dx.doi.org/10.1063/1.3431299

[101] X. Xie, R. Bouchand, D. Nicolodi, M. Giunta, W. Hänsel, M. Lezius, A. Joshi, S. Datta, C. Alexandre, M. Lours, P.-A. Tremblin, G. Santarelli, R. Holzwarth, and Y. Le Coq, "Photonic microwave signals with zeptosecond-level absolute timing noise," *Nat Photon*, vol. 11, no. 1, pp. 44–47, Jan. 2017. [Online]. Available: http://dx.doi.org/10.1038/nphoton.2016.215

[102] P. Wolf, G. Petit, E. Peik, C. Tamm, H. Schnatz, B. Lipphardt, S. Weyers, R. Wynands, J.-Y. Richard, S. Bize, F. Chapelet, F. Pereira dos Santos, and A. Clairon, "Comparing high accuracy frequency standards via tai," in *Frequency and Time Forum (EFTF), 2006 20th European*, 2006, pp. 476–485.

[103] T. E. Parker, "Long-term comparison of caesium fountain primary frequency standards," *Metrologia*, vol. 47, p. 1, 2010. [Online]. Available: http://stacks.iop.org/0026-1394/47/i=1/a=001

[104] ——, "Invited review article: The uncertainty in the realization and dissemination of the SI second from a systems point of view," *Review of Scientific Instruments*, vol. 83, no. 2, p. 021102, 2012. [Online]. Available: http://link.aip.org/link/?RSI/83/021102/1

[105] G. Petit and G. Panfilo, "Comparison of frequency standards used for TAI," *Instrumentation and Measurement, IEEE Transactions on*, vol. 62, no. 99, p. 1550, 2013.

[106] G. Panfilo and T. E. Parker, "A theoretical and experimental analysis of frequency transfer uncertainty, including frequency transfer into tai," *Metrologia*, vol. 47, no. 5, p. 552, 2010. [Online]. Available: http://stacks.iop.org/0026-1394/47/i=5/a=005

[107] A. Bauch, J. Achkar, S. Bize, D. Calonico, R. Dach, R. Hlavac, L. Lorini, T. Parker, G. Petit, D. Piester, K. Szymaniec, and P. Uhrich, "Comparison between frequency standards in europe and the USA at the 10^{-15} uncertainty level," *Metrologia*, vol. 43, no. 1, pp. 109–120, 2006. [Online]. Available: http://stacks.iop.org/0026-1394/43/109

[108] C. Lisdat, G. Grosche, N. Quintin, C. Shi, S. Raupach, C. Grebing, D. Nicolodi, F. Stefani, A. Al-Masoudi, S. Dorscher, S. Hafner, J.-L. Robyr, N. Chiodo, S. Bilicki, E. Bookjans, A. Koczwara, S. Koke, A. Kuhl, F. Wiotte, F. Meynadier, E. Camisard, M. Abgrall, M. Lours, T. Legero, H. Schnatz, U. Sterr, H. Denker, C. Chardonnet, Y. Le Coq, G. Santarelli, A. Amy-Klein, R. Le Targat, J. Lodewyck, O. Lopez, and P.-E. Pottie, "A clock network for geodesy and fundamental science," *Nat Commun*, vol. 7, p. 12443, Aug. 2016. [Online]. Available: http://dx.doi.org/10.1038/ncomms12443

[109] J. Guéna, S. Weyers, M. Abgrall, C. Grebing, V. Gerginov, P. Rosenbusch, S. Bize, B. Lipphardt, H. Denker, N. Quintin, S. M. F. Raupach, D. Nicolodi, F. Stefani, N. Chiodo, S. Koke, A. Kuhl, F. Wiotte, F. Meynadier, E. Camisard, C. Chardonnet, Y. L. Coq, M. Lours, G. Santarelli, A. Amy-Klein, R. L. Targat, O. Lopez, P. E. Pottie, and G. Grosche, "First international comparison of fountain primary frequency standards via a long distance optical fiber link," *Metrologia*, vol. 54, no. 3, p. 348, 2017. [Online]. Available: http://stacks.iop.org/0026-1394/54/i=3/a=348

[110] F. Riehle, P. Gill, F. Arias, and L. Robertsson, "The CIPM list of recommended frequency standard values: guidelines and procedures,"

Metrologia, vol. 55, no. 2, p. 188, 2018. [Online]. Available: http://stacks.iop.org/0026-1394/55/i=2/a=188

[111] S. Bize, Y. Sortais, M. Santos, C. Mandache, A. Clairon, and C. Salomon, "High-accuracy measurement of the ^{87}Rb ground-state hyperfine splitting in an atomic fountain," *Europhys. Lett.*, vol. 45, no. 5, p. 558, 1999. [Online]. Available: https://doi.org/10.1209/epl/i1999-00203-9

[112] H. Marion, F. Pereira Dos Santos, M. Abgrall, S. Zhang, Y. Sortais, S. Bize, I. Maksimovic, D. Calonico, J. Grünert, C. Mandache, P. Lemonde, G. Santarelli, P. Laurent, A. Clairon, and C. Salomon, "Search for variations of fundamental constants using atomic fountain clocks," *Phys. Rev. Lett.*, vol. 90, p. 150801, 2003. [Online]. Available: https://doi.org/10.1103/PhysRevLett.90.150801

[113] J. Guéna, M. Abgrall, A. Clairon, and S. Bize, "Contributing to TAI with a secondary representation of the si second," *Metrologia*, vol. 51, no. 1, p. 108, 2014. [Online]. Available: http://stacks.iop.org/0026-1394/51/i=1/a=108

[114] X. Baillard, M. Fouché, R. L. Targat, P. G. Westergaard, A. Lecallier, Y. L. Coq, G. D. Rovera, S. Bize, and P. Lemonde, "Accuracy evaluation of an optical lattice clock with bosonic atoms," *Opt. Lett.*, vol. 32, p. 1812, 2007. [Online]. Available: https://doi.org/10.1364/OL.32.001812

[115] X. Baillard, M. Fouché, R. Le Targat, P. G. Westergaard, A. Lecallier, F. Chapelet, M. Abgrall, G. D. Rovera, P. Laurent, P. Rosenbusch, S. Bize, G. Santarelli, A. Clairon, P. Lemonde, G. Grosche, B. Lipphardt, and H. Schnatz, "An optical lattice clock with spin-polarized ^{87}sr atoms," *The European Physical Journal D*, vol. 48, no. 1, pp. 11–17, 2008. [Online]. Available: http://dx.doi.org/10.1140/epjd/e2007-00330-3

[116] R. Le Targat, L. Lorini, Y. Le Coq, M. Zawada, J. Guéna, M. Abgrall, M. Gurov, P. Rosenbusch, D. G. Rovera, B. Nagórny, R. Gartman, P. G. Westergaard, M. E. Tobar, M. Lours, G. Santarelli, A. Clairon, S. Bize, P. Laurent, P. Lemonde, and J. Lodewyck, "Experimental realization of an optical second with strontium lattice clocks," *Nat Commun*, vol. 4, p. 2109, Jul. 2013. [Online]. Available: http://dx.doi.org/10.1038/ncomms3109

[117] J. Lodewyck, S. Bilicki, E. Bookjans, J.-L. Robyr, C. Shi, G. Vallet, R. L. Targat, D. Nicolodi, Y. L. Coq, J. Guéna, M. Abgrall, P. Rosenbusch, and S. Bize, "Optical to microwave clock frequency ratios with a nearly continuous strontium optical lattice clock," *Metrologia*, vol. 53, no. 4, p. 1123, 2016. [Online]. Available: http://stacks.iop.org/0026-1394/53/i=4/a=1123

[118] G. Petit, F. Arias, and G. Panfilo, "International atomic time: Status and future challenges," *Comptes Rendus Physique*, vol. 16, no. 5, pp. 480 – 488, 2015, the measurement of time / La mesure du temps. [Online]. Available: http://www.sciencedirect.com/science/article/pii/S1631070515000535

[119] See *Circular T* and fountain reports on the BIPM website. [Online]. Available: https://www.bipm.org/fr/bipm-services/timescales/time-ftp/Circular-T.html

[120] H. Hachisu, G. Petit, F. Nakagawa, Y. Hanado, and T. Ido, "SI-traceable measurement of an optical frequency at the low 10^{-16} level without a local primary standard," *Opt. Express*, vol. 25, no. 8, pp. 8511–8523, Apr 2017. [Online]. Available: http://www.opticsexpress.org/abstract.cfm?URI=oe-25-8-8511

[121] G. D. Rovera, S. Bize, B. Chupin, J. Guéna, P. Laurent, P. Rosenbusch, P. Uhrich, and M. Abgrall, "UTC(OP) based on LNE-SYRTE atomic fountain primary frequency standards," *Metrologia*, vol. 53, no. 3, p. S81, 2016. [Online]. Available: http://stacks.iop.org/0026-1394/53/i=3/a=S81

[122] A. Bauch, S. Weyers, D. Piester, E. Staliuniene, and W. Yang, "Generation of UTC(PTB) as a fountain-clock based time scale," *Metrologia*, vol. 49, no. 3, p. 180, 2012. [Online]. Available: http://stacks.iop.org/0026-1394/49/i=3/a=180

[123] Décret n°2017-292 du 06 mars 2017 relatif au temps légal français. [Online]. Available: https://www.legifrance.gouv.fr/eli/decret/2017/3/6/2017-292/jo/texte

[124] A. Bauch, "Time and frequency comparisons using radiofrequency signals from satellites," *Comptes Rendus Physique*, vol. 16, no. 5, pp. 471 – 479, 2015, the measurement of time / La mesure du temps. [Online]. Available: http://www.sciencedirect.com/science/article/pii/S1631070515000201

[125] G. P. Petit, A. Kanj, S. Loyer, J. Delporte, F. Mercier, and F. Perosanz, "1x10-16 frequency transfer by gps ppp with integer ambiguity resolution," *Metrologia*, vol. 52, no. 2, p. 301, 2015. [Online]. Available: http://stacks.iop.org/0026-1394/52/i=2/a=301

[126] L. Cacciapuoti and C. Salomon, "Space clocks and fundamental tests: The ACES experiment," *The European Physical Journal Special Topics*, vol. 172, pp. 57–68, 2009. [Online]. Available: http://dx.doi.org/10.1140/epjst/e2009-01041-7

[127] L. Cacciapuoti, N. Dimarcq, G. Santarelli, P. Laurent, P. Lemonde, A. Clairon, P. Berthoud, A. Jornod, F. Reina, S. Feltham, and C. Salomon, "Atomic clock ensemble in space: Scientific objectives and mission status," *Nuclear Physics B - Proceedings Supplements*, vol. 166, pp. 303 – 306, 2007, proceedings of the Third International Conference on Particle and Fundamental Physics in Space. [Online]. Available: http://www.sciencedirect.com/science/article/pii/S0920563206010425

[128] M. Abgrall, B. Chupin, L. D. Sarlo, J. Guéna, P. Laurent, Y. L. Coq, R. L. Targat, J. Lodewyck, M. Lours, P. Rosenbusch, G. D. Rovera, and S. Bize, "Atomic fountains and optical clocks at SYRTE: Status and perspectives," *Comptes Rendus Physique*, vol. 16, no. 5, pp. 461 – 470, 2015, the measurement of time / La mesure du temps. [Online]. Available: http://www.sciencedirect.com/science/article/pii/S1631070515000614

[129] M. Gurov, J. McFerran, B. Nagorny, R. Tyumenev, Z. Xu, Y. Le Coq, R. Le Targat, P. Lemonde, J. Lodewyck, and S. Bize, "Optical lattice clocks as candidates for a possible redefinition of the si second," *Instrumentation and Measurement, IEEE Transactions on*, vol. 62, no. 6, pp. 1568–1573, 2013.

[130] X. Baillard, M. Fouché, R. L. Targat, P. G. Westergaard, A. Lecallier, F. Chapelet, M. Abgrall, G. D. Rovera, P. Laurent, P. Rosenbusch, S. Bize, G. Santarelli, A. Clairon, P. Lemonde, G. Grosche, B. Lipphardt, and H. Schnatz, "An optical lattice clock with spin-polarized ^{87}Sr atoms," *Eur. Phys. J. D*, vol. 48, p. 11, 2008. [Online]. Available: http://dx.doi.org/10.1140/epjd/e2007-00330-3

[131] J.-P. Uzan, "Varying constants, gravitation and cosmology," *Living Reviews in Relativity*, vol. 14, no. 2, 2011. [Online]. Available: http://www.livingreviews.org/lrr-2011-2

[132] C. M. Will, "The confrontation between general relativity and experiment," *Living Reviews in Relativity*, vol. 17, no. 1, p. 4, Jun 2014. [Online]. Available: https://doi.org/10.12942/lrr-2014-4

[133] S. Reynaud, C. Salomon, and P. Wolf, "Testing general relativity with atomic clocks," *Space Science Reviews*, vol. 148, no. 1, pp. 233–247, Dec. 2009. [Online]. Available: http://dx.doi.org/10.1007/s11214-009-9539-0

[134] V. V. Flambaum and A. F. Tedesco, "Dependence of nuclear magnetic moments on quark masses and limits on temporal variation of fundamental constants from atomic clock experiments," *Phys. Rev. C*, vol. 73, no. 5, p. 055501, 2006. [Online]. Available: http://link.aps.org/abstract/PRC/v73/e055501

[135] T. H. Dinh, A. Dunning, V. A. Dzuba, and V. V. Flambaum, "Sensitivity of hyperfine structure to nuclear radius and quark mass variation," *Phys. Rev. A*, vol. 79, p. 054102, May 2009. [Online]. Available: http://link.aps.org/doi/10.1103/PhysRevA.79.054102

[136] V. A. Dzuba and V. V. Flambaum, "Relativistic corrections to transition frequencies of Ag *i*, Dy *i*, Ho *i*, Yb *ii*, Yb *iii*, Au *i*, and Hg *ii* and search for variation of the fine-structure constant," *Phys. Rev. A*, vol. 77, p. 012515, Jan 2008. [Online]. Available: http://link.aps.org/doi/10.1103/PhysRevA.77.012515

[137] V. V. Flambaum and V. A. Dzuba, "Search for variation of the fundamental constants in atomic, molecular, and nuclear spectra," *Can. J. Phys.*, vol. 87, p. 25, 2009.

[138] J. Webb, V. Flambaum, C. Churchill, M. Drinkwater, and J. Barrow, "Search for time variation of the fine structure constant," *Phys. Rev. Lett.*, vol. 82, no. 5, p. 884, 1999.

[139] J. Webb, M. Murphy, V. Flambaum, V. Dzuba, J. Barrow, C. Churchill, J. Prochaska, and A. Wolfe, "Further evidence for cosmological evolution of the fine structure constant," *Phys. Rev. Lett.*, vol. 87, p. 091301, 2001.

[140] R. Srianand, H. Chand, P. Petitjean, and B. Aracil, "Limits on the time variation of the electromagnetic fine-structure constant in the low energy limit from absorption lines in the spectra of distant quasars," *Phys. Rev. Lett.*, vol. 92, no. 12, p. 121302, Mar 2004.

[141] A. Ivanchik, P. Petitjean, D. Varshalovich, B. Aracil, R. Srianand, H. Chand, C. Ledoux, and P. Boissé, "A new constraint on the time dependence of the proton-to-electron mass ratio," *A&A*, vol. 440, no. 1, pp. 45–52, 2005. [Online]. Available: http://dx.doi.org/10.1051/0004-6361:20052648

[142] E. Reinhold, R. Buning, U. Hollenstein, A. Ivanchik, P. Petitjean, and W. Ubachs, "Indication of a cosmological variation of the proton-electron mass ratio based on laboratory measurement and reanalysis of $h2$ spectra," *Phys. Rev. Lett.*, vol. 96, no. 15, p. 151101, Apr 2006.

[143] T. Damour and A. Polyakov, "The string dilaton and a least coupling principle," *Nucl. Phys. B*, vol. 423, p. 532, 1994.

[144] T. Damour, F. Piazza, and G. Veneziano, "Runaway dilaton and equivalence principle violations," *Phys. Rev. Lett*, vol. 89, p. 081601, 2002.

[145] J. Guéna, M. Abgrall, D. Rovera, P. Rosenbusch, M. E. Tobar, P. Laurent, A. Clairon, and S. Bize, "Improved tests of local position invariance using ^{87}Rb and ^{133}Cs fountains," *Phys. Rev. Lett.*, vol. 109, p. 080801, Aug 2012. [Online]. Available: http://link.aps.org/doi/10.1103/PhysRevLett.109.080801

[146] M. E. Tobar, P. L. Stanwix, J. J. McFerran, J. Guéna, M. Abgrall, S. Bize, A. Clairon, P. Laurent, P. Rosenbusch, D. Rovera, and G. Santarelli, "Testing local position and fundamental constant invariance due to periodic gravitational and boost using long-term comparison of the syrte atomic fountains and h-masers," *Phys. Rev. D*, vol. 87, p. 122004, Jun 2013. [Online]. Available: http://link.aps.org/doi/10.1103/PhysRevD.87.122004

[147] S. Bize, S. Diddams, U. Tanaka, C. Tanner, W. Oskay, R. Drullinger, T. Parker, T. Heavner, S. Jefferts, L. Hollberg, W. Itano, and J. Bergquist, "Testing the stability of fundamental constants with the $^{199}Hg^{+}$ single-ion optical clock," *Phys. Rev. Lett.*, vol. 90, p. 150802, 2003.

[148] S. Blatt, A. D. Ludlow, G. K. Campbell, J. W. Thomsen, T. Zelevinsky, M. M. Boyd, J. Ye, X. Baillard, M. Fouché, R. L. Targat, A. Brusch, P. Lemonde, M. Takamoto, F.-L. Hong, H. Katori, and V. V. Flambaum, "New limits on coupling of fundamental constants to gravity using ^{87}Sr optical lattice clocks," *Phys. Rev. Lett.*, vol. 100, p. 140801, 2008.

[149] C. Grebing, A. Al-Masoudi, S. Dörscher, S. Häfner, V. Gerginov, S. Weyers, B. Lipphardt, F. Riehle, U. Sterr, and C. Lisdat, "Realization of a timescale with an accurate optical lattice clock," *Optica*, vol. 3, no. 6, pp. 563–569, Jun 2016. [Online]. Available: http://www.osapublishing.org/optica/abstract.cfm?URI=optica-3-6-563

[150] M. Niering, R. Holzwarth, J. Reichert, P. Pokasov, T. Udem, M. Weitz, T. W. Hänsch, P. Lemonde, G. Santarelli, M. Abgrall, P. Laurent, C. Salomon, and A. Clairon, "Measurement of the hydrogen 1S-2S transition frequency by phase coherent comparison with a microwave cesium fountain clock," *Phys. Rev. Lett.*, vol. 84, p. 5496, 2000. [Online]. Available: https://doi.org/10.1103/PhysRevLett.84.5496

[151] M. Fischer, N. Kolachevsky, M. Zimmermann, R. Holzwarth, T. Udem, T. W. Hänsch, M. Abgrall, J. Grunert, I. Maksimovic, S. Bize, H. Marion, F. P. D. Santos, P. Lemonde, G. Santarelli, P. Laurent, A. Clairon, C. Salomon, M. Haas, U. D. Jentschura, and C. H. Keitel, "New limits on the drift of fundamental constants from laboratory measurements," *Phys. Rev. Lett.*, vol. 92, p. 230802, 2004. [Online]. Available: https://doi.org/10.1103/PhysRevLett.92.230802

[152] C. G. Parthey, A. Matveev, J. Alnis, B. Bernhardt, A. Beyer, R. Holzwarth, A. Maistrou, R. Pohl, K. Predehl, T. Udem, T. Wilken, N. Kolachevsky, M. Abgrall, D. Rovera, C. Salomon, P. Laurent, and T. W. Hänsch, "Improved measurement of the hydrogen 1S-2S transition frequency," *Phys. Rev. Lett.*, vol. 107, p. 203001, Nov 2011. [Online]. Available: http://link.aps.org/doi/10.1103/PhysRevLett.107.203001

[153] A. Matveev, C. G. Parthey, K. Predehl, J. Alnis, A. Beyer, R. Holzwarth, T. Udem, T. Wilken, N. Kolachevsky, M. Abgrall, D. Rovera, C. Salomon, P. Laurent, G. Grosche, O. Terra, T. Legero, H. Schnatz, S. Weyers, B. Altschul, and T. W. Hänsch, "Precision measurement of the hydrogen 1s-2s frequency via a 920-km fiber link," *Phys. Rev. Lett.*, vol. 110, p. 230801, Jun 2013. [Online]. Available: http://link.aps.org/doi/10.1103/PhysRevLett.110.230801

[154] P. J. Mohr, B. N. Taylor, and D. B. Newell, "Codata recommended values of the fundamental physical constants: 2010," *Rev. Mod. Phys.*, vol. 84, pp. 1527–1605, Nov 2012. [Online]. Available: http://link.aps.org/doi/10.1103/RevModPhys.84.1527

[155] R. Pohl, A. Antognini, F. Nez, F. D. Amaro, F. Biraben, J. M. R. Cardoso, D. S. Covita, A. Dax, S. Dhawan, L. M. P. Fernandes, A. Giesen, T. Graf, T. W. Hänsch, P. Indelicato, L. Julien, C.-Y. Kao, P. Knowles, E.-O. Le Bigot, Y.-W. Liu, J. A. M. Lopes, L. Ludhova, C. M. B. Monteiro, F. Mulhauser, T. Nebel, P. Rabinowitz, J. M. F. dos Santos, L. A. Schaller, K. Schuhmann, C. Schwob, D. Taqqu, J. F. C. A. Veloso, and F. Kottmann, "The size of the proton," *Nature*, vol. 466, no. 7303, pp. 213–216, Jul. 2010. [Online]. Available: http://dx.doi.org/10.1038/nature09250

[156] A. Antognini, F. Nez, K. Schuhmann, F. D. Amaro, F. Biraben, J. M. R. Cardoso, D. S. Covita, A. Dax, S. Dhawan, M. Diepold, L. M. P. Fernandes, A. Giesen, A. L. Gouvea, T. Graf, T. W. HÃd'nsch, P. Indelicato, L. Julien, C.-Y. Kao, P. Knowles, F. Kottmann, E.-O. Le Bigot, Y.-W. Liu, J. A. M. Lopes, L. Ludhova, C. M. B. Monteiro, F. Mulhauser, T. Nebel, P. Rabinowitz, J. M. F. dos Santos, L. A. Schaller, C. Schwob, D. Taqqu, J. F. C. A. Veloso, J. Vogelsang, and R. Pohl, "Proton structure from the measurement of 2s-2p transition frequencies of muonic hydrogen," *Science*, vol. 339, no. 6118, pp. 417–420, 2013. [Online]. Available: http://www.sciencemag.org/content/339/6118/417.abstract

[157] R. Pohl, F. Nez, T. Udem, A. Antognini, A. Beyer, H. Fleurbaey, A. Grinin, T. W. Hänsch, L. Julien, F. Kottmann, J. J. Krauth, L. Maisenbacher, A. Matveev, and F. Biraben, "Deuteron charge radius and rydberg constant from spectroscopy data in atomic deuterium," *Metrologia*, vol. 54, no. 2, p. L1, 2017. [Online]. Available: http://stacks.iop.org/0026-1394/54/i=2/a=L1

[158] N. Leefer, C. T. M. Weber, A. Cingöz, J. R. Torgerson, and D. Budker, "New limits on variation of the fine-structure constant using atomic dysprosium," *Phys. Rev. Lett.*, vol. 111, p. 060801, Aug 2013. [Online]. Available: http://link.aps.org/doi/10.1103/PhysRevLett.111.060801

[159] V. V. Flambaum, "Enhanced effect of temporal variation of the fine-structure constant in diatomic molecules," *Phys. Rev. A*, vol. 73, no. 3, p. 034101, 2006. [Online]. Available: http://link.aps.org/abstract/PRA/v73/e034101

[160] E. Peik and C. Tamm, "Nuclear laser spectroscopy of the 3.5 ev transition in th-229," *EPL (Europhysics Letters)*, vol. 61, no. 2, p. 181, 2003. [Online]. Available: http://stacks.iop.org/0295-5075/61/i=2/a=181

[161] J. C. Berengut, V. A. Dzuba, and V. V. Flambaum, "Enhanced laboratory sensitivity to variation of the fine-structure constant using highly charged ions," *Phys. Rev. Lett.*, vol. 105, no. 12, p. 120801, Sep 2010.

[162] T. Damour and J. F. Donoghue, "Equivalence principle violations and couplings of a light dilaton," *Phys. Rev. D*, vol. 82, p. 084033, Oct 2010. [Online]. Available: https://link.aps.org/doi/10.1103/PhysRevD.82.084033

[163] Y. V. Stadnik and V. V. Flambaum, "Searching for topological defect dark matter via nongravitational signatures," *Phys. Rev. Lett.*, vol. 113, p. 151301, Oct 2014. [Online]. Available: http://link.aps.org/doi/10.1103/PhysRevLett.113.151301

[164] ——, "Can dark matter induce cosmological evolution of the fundamental constants of nature?" *Phys. Rev. Lett.*, vol. 115, p. 201301, Nov 2015. [Online]. Available: http://link.aps.org/doi/10.1103/PhysRevLett.115.201301

[165] A. Arvanitaki, J. Huang, and K. Van Tilburg, "Searching for dilaton dark matter with atomic clocks," *Phys. Rev. D*, vol. 91, p. 015015, Jan 2015. [Online]. Available: https://link.aps.org/doi/10.1103/PhysRevD.91.015015

[166] A. Hees, J. Guéna, M. Abgrall, S. Bize, and P. Wolf, "Searching for an oscillating massive scalar field as a dark matter candidate using atomic hyperfine frequency comparisons," *Phys. Rev. Lett.*, vol. 117, p. 061301, Aug 2016. [Online]. Available: http://link.aps.org/doi/10.1103/PhysRevLett.117.061301

[167] P. J. McMillan, "Mass models of the milky way," *Monthly Notices of the Royal Astronomical Society*, vol. 414, no. 3, pp. 2446–2457, 2011. [Online]. Available: https://doi.org/10.1111/j.1365-2966.2011.18564.x

[168] K. Van Tilburg, N. Leefer, L. Bougas, and D. Budker, "Search for ultralight scalar dark matter with atomic spectroscopy," *Phys. Rev. Lett.*, vol. 115, p. 011802, Jun 2015. [Online]. Available: http://link.aps.org/doi/10.1103/PhysRevLett.115.011802

[169] Y. V. Stadnik and V. V. Flambaum, "Improved limits on interactions of low-mass spin-0 dark matter from atomic clock spectroscopy," *Phys. Rev. A*, vol. 94, p. 022111, Aug 2016. [Online]. Available: https://link.aps.org/doi/10.1103/PhysRevA.94.022111

[170] A. A. Michelson and E. W. Morley, "On the relative motion of the earth and the luminiferous ether," *Am. J. Sci.*, vol. 34, p. 333, 1887.

[171] R. J. Kennedy and E. M. Thorndike, "Experimental establishment of the relativity of time," *Phys. Rev.*, vol. 42, pp. 400–418, Nov 1932. [Online]. Available: https://link.aps.org/doi/10.1103/PhysRev.42.400

[172] H. E. Ives and G. R. Stilwell, "An experimental study of the rate of a moving atomic clock," *J. Opt. Soc. Am.*, vol. 28, no. 7, pp. 215–226, 1938. [Online]. Available: http://www.opticsinfobase.org/abstract.cfm?URI=josa-28-7-215

[173] G. Hinshaw, J. L. Weiland, R. S. Hill, N. Odegard, D. Larson, C. L. Bennett, J. Dunkley, B. Gold, M. R. Greason, N. Jarosik, E. Komatsu, M. R. Nolta, L. Page, D. N. Spergel, E. Wollack, M. Halpern, A. Kogut, M. Limon, S. S. Meyer, G. S. Tucker, and E. L. Wright, "Five-year wilkinson microwave anisotropy probe observations: Data processing, sky maps, and basic results," *The Astrophysical Journal Supplement Series*, vol. 180, no. 2, p. 225, 2009. [Online]. Available: http://stacks.iop.org/0067-0049/180/i=2/a=225

[174] P. Wolf, S. Bize, A. Clairon, A. N. Luiten, G. Santarelli, and M. E. Tobar, "Tests of lorentz invariance using a microwave resonator," *Phys. Rev. Lett.*, vol. 90, p. 060402, Feb 2003. [Online]. Available: http://link.aps.org/doi/10.1103/PhysRevLett.90.060402

[175] P. Wolf, S. Bize, A. Clairon, G. Santarelli, M. E. Tobar, and A. N. Luiten, "Improved test of lorentz invariance in electrodynamics," *Phys. Rev. D*, vol. 70, no. 5, p. 051902, Sep 2004.

[176] P. Wolf, M. E. Tobar, S. Bize, A. Clairon, A. N. Luiten, and G. Santarelli, "Whispering gallery resonators and tests of lorentz invariance," *General Relativity and Gravitation*, vol. 36, no. 10, pp. 2351–2372, Oct 2004. [Online]. Available: https://doi.org/10.1023/B:GERG.0000046188.87741.51

[177] M. E. Tobar, P. Wolf, S. Bize, G. Santarelli, and V. Flambaum, "Testing local lorentz and position invariance and variation of fundamental constants by searching the derivative of the comparison frequency between a cryogenic sapphire oscillator and hydrogen maser," *Phys. Rev. D*, vol. 81, no. 2, p. 022003, Jan 2010.

[178] H. P. Robertson, "Postulate versus observation in the special theory of relativity," *Rev. Mod. Phys.*, vol. 21, pp. 378–382, Jul 1949. [Online]. Available: https://link.aps.org/doi/10.1103/RevModPhys.21.378

[179] R. Mansouri and R. U. Sexl, "A test theory of special relativity: I. simultaneity and clock synchronization," *General Relativity and Gravitation*, vol. 8, no. 7, pp. 497–513, Jul 1977. [Online]. Available: https://doi.org/10.1007/BF00762634

[180] ——, "A test theory of special relativity: Ii. first order tests," *General Relativity and Gravitation*, vol. 8, no. 7, pp. 515–524, Jul 1977.

[181] ——, "A test theory of special relativity: Iii. second-order tests," *General Relativity and Gravitation*, vol. 8, no. 10, pp. 809–814, Oct 1977. [Online]. Available: https://doi.org/10.1007/BF00759585

[182] A. Brillet and J. L. Hall, "Improved laser test of the isotropy of space," *Phys. Rev. Lett.*, vol. 42, pp. 549–552, Feb 1979. [Online]. Available: https://link.aps.org/doi/10.1103/PhysRevLett.42.549

[183] D. Hils and J. L. Hall, "Improved kennedy-thorndike experiment to test special relativity," *Phys. Rev. Lett.*, vol. 64, pp. 1697–1700, Apr 1990. [Online]. Available: https://link.aps.org/doi/10.1103/PhysRevLett.64.1697

[184] P. L. Stanwix, M. E. Tobar, P. Wolf, M. Susli, C. R. Locke, E. N. Ivanov, J. Winterflood, and F. van Kann, "Test of lorentz invariance in electrodynamics using rotating cryogenic sapphire microwave oscillators," *Phys. Rev. Lett.*, vol. 95, p. 040404, Jul 2005. [Online]. Available: https://link.aps.org/doi/10.1103/PhysRevLett.95.040404

[185] P. L. Stanwix, M. E. Tobar, P. Wolf, C. R. Locke, and E. N. Ivanov, "Improved test of lorentz invariance in electrodynamics using rotating cryogenic sapphire oscillators," *Phys. Rev. D*, vol. 74, p. 081101, Oct 2006. [Online]. Available: https://link.aps.org/doi/10.1103/PhysRevD.74.081101

[186] S. Herrmann, A. Senger, K. Möhle, M. Nagel, E. V. Kovalchuk, and A. Peters, "Rotating optical cavity experiment testing lorentz invariance at the 10^{-17} level," *Phys. Rev. D*, vol. 80, no. 10, p. 105011, Nov 2009.

[187] D. Colladay and V. A. Kostelecký, "CPT," *Phys. Rev. D*, vol. 55, pp. 6760–6774, Jun 1997. [Online]. Available: https://link.aps.org/doi/10.1103/PhysRevD.55.6760

[188] ——, "Lorentz-violating extension of the standard model," *Phys. Rev. D*, vol. 58, p. 116002, Oct 1998. [Online]. Available: https://link.aps.org/doi/10.1103/PhysRevD.58.116002

[189] V. A. Kostelecký, "Gravity, lorentz violation, and the standard model," *Phys. Rev. D*, vol. 69, p. 105009, May 2004. [Online]. Available: https://link.aps.org/doi/10.1103/PhysRevD.69.105009

[190] H. Müller, S. Herrmann, C. Braxmaier, S. Schiller, and A. Peters, "Modern michelson-morley experiment using cryogenic optical resonators," *Phys. Rev. Lett.*, vol. 91, p. 020401, Jul 2003. [Online]. Available: https://link.aps.org/doi/10.1103/PhysRevLett.91.020401

[191] V. A. Kostelecký and N. Russell, "Data tables for lorentz and *cpt* violation," *Rev. Mod. Phys.*, vol. 83, no. 1, pp. 11–32, Mar 2011.

[192] ——, "Data tables for lorentz and *cpt* violation: update to rev. mod. phys. 83, 11 (2011)," *arxiv 0801.0287v10*, 2008. [Online]. Available: https://arxiv.org/abs/0801.0287v10

[193] V. W. Hughes, H. G. Robinson, and V. Beltran-Lopez, "Upper limit for the anisotropy of inertial mass from nuclear resonance experiments," *Phys. Rev. Lett.*, vol. 4, pp. 342–344, Apr 1960. [Online]. Available: https://link.aps.org/doi/10.1103/PhysRevLett.4.342

[194] R. W. P. Drever, "Upper limit to anisotropy of inertial mass from nuclear resonance," *Philosophical Magazine*, vol. 5, no. 52, pp. 409–411, 1960. [Online]. Available: http://dx.doi.org/10.1080/14786436008235858

[195] ——, "A search for anisotropy of inertial mass using a free precession technique," *Philosophical Magazine*, vol. 6, no. 65, pp. 683–687, 1961. [Online]. Available: http://www.tandfonline.com/doi/abs/10.1080/14786436108244418

[196] R. Bluhm, V. A. Kostelecký, C. D. Lane, and N. Russell, "Probing lorentz and CPT violation with space-based experiments," *Phys. Rev. D*, vol. 68, p. 125008, Dec 2003. [Online]. Available: https://link.aps.org/doi/10.1103/PhysRevD.68.125008

[197] H. Pihan-Le Bars, C. Guerlin, R.-D. Lasseri, J.-P. Ebran, Q. G. Bailey, S. Bize, E. Khan, and P. Wolf, "Lorentz-symmetry test at planck-scale suppression with nucleons in a spin-polarized ^{133}Cs cold atom clock," *Phys. Rev. D*, vol. 95, p. 075026, Apr 2017. [Online]. Available: https://link.aps.org/doi/10.1103/PhysRevD.95.075026

[198] P. Peterman, K. Gibble, P. Laurent, and C. Salomon, "Microwave lensing frequency shift of the pharao laser-cooled microgravity atomic clock," *Metrologia*, vol. 53, no. 2, p. 899, 2016. [Online]. Available: http://stacks.iop.org/0026-1394/53/i=2/a=899

[199] M. Swallows, M. Martin, M. Bishof, C. Benko, Y. Lin, S. Blatt, A. Rey, and J. Ye, "Operating a ^{87}Sr optical lattice clock with high precision and at high density," *Ultrasonics, Ferroelectrics and Frequency Control, IEEE Transactions on*, vol. 59, no. 3, pp. 416 –425, march 2012.

[200] T. Kessler, C. Hagemann, C. Grebing, T. Legero, U. Sterr, F. Riehle, M. J. Martin, L. Chen, and J. Ye, "A sub-40-mHz-linewidth laser based on a silicon single-crystal optical cavity," *Nature Photonics*, vol. 6, no. 10, pp. 687–692, Oct. 2012.

[201] S. Häfner, S. Falke, C. Grebing, S. Vogt, T. Legero, M. Merimaa, C. Lisdat, and U. Sterr, "8×10^{-17} fractional laser frequency instability with a long room-temperature cavity," *Opt. Lett.*, vol. 40, no. 9, pp. 2112–2115, May 2015. [Online]. Available: http://ol.osa.org/abstract.cfm?URI=ol-40-9-2112

[202] D. G. Matei, T. Legero, S. Häfner, C. Grebing, R. Weyrich, W. Zhang, L. Sonderhouse, J. M. Robinson, J. Ye, F. Riehle, and U. Sterr, "1.5 μm lasers with sub 10 mHz linewidth," *Phys. Rev. Lett.*, vol. 118, p. 263202, Jun 2017. [Online]. Available: https://link.aps.org/doi/10.1103/PhysRevLett.118.263202

[203] J. A. Sherman, N. D. Lemke, N. Hinkley, M. Pizzocaro, R. W. Fox, A. D. Ludlow, and C. W. Oates, "High-accuracy measurement of atomic polarizability in an optical lattice clock," *Phys. Rev. Lett.*, vol. 108, p. 153002, Apr 2012. [Online]. Available: http://link.aps.org/doi/10.1103/PhysRevLett.108.153002

[204] K. Beloy, J. A. Sherman, N. D. Lemke, N. Hinkley, C. W. Oates, and A. D. Ludlow, "Determination of the $5d6s\ ^3D_1$ state lifetime and blackbody-radiation clock shift in yb," *Phys.*

Rev. A, vol. 86, p. 051404, Nov 2012. [Online]. Available: http://link.aps.org/doi/10.1103/PhysRevA.86.051404

[205] T. Middelmann, S. Falke, C. Lisdat, and U. Sterr, "High accuracy correction of blackbody radiation shift in an optical lattice clock," *Phys. Rev. Lett.*, vol. 109, p. 263004, Dec 2012. [Online]. Available: http://link.aps.org/doi/10.1103/PhysRevLett.109.263004

[206] V. D. Ovsiannikov, S. I. Marmo, V. G. Palchikov, and H. Katori, "Higher-order effects on the precision of clocks of neutral atoms in optical lattices," *Phys. Rev. A*, vol. 93, p. 043420, Apr 2016. [Online]. Available: http://link.aps.org/doi/10.1103/PhysRevA.93.043420

[207] M.-A. Bouchiat, "Linear stark shift in dressed atoms as a signal to measure a nuclear anapole moment with a cold-atom fountain or interferometer," *Phys. Rev. Lett.*, vol. 98, no. 4, p. 043003, Jan 2007.

[208] A. Einstein, "Über den einflußder schwerkraft auf die ausbreitung des lichtes," *Ann. Phys.*, vol. 35, no. 10, pp. 898–908, 1911. [Online]. Available: http://dx.doi.org/10.1002/andp.19113401005

[209] R. Pound and G. Rebka, "Apparent weight of photons," *Phys. Rev. Lett.*, vol. 4, p. 337, 1960.

[210] M. Vermeer, "Chronometric levelling," Finnish Geodetic Institute, Tech. Rep., 1983.

[211] G. Lion, I. Panet, P. Wolf, C. Guerlin, S. Bize, and P. Delva, "Determination of a high spatial resolution geopotential model using atomic clock comparisons," *Journal of Geodesy*, pp. 1–15, 2017. [Online]. Available: http://dx.doi.org/10.1007/s00190-016-0986-6

[212] S. B. Koller, J. Grotti, S. Vogt, A. Al-Masoudi, S. Dörscher, S. Häfner, U. Sterr, and C. Lisdat, "Transportable optical lattice clock with 7×10^{-17} uncertainty," *Phys. Rev. Lett.*, vol. 118, p. 073601, Feb 2017. [Online]. Available: http://link.aps.org/doi/10.1103/PhysRevLett.118.073601

[213] K. Bongs, Y. Singh, L. Smith, W. He, O. Kock, D. ÅŽwierad, J. Hughes, S. Schiller, S. Alighanbari, S. Origlia, S. Vogt, U. Sterr, C. Lisdat, R. L. Targat, J. Lodewyck, D. Holleville, B. Venon, S. Bize, G. P. Barwood, P. Gill, I. R. Hill, Y. B. Ovchinnikov, N. Poli, G. M. Tino, J. Stuhler, and W. Kaenders, "Development of a strontium optical lattice clock for the SOC mission on the ISS,"

Comptes Rendus Physique, vol. 16, no. 5, pp. 553 – 564, 2015, the measurement of time / La mesure du temps. [Online]. Available: http://www.sciencedirect.com/science/article/pii/S1631070515000602

[214] T. Takano, M. Takamoto, I. Ushijima, N. Ohmae, T. Akatsuka, A. Yamaguchi, Y. Kuroishi, H. Munekane, B. Miyahara, and H. Katori, "Geopotential measurements with synchronously linked optical lattice clocks," *Nat Photon*, vol. advance online publication, Aug. 2016. [Online]. Available: http://dx.doi.org/10.1038/nphoton.2016.159

[215] J.-D. Deschênes, L. C. Sinclair, F. R. Giorgetta, W. C. Swann, E. Baumann, H. Bergeron, M. Cermak, I. Coddington, and N. R. Newbury, "Synchronization of distant optical clocks at the femtosecond level," *Phys. Rev. X*, vol. 6, p. 021016, May 2016. [Online]. Available: http://link.aps.org/doi/10.1103/PhysRevX.6.021016

[216] F. R. Giorgetta, W. C. Swann, L. C. Sinclair, E. Baumann, I. Coddington, and N. R. Newbury, "Optical two-way time and frequency transfer over free space," *Nat Photon*, vol. 7, no. 6, pp. 434–438, Jun. 2013. [Online]. Available: http://dx.doi.org/10.1038/nphoton.2013.69